CANADIAN THESES

THÈSES CANADIENNES

NOTICE

The quality of this microfiche is heavily dependent upon the quality of the original thesis submitted for microfilming. Every effort has been made to ensure the highest quality of reproduction possible.

If pages are missing, contact the university which granted the degree.

Some pages may have indistinct print especially if the original pages were typed with a poor typewriter ribbon or if the university sent us an inferior photocopy.

Previously copyrighted materials (journal articles, published tests, etc.) are not filmed.

Reproduction in full or in part of this film is governed by the Canadian Copyright Act, R.S.C. 1970, c. C-30. Please read the authorization forms which accompany this thesis.

AVIS

La qualité de cette microfiche dépend grandement de la qualité de la thèse soumise au microfilmage. Nous avons tout fait pour assurer une qualité supérieure de reproduction.

S'il manque des pages, veuillez communiquer avec l'université qui a conféré le grade.

La qualité d'impression de certaines pages peut laisser à désirer, surtout si les pages originales ont été dactylographiées à l'aide d'un ruban usé ou si l'université nous a fait parvenir une photocopie de qualité inférieure.

Les documents qui font déjà l'objet d'un droit d'auteur (articles de revue, examens publiés, etc.) ne sont pas microfilmés.

La reproduction, même partielle, de ce microfilm est soumise à la Loi canadienne sur le droit d'auteur, SRC 1970, c. C-30. Veuillez prendre connaissance des formules d'autorisation qui accompagnent cette thèse.

THIS DISSERTATION
HAS BEEN MICROFILMED
EXACTLY AS RECEIVED

LA THÈSE A ÉTÉ
MICROFILMÉE TELLE QUE
NOUS L'AVONS REÇUE

Canada

NL 339 (r. 86/01)

TSI-OQPSK FOR MULTIPLE CARRIER AND NONLINEARLY AMPLIFIED SYSTEMS

by

Hiep Pham Van

Thesis submitted to the School of Graduate Studies,
University of Ottawa, in partial fulfillment of
the requirements for the degree of
Master of Applied Science

Department of Electrical Engineering
University of Ottawa
Ottawa, Ontario
May 1983

ABSTRACT

In this thesis a *new class* of *Two-Symbol-Interval* (TSI) baseband pulse shapes is introduced. The power spectral density (PSD) and the probability of error (P_e) performance of TSI-OQPSK modems operated in a power and spectral efficient multi-carrier satellite system are analyzed. Power efficiency is achieved by operating the high-power-amplifiers (HPA) in full saturation. It is shown that the spectral restoration (spreading) caused by saturated HPA or by ideal hardlimited output amplifiers is much *lower* in the case of TSI-OQPSK systems than for conventional QPSK, OQPSK and MSK systems.

A new filtering strategy called *Sum of Approximate Eye* (SAE) is also introduced. It is shown that the SAE filter improves the P_e performance of our general-class of TSI-OQPSK modems, operated in a nonlinear (hardlimited and/or saturated HPA) and adjacent channel interference environment.

The hardware design of a TSI-OQPSK modem is presented, and implemented. Using our hardware system, the P_e performance of a TSI-OQPSK (n = 1) modem is evaluated and compared to our computer simulated results. It is shown that in the most spectral efficient narrow-channel spacing case, $(\Delta f \cdot T_b) \leq 1$, TSI-OQPSK systems have *the best* P_e *performance*.

ACKNOWLEDGEMENTS

The author would like to extend his gratitude to many people who helped him directly or indirectly, in making this work a success.

Thanks are due to his supervisor, Professor Kamilo Feher, for his helpful suggestions, encouragement, and numerous constructive criticisms.

Thanks are due to his friends, Tho Le-Ngoc, Steve Hatzigeorgiou, and Greg Shaw for their comments and suggestions.

Finally, the author would like to thank his wife, Hong, for encouraging him to complete this work.

TABLE OF CONTENTS

LIST OF FIGURES

LIST OF FIGURES (Cont'd)

LIST OF FIGURES (Cont'd)

LIST OF FIGURES (Cont'd)

LIST OF FIGURES (Cont'd)

LIST OF FIGURES (Cont'd)

LIST OF FIGURES (Cont'd)

LIST OF TABLES

LIST OF SYMBOLS AND ABBREVIATIONS

TSI	Two Symbol Interval
PSD	Power Spectral Density
P_e	Probability of error
TSI-OQPSK	Two Symbol Interval Offset Quadrature Phase Shift Keying
HPA	High Power Amplifier
QPSK	Quadrature Phase Shift Keying
OQPSK	Offset Quadrature Phase Shift Keying
MSK	Minimum Shift Keying
SAE	Sum of Approximate Eye
NRZ	Non Return to Zero
BER	Bit Error Rate
PSK	Phase Shift Keying
BPSK	Binary Phase Shift Keying
QAM	Quadrature Amplitude Modulation
QPR	Quadrature Partial Response
APK	Amplitude Phase Shift Keying
AM	Amplitude Modulation
PM	Phase Modulation
RZ	Return to Zero
ISI	InterSymbol Interference
SQORC	Staggered Quadrature Overlapped Raised Cosine
BPF	Band Pass Filter

ACI	Adjacent Channel Interference
FFT	Fast Fourier Transform
AWGN	Additive White Gaussian Noise
IJF OQPSK	Interference and Jitter Free Offset Quadrature Phase Shift Keying
NLSF	Nonlinear Switching Filter
BIP	Bipolar signals
LPF	Low Pass Filter
TSI-QPSK	Two Symbol Interval Quadrature Phase Shift Keying
WGN	White Gaussian Noise
Δf	Distance between two adjacent carrier frequencies
T_s	Symbol duration
b/s	Bits per second
f_s	Symbol rate
b/s/Hz	Bits per second per Hertz
S/N	Signal to Noise ratio
E_b/N_o	Energy per bit to Noise density ratio
C/N	Carrier to Noise ratio
f_b	Bit rate
σ^2	Noise variance
α	Roll-off factor of Raised Cosine filter
C/I	Carrier to Interference power ratio
F	Fourier Transform
F^{-1}	Inverse Fourier Transform
T_b	Bit rate duration
APK	Amplitude Phase Shift Keying

CHAPTER ONE

INTRODUCTION

The increasing use of data transmission for voice encoded digital signals and telegraph signals has led to an accelerated need for more and better communication channels between machines and between machines and people. Because of the increasing use of data transmission and the increased number of users, bandwidth is becoming more precious. It is also desirable to achieve the bandwidth efficiency needed, with as low average signal power as possible. Unfortunately, the lower the signal power, the poorer the system's performance, (all other parameters are constant). The performance of a digital system is specified by the bit error rate (BER). BER is defined as the ratio of the number of bits in error in a time interval t, to the total number of bits transmitted in that t seconds. For a large number of transmitted bits, the BER approximates the probability that any bit is incorrectly received (called probability of error: P_e). We note that the term BER is used in practical measurement while the term P_e is used in theoretical analysis. The objective of the design of any modern modulation system is to maximize the use of the channels (i.e. its spectral efficiency which is measured in bit/second/Hertz) and to minimize the P_e of the

system as a function of signal to noise (S/N) ratio, while operating in the presence of noise and interference. Other factors, such as hardware simplicity, cost reliability and maintainability, must also be taken into account.

Phase Shift Keying (PSK) is a technique which can enable the data transmitting system to increase the transmitted rate in a given bandwidth. There are many different PSK systems which have different bandwidth efficiencies, such as Binary PSK (BPSK) [19, 20, 24], Quadrature PSK (QPSK) [19, 20, 24], M-ary PSK [19, 20, 25] and M-ary APK [19, 20, 48, 29]. For a given bandwidth and limited signal power, a QPSK system has more advantages than other PSK systems.

The Energy per bit-to-noise density ratio (E_b/N_o) requirement of a QPSK system is almost the same as that of a BPSK system but the bandwidth efficiency of a QPSK system is double that of the other, (QPSK system: 2b/s/Hz, BPSK system: 1b/s/Hz). (We note that the channel bandwidth is defined by Nyquist filter with $\alpha = 0.0$). To obtain 4b/s/Hz (16 PSK or 16 APK), M-ary PSK ($M \geq 4$) requires at least 8 dB of carrier power more than QPSK. We also note that M-ary PSK or M-ary APK ($M \geq 4$) systems degrade significantly in a nonlinearly amplified satellite channel [6, 19, 20].

Because of these advantages, QPSK modulation techniques have been extensively used in high and medium speed digital microwave and satellite systems.

Since the power spectra of unfiltered QPSK signals exhibit sidelobes that may interfere with adjacent channels, a certain amount of filtering is necessary at the transmitter. However, this filtering results in a great amount of envelope fluctuation in the signal, which leads to a considerable out-of-band spectral regeneration due to the AM/AM and AM/PM nonlinear effects of the transmit high power amplifier (HPA). The regenerated spectral sidelobes introduce adjacent channel interference and degrade the P_e performance of the system (See Fig. 1). In order to reduce the spectral sidelobe regeneration (due to nonlinear effects), a number of modulation techniques has been introduced [1-5, 7-9, 15-17, 19, 20, 23, 32-36, 39-47].

Among these modulation techniques, Minimum Shift Keying (MSK) and Staggered QPSK (SQPSK) or Offset Keyed QPSK (OQPSK) are the most widely publised and had been used in digital microwave and satellite systems.

The only difference between the QPSK and OQPSK schemes is in the alignment of the in-phase and quadrature baseband components of the modulated signals. The result is that only 90° phase transitions occur in the modulator output signals. Like QPSK, an unfiltered OQPSK signal has a constant envelope. However, for filtered OQPSK signals, the result has a maximum envelope variation of 3 dB (70%) compared to the 100% envelope variation for conventional QPSK signals.

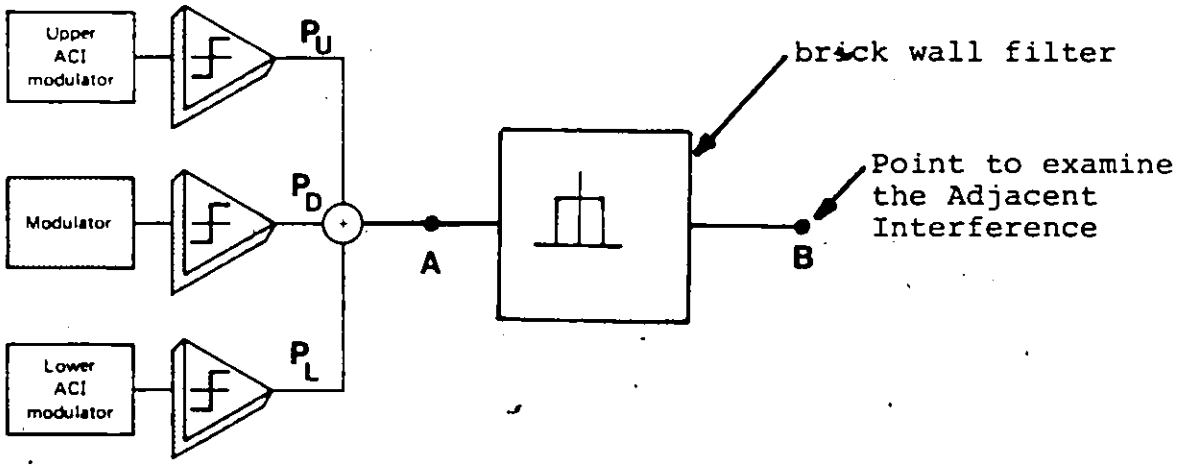

(a) Block diagram of an adjacent channel environment

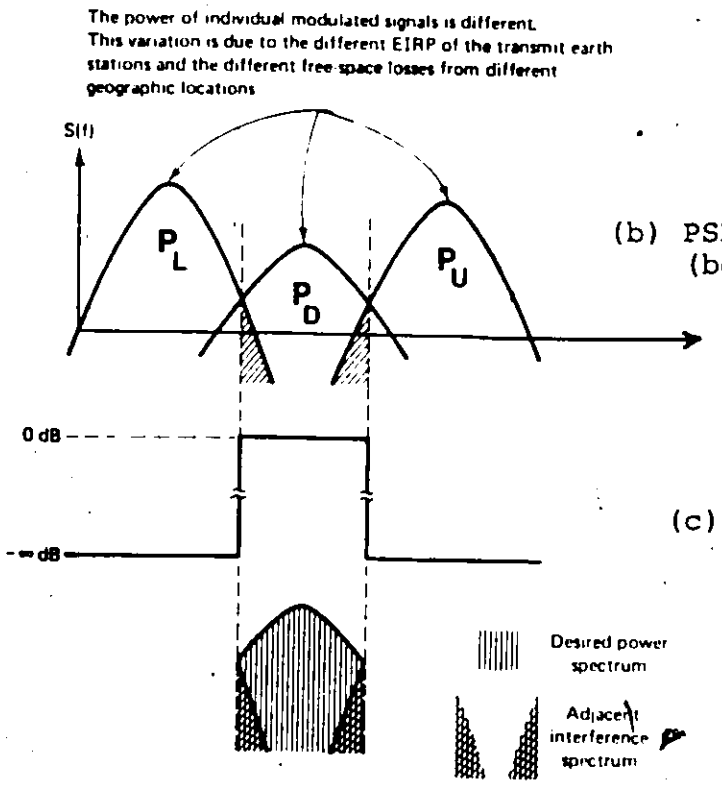

(b) PSDs at point A (before the filter)

(c) Brick wall filter

(d) Adjacent channel interference at Point B (after the filter)

Fig. 1. An example of an adjacent channel interference environment

Because of the different envelope fluctuations, the two modulated signals respond differently in a nonlinearly amplified channel; a OQPSK modulated signal has much less spectral sidelobe regeneration than a QPSK signal.

MSK is considered to be a form of OQPSK, in which the symbol pulse shape is a half cycle sinusoid rather than the usual rectangular form. It may also be viewed as a special case of continuous-phase-frequency-shift-keying (CPFSK) [50] with a frequency deviation ratio equal to 0.5. In this view, it is also known as Fast FSK (FFSK) because it can transmit faster pulse trains than any other ordinary FSK of equal bandwidth and signal to noise ratio. Due to its *constant envelope* and continuous phase transitions, MSK signals retain relatively low spectral sidelobe regeneration in a non-linearly amplified channel [1-6, 36-38].

In general the baseband pulse shape, phase transition and envelope fluctuation of a modulated signal are the major parameters affecting its spectral properties. For this reason, efforts have been expended to search for better pulse shapes, phase transition and envelope fluctuation.

This thesis introduces a new class of TWO SYMBOL INTERVAL (TSI) pulse shapes formed by means of sinusoidal waveforms having different amplitudes and periods. The choices of these shapes are based on the previous research results and publications [7,9,18] by Dr. K. Feher's team. This new class of

signals, when applied to an Offset-Quadrature-Phase-Shift-Keying (OQPSK) modulator and passed through a nonlinear system (such as a hardlimiter or a saturated High-Power-Amplifier), has some spectral advantages over conventional MSK, QPSK and OQPSK signals.

A new filtering strategy called SUM OF APPROXIMATE EYE is also introduced in this thesis. This SAE filter is obtained by taking the ratio of the raised cosine filter transfer function and the square root of the sum of the PSDs of the two separate overlapping eye diagrams of the receive eye diagram. The results show that SAE filters improve significantly the P_e performance of TSI-OQPSK modems as compared with Linear Zero Forcing filters [12, 13, 20, 24, 25] in a nonlinearly amplified channel.

We use extensive computer simulations to evaluate the probability of error (P_e) performance of different systems. The accuracy of our computer simulation was verified by comparing the computer generated $P_e = f(E_b/N_o)$ results with our measurement results performed on the same hardware system.

Our new class of TSI pulse shapes is introduced and analyzed in Chapter Two. The phase transitions of these TSI-OQPSK modulated signals are derived and found to be smoother than those of conventional MSK signals. The measured PSD of hardlimited TSI-OQPSK signals is in close agreement with our

computer simulated results. It is shown that these PSDs are narrower (for main lobes) and lower (for side lobes) than those of hardlimited QPSK, OQPSK and MSK modulated signals.

Two types of detection filters are examined in Chapter Three. A new filtering strategy is introduced and called "Sum of Approximate Eye". The results show that the SAE filter greatly improves the P_e performance of hardlimited TSI-OQPSK systems, over the conventional Linear-Zero-Forcing-Filter.

In Chapter Four, the adjacent channel experimental model is presented. Two types of nonlinear amplifiers are used in our evaluation - Hardlimiter and Saturated INTELSAT V type HPA. In this thesis we assume that the carrier and the symbol timing recovery circuit degradations are negligible and that the channel filters are equalized.

For all different configurations of nonlinear amplifiers (hardlimiter and HPA), the results indicate that TSI-OQPSK modems have a better P_e performance than conventional QPSK, OQPSK and MSK modems when the channel spacing is less than 1.0 times the bit rate ($\Delta f.T_b \leq 1$).

In Chapter Five two different types of TSI pulse shape encoders, called Nonlinear Switching Filter (NLSF) and Pulse Overlapping, are presented. The complete design of a

TSI-OQPSK n = 1 modem is also described. Our measurement results indicate an approximately 1 dB variation from our computer simulated results. These differences are caused by hardware - imperfections and the type of filter in use.

CHAPTER TWO

TWO SYMBOL INTERVAL OFFSET-QUADRATURE-PHASE-SHIFT-KEYED (TSI-OQPSK) MODEMS

In a conventional Quadrature-Phase-Shift-Keyed (QPSK) system, saturated high power amplifiers (HPA) restore the spectral sidelobes of the filtered and modulated signal [3-6, 19-20, 37-38]. Two parameters which have a significant affect on the restoration of the spectral sidelobes (in a nonlinearly amplified channel) are envelope fluctuation and phase transitions. The regenerated spectral sidelobes, resulting from AM to AM and AM to PM conversion in nonlinear amplifiers, introduce adjacent channel interference and degrade the probability of error performance of the system.

In this chapter a generalized Class of Two-Symbol-Interval (TSI) pulse shapes constructed from sinusoidal waveform is introduced. The properties of the modulated TSI signals, using an Offset-Quadrature-Phase-Shift-Keyed (OQPSK) modulator, are analyzed. The results indicate that TSI-OQPSK signals have better PSDs than conventional QPSK, OQPSK and MSK signals in a narrow channel spacing and nonlinearly amplified environment.

2.1 Two-Symbol-Interval Pulse Shapes

Our new class of TSI pulse shapes is defined by

$$s_n(t) = \begin{cases} \frac{1}{2}\left\{1 - \dfrac{\sin\left[\pi/nT_s\left(|t| - T_s/2\right)\right]}{\sin\left(\pi/2n\right)}\right\} & |t| \le T_s \\ 0 & \text{elsewhere} \end{cases} \qquad n = 1, 2 \ldots (2.1)$$

The maximal value of $s_n(t)$ equals one, at $t = 0$, and the minimal value equals zero at $t = \pm T_s$. These values must hold in order to have an intersymbol-interference (ISI) free condition. The amplitudes of $s_n(t)$ at $t = \pm T_s/2$ must be equal to 0.5 in order to have a jitter free condition.

The pulse shapes $s_n(t)$ (as shown in Fig. 2.1) can be separated into a pair of even and odd single interval pulses $s_{en}(t)$ and $s_{on}(t)$ given by

$$s_{en}(t) = \begin{cases} s_n(t-T_s/2) + s_n(t+T_s/2) & |t| \le \dfrac{T_s}{2} \quad \text{even pulse} \\ 0 & \text{elsewhere} \end{cases}$$

$$s_{on}(t) = \begin{cases} s_n(t+T_s/2) - s_n(t-T_s/2) & |t| \le \dfrac{T_s}{2} \quad \text{odd pulse} \\ 0 & \text{elsewhere} \end{cases}$$

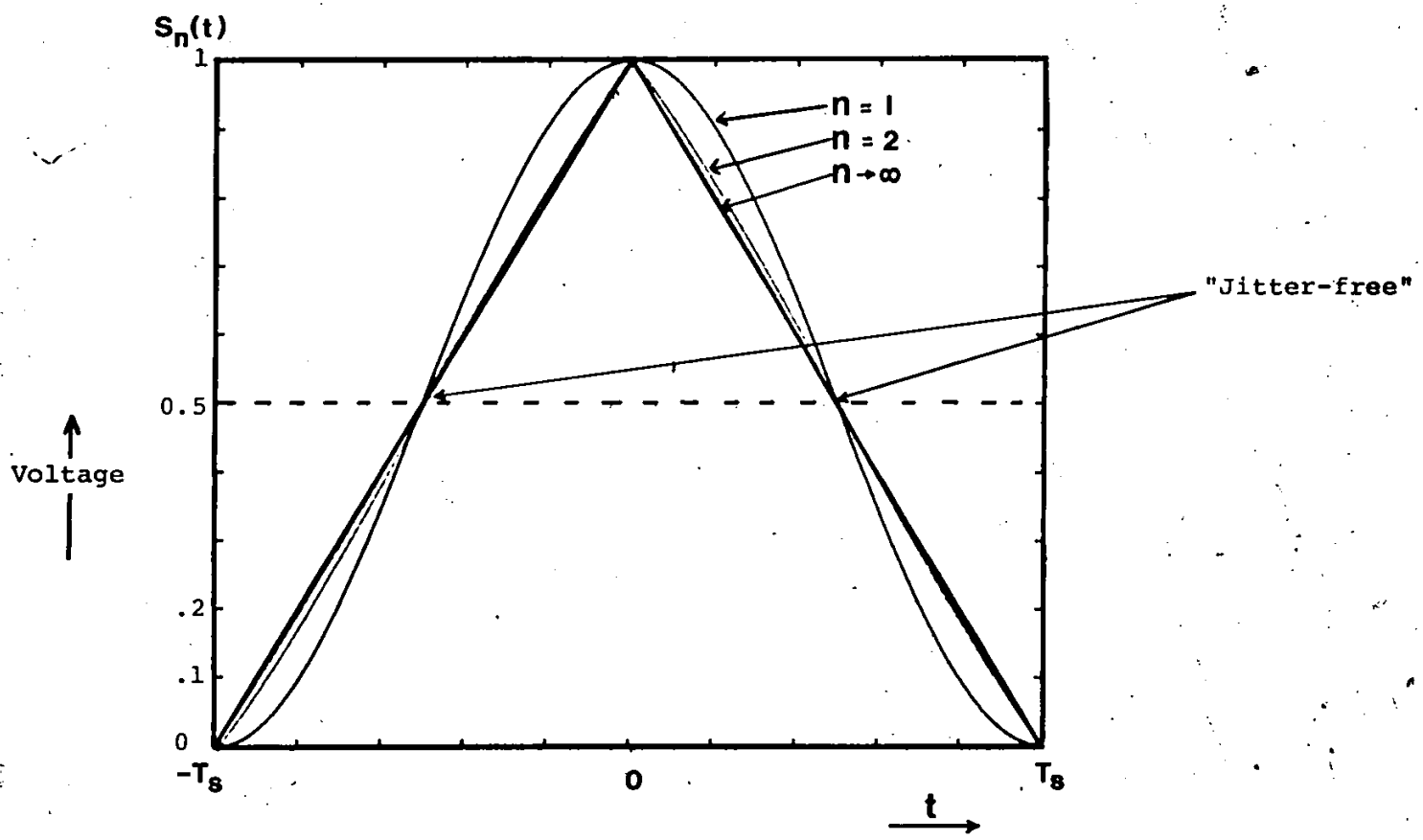

Fig.2.1: Two-symbol-interval pulse shapes $s_n(t)$. These pulse shapes transmitted in a synchronous sequence form the $Y_{In}(t)$ and $Y_{Qn}(t)$ data streams.

Hence, the even and odd functions of $s_n(t)$ given in equation (2.1) can be found as:

$$s_{en}(t) = \begin{cases} 1 & |t| \leq T_s/2 \\ 0 & \text{elsewhere} \end{cases} \qquad (2.2)$$

$$s_{on}(t) = \begin{cases} \dfrac{\sin\left(\frac{\pi t}{nT_s}\right)}{\sin\left(\pi/2n\right)} & |t| \leq T_s/2 \\ 0 & \text{elsewhere} \end{cases}$$

Fig. 2.2 shows the even and odd pulse shapes of $s_n(t)$.

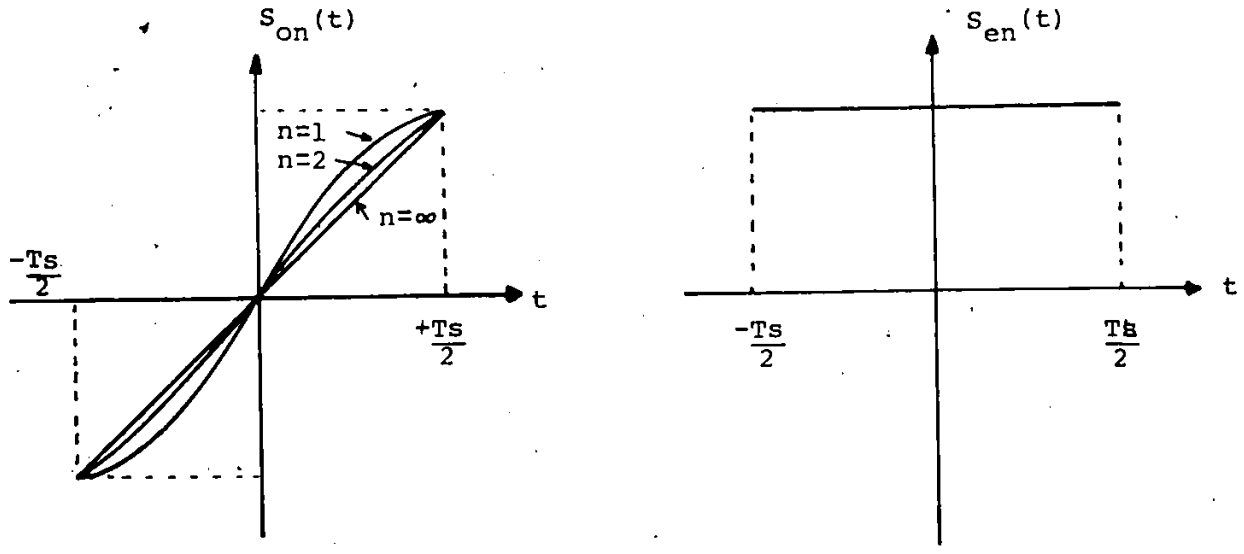

Fig. 2.2 : Even and odd pulse shapes of TSI pulse shapes

The amplitudes of $s_{on}(t)$ are always equal to either +1 or -1 at the transition points ($t = \pm T_s/2$) to eliminate any discontinuity that may occur when the waveforms are generated [7, 9, 14, 15]. For all values of n, the values of $S_{en}(t)$ are the same and equal 1.

2.2 Two-Symbol-Interval Modulator

The block diagram of a TSI-OQPSK modulator is shown in Fig. 2.3. It is similar to that of the conventional premodulation filtered OQPSK modulator [1-5, 23, 36], except that the two low-pass filters are replaced by two TSI encoders. The input binary data stream, x(t), having a bit rate $f_b = \frac{1}{T_b}$, is converted into two Non Return to Zero (NRZ) data streams $x_I(t)$ and $x_Q(t)$. These data streams have symbol durations which are twice the bit duration T_b, that is $T_s = 2T_b$. Both data streams, namely $x_I(t)$ and the delayed data stream $x_Q(t-T_b)$ are fed into two TSI encoders, which convert these streams into the in-phase and quadrature ($y_I(t)$ and $y_Q(t)$) streams of the modulator.

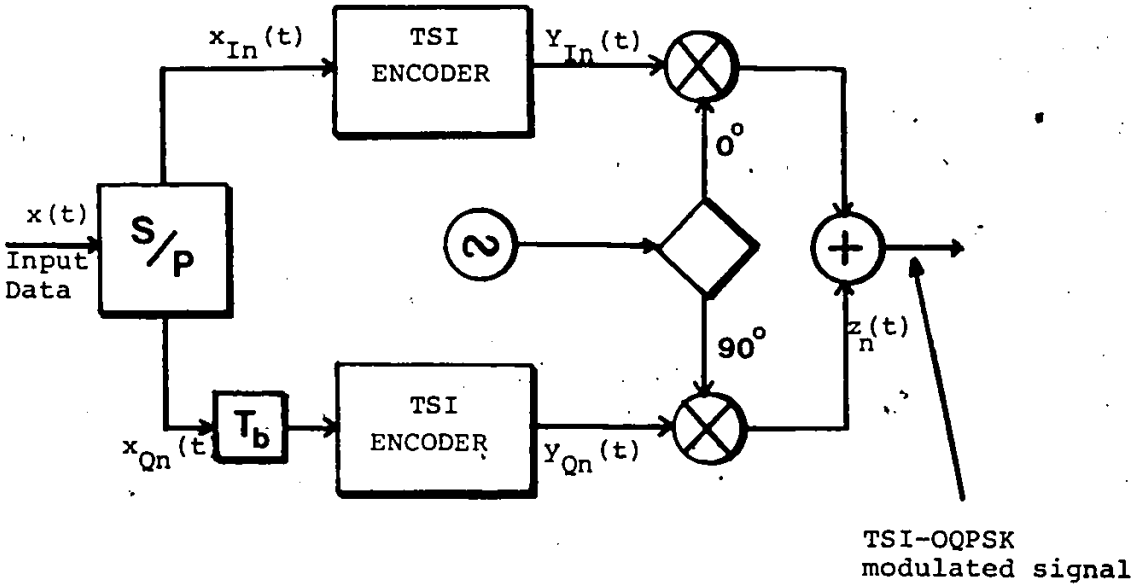

Fig. 2.3: Block diagram of a Two-Symbol-Interval-OQPSK modulator (TSI-OQPSK)

2.2.1 The in-phase and quadrature TSI signals

The equation of the input binary data stream x(t) (Fig. 2.3) can be defined as:

$$x(t) = \sum_{k=-\infty}^{+\infty} x_k g(t-kT_b) \qquad (2.3)$$

(x_k is a random variable number)

where $x_k = \pm A$, with the probability of $x_k = +A$ is equal to the probability of $x_k = -A$ and equal to 0.5. "A" is a constant and equal to the input signal level.

$$g(t-kT_b) = \begin{cases} 1, & |t-kT_b| \leq T_b/2 \\ 0, & |t-kT_b| \geq T_b/2 \end{cases} \qquad (2.4)$$

From the previous definitions of the in-phase $x_I(t)$ and the quadrature $x_Q(t)$ streams, the equations of $x_I(t)$ and $x_Q(t)$ are:

$$x_I(t) = \sum_{i=-\infty}^{+\infty} x_i g(t-iT_b) \qquad (2.5)$$

$i = 1, 3, 5, \ldots$.odd values

$$x_Q(t) = \sum_{j=-\infty}^{+\infty} x_j g(t-jT_b) \qquad (2.6)$$

$j = 0, 2, 4, \ldots$.even values

Note that $x_I(t)$ equals the odd binary stream of $x(t)$ and $x_Q(t)$ equals the even binary stream of $x(t)$.

The T_b delayed data stream of $x_Q(t)$ can be found as:

$$x_Q(t-T_b) = \sum_{j=-\infty}^{+\infty} x_j g\{t-(j+1)T_b\} \qquad j = 0,2,4,\ldots\text{even values}$$

From the definition of $x_Q(t-T_b)$, we can see that the data stream $x_I(t)$ is offset by T_b from the $x_Q(t-T_b)$ data stream. This condition implies that the maximum (or minimum) amplitudes of one filtered data stream ($x_I(t)$ or $x_Q(t-T_b)$) occur at the instant where the other filtered data stream has a transition.

The encoded $y_{In}(t)$ and $y_{Qn}(t)$ streams, indicated in Fig. 2.3, represent synchronous streams of the in-phase and quadrature phase two-symbol interval $s_n(t)$ pulses. The equations of $y_{In}(t)$ and $y_{Qn}(t)$ are found as

$$y_{In}(t) = T_n\{x_I(t)\} \qquad (2.7)$$

$$y_{Qn}(t) = T_n\{x_Q(t-T_b)\}$$

where T_n is the n-typed TSI pulse shape transform and defined by

$$T_n \left\{ \sum_{k=-\infty}^{\infty} x_k g(t-kT_s) \right\} = \sum_{k=-\infty}^{\infty} y_{nk}(t)$$

and

$$y_{nk}(t) = \begin{cases} s_{en}(t-kT_s), \text{ if } x_k = x_{k-1} = +A \\ -s_{en}(t-kT_s), \text{ if } x_k = x_{k-1} = -A \\ s_{on}(t-kT_s), \text{ if } x_k = +A \text{ and } x_{k-1} = -A \\ -s_{on}(t-kT_s), \text{ if } x_k = -A \text{ and } x_{k-1} = +A \end{cases} \quad (2.8)$$

Note that x_k and x_{k-1} are the two consecutive symbols of the in-phase $x_I(t)$ or the quadrature $x_Q(t-T_b)$ data streams.

Figure 2.4 shows the computer generated-signal-eye-diagrams for n = 1, 2, 3 and $n \rightarrow \infty$ at the output of the TSI encoders . These eye diagrams exhibit neither jitter nor intersymbol-interference. Measured signal eye diagrams for n = 1, n = 2 and $n \rightarrow \infty$ are shown in Fig. 2.5. (The input signal of our hardware or computer simulated TSI encoders is a pseudo random data with symbol duration T_s).

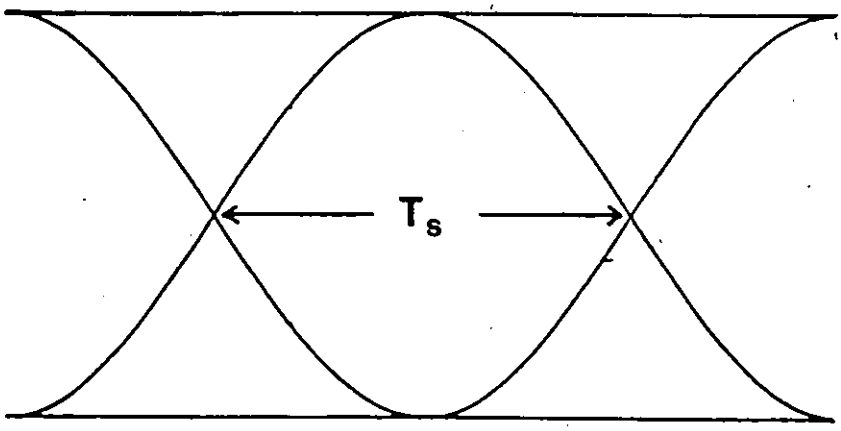

a/ n = 1

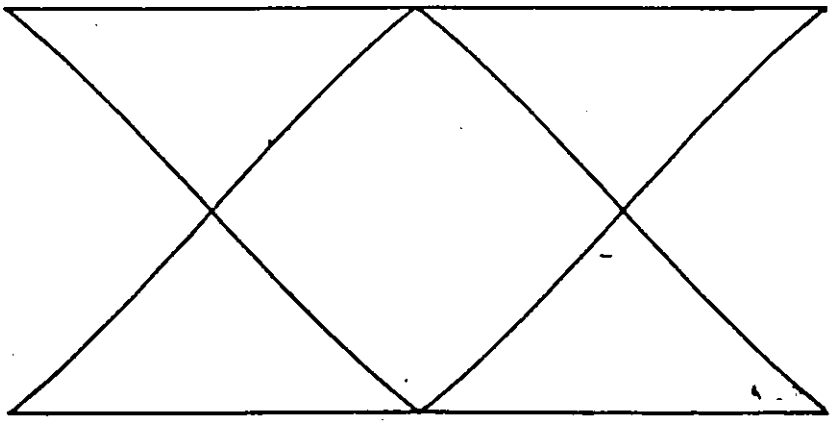

b/ n = 2

Fig.2.4 : Signal eye diagrams generated by TSI encoders

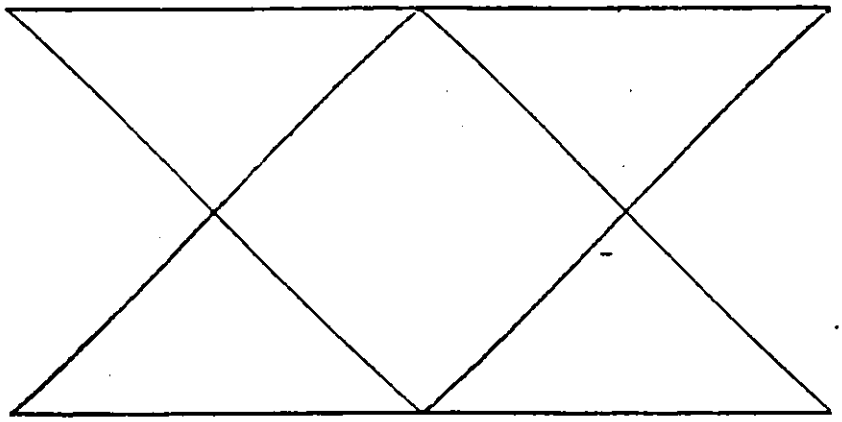

c/ n = 3

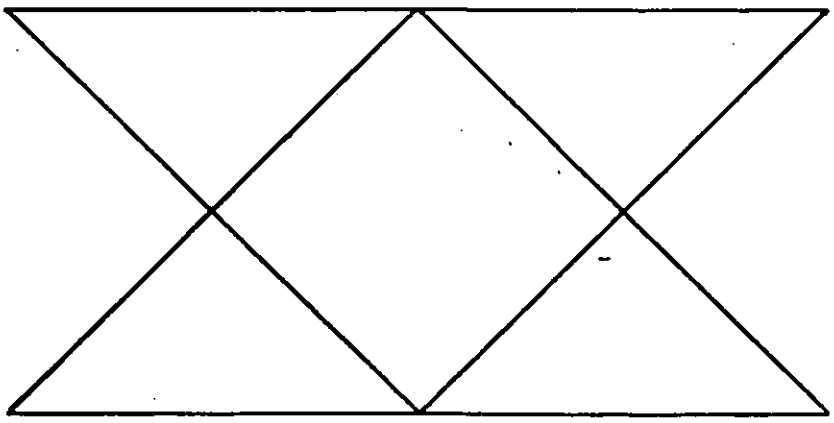

d/ n ⟶ ∞

Fig. 2.4: Signal eye diagrams generated by TSI encoders

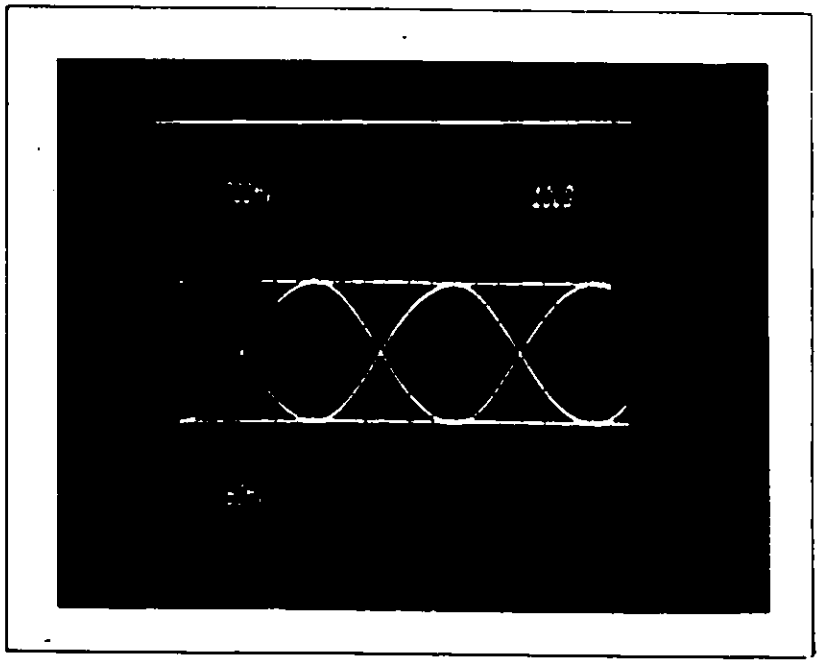

vert: 200mv/div

horiz: 10us/div

symbol rate: 32 kb/s

Fig. 2.5a Measured signal eye diagram at the output of the TSI- encoder (n = 1)

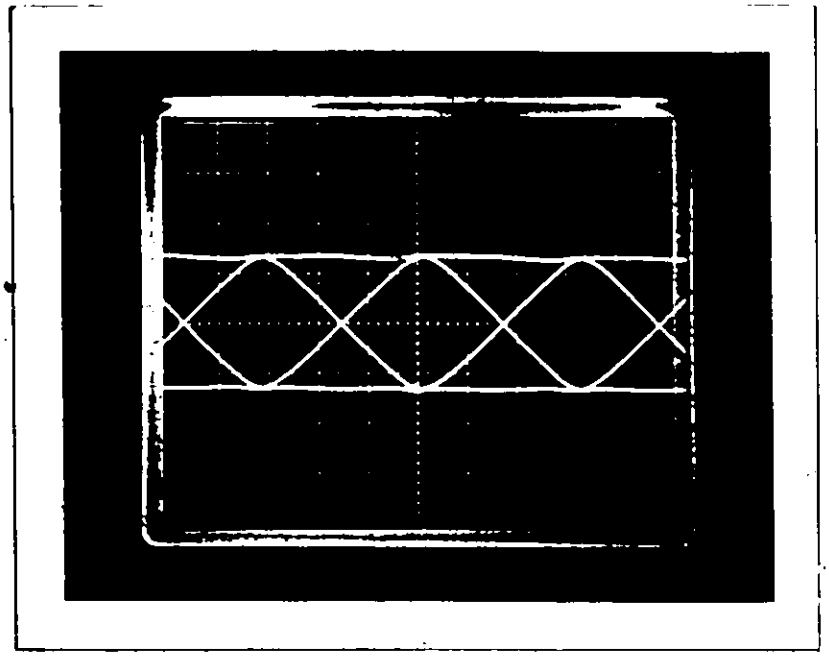

vert: 200mv/div

horiz: 10us/div

symbol rate: 32 kb/s

Fig. 2.5b Measured signal eye diagram at the output of the TSI encoder (n = 2)

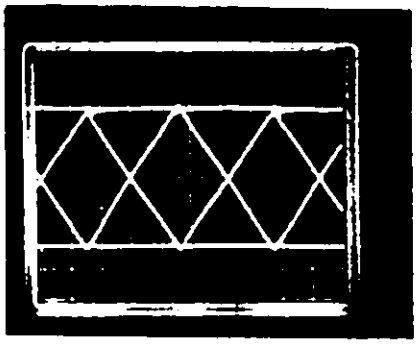

vert: 200mv/div

noriz: 10us/div

symbol rate: 32 kb/s

Fig. 2.5c Measured signal eye diagram at the output of the TSI encoder ($n \to \infty$)

(Courtesy of Dr. J. Huang, Aydin, CA)

Note that the signal eye diagrams are almost the same when n is greater than 2. In the following sections we will show that the PSDs of TSI-OQPSK signals for $n \geq 2$ have practically the same main lobe.

2.2.2 Power Spectral Density of TSI Signals

In order to derive the PSDs of TSI signals and simplify our equations, let us define

$$\begin{aligned} s_1(t-kT_s) &= s_{en}(t-kT_s) \\ s_2(t-kT_s) &= -s_{en}(t-kT_s) \\ s_3(t-kT_s) &= s_{on}(t-kT_s) \\ s_4(t-kT_s) &= -s_{on}(t-kT_s) \end{aligned} \tag{2.9}$$

Then for every T_s, seconds, the (TSI) encoder shown in Fig. 2.3, transmits an elementary signal $Y_{nk}(t)$ from the set of 4 basic signals $\{ s_1(t-kT_s), s_2(t-kT_s), s_3(t-kT_s), s_4(t-kT_s) \}$, determined by the previous elementary signals $Y_{n(k-1)}(t)$ and present input x_k. Therefore, the TSI signal encoder can be statistically represented by a 4-state Markov chain [21] as shown in Fig. 2.6. The encoded signal for a specified value of n called y(t) has a set of stationary probabilities.

$$\{ p_i,\ i = 1,\ 2,\ 3,\ 4 \}$$

and a set of transition probabilities

(a) Transition diagram of y(t)

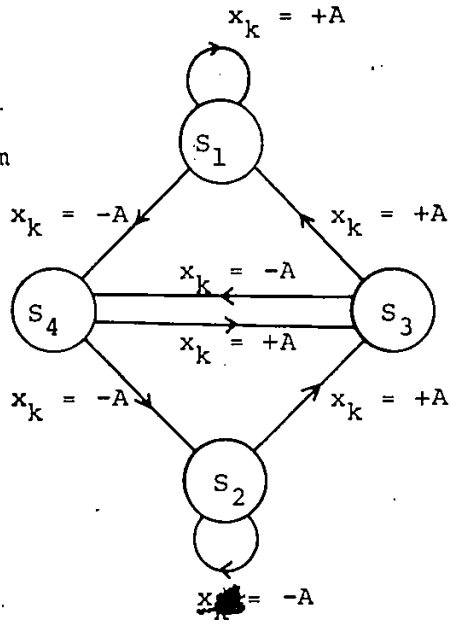

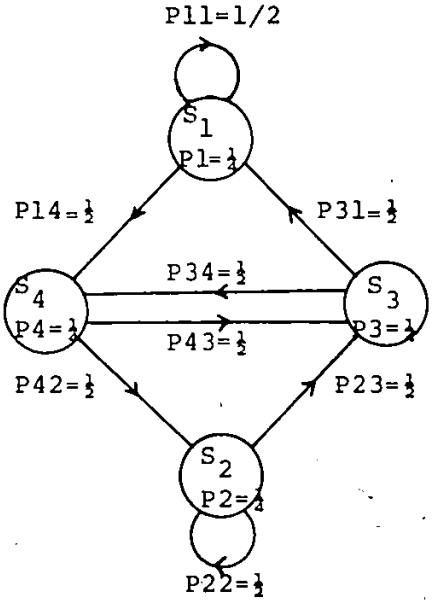

(b) 4-state Markov chain model of the TSI signal encoder

Fig. 2.6 4-state Markov chain representation of the TSI signal encoding

$$\{ p_{ij},\ i, j = 1, 2, 3, 4 \}$$

where the states are the basic signals s_i, $i = 1, 2, 3, 4$ and the stationary and transition probabilities are defined as

$$p_i = P\{y_k(t) = s_i\ (t-kT_s)\}$$

$$p_{ij} = P\{y_k(t) = s_j(t-kT_s) \mid y_{k-1}(t) = s_i\ (t-(k-1)T_s)\}$$

for $i, j = 1, 2, 3, 4$

Based on Eq. 2.8 and 2.9, it can be shown that

$$p_1 = P\{y_k(t) = s_1(t-kT_s)\} = P\{x_k = +A,\ x_{k-1} = -A\}$$

$$= P\{x_k = +A\} \cdot P\{x_{k-1} = -A\} = 1/4$$

since x_k and x_{k-1} are statistically independent Other p_i's, $i = 1, 2, 3, 4$ can be obtained in the similar manner and

$$p_i = 1/4 \text{ for } i = 1, 2, 3, 4,$$

From an examination of Fig. 2.6a, it follows that

$$p_{11} = P\left\{ y_k(t) = s_1(t-kT_s) \;/\; y_{k-1}(t) = s_1(t-(k-1)T_s) \right\}$$

$$= P\left\{ x_k = +A \;/\; y_{k-1}(t) = s_1(t-(k-1)T_s) \right\}$$

$$= P\left\{ x_k = +A \right\} = 1/2$$

Since x_k and $y_{k-1}(t)$ are statistically independent,

$$p_{12} = P\left\{ y_k(t) = s_2(t-kT_s) \;/\; y_{k-1}(t) = s_1(t-(k-1)T_s) \right\}$$

$$= 0$$

Since there is no transition from s_1 to s_2 (Fig. 2.6a). Similarly, other p_{ij}'s can be obtained. They are arranged as entries of the transition matrix P,

$$P = \begin{bmatrix} p_{11} & p_{12} & p_{13} & p_{14} \\ p_{21} & p_{22} & p_{23} & p_{24} \\ p_{31} & p_{32} & p_{33} & p_{34} \\ p_{41} & p_{42} & p_{43} & p_{44} \end{bmatrix} = \frac{1}{2} \begin{bmatrix} 1 & 0 & 0 & 1 \\ 0 & 1 & 1 & 0 \\ 1 & 0 & 0 & 1 \\ 0 & 1 & 1 & 0 \end{bmatrix}$$

From this statistical description, the power spectral density (PSD) of the encoded signal y(t) is given by [22, 51]

$$Y(f) = \frac{1}{T_s^2} \sum_{n=-\infty}^{+\infty} \left| \sum_{i=1}^{4} p_i S_i\left(\frac{n}{T_s}\right) \right|^2 \delta\left(f - \frac{n}{T_s}\right)$$

$$+ \frac{1}{T_s} \sum_{i=1}^{4} p_i \left| S_i(f) \right|^2 - \frac{1}{T_s} \left| \sum_{i=1}^{4} p_i S_i(f) \right|^2$$

$$+ \frac{2}{T_s} \operatorname{Re}\left\{ \sum_{i=1}^{4} \sum_{k=1}^{4} p_i S_i^*(f)\, S_k(f)\, S_{ik} \right\} \qquad (2.10)$$

where

$S_i(f)$ is the Fourier transform of $s_i(t)$,

$S^*_i(f)$ is the complex conjugate of $S_i(f)$

$$S_{ij} = \sum_{n=1}^{\infty} p_{ij}^{(n)}\, e^{-j2\pi n f T_s}$$

$p_{ij}^{(n)}$ is the ij^{th} entry of the n-step transition matrix P^n.

$\delta(f)$ is the Dirac delta function

$$P^n = P \times P \times P \times \ldots \times P$$

n times

and

Re $\{\ldots\}$ is the real part of $\{\ldots\}$

From the derivation in Appendix I.1 the PSD of y(t) is represented by

$$Y(f) = \frac{1}{T_s} \left(S_e(f) \cos \pi f T_s + j S_o(f) \sin \pi f T_s\right)^2 \qquad (2.11)$$

where $S_e(f)$ and $S_o(f)$ are the Fourier transforms of $s_e(t)$ and $s_o(t)$ respectively.

From equation (2.2), the Fourier transforms of $s_{en}(t)$ and $s_{on}(t)$ are found to be: (details are shown in Appendix I.2).

$$S_{en}(f) = \frac{\sin(\pi f T_s)}{\pi f} \tag{2.12}$$

$$S_{on}(f) = \frac{jnT_s}{\sin(\frac{\pi}{2n})} \left\{ \frac{\sin(\pi f T_s + \frac{\pi}{2n})}{(1+2nfT_s)} + \frac{\sin(\pi f T_s - \frac{\pi}{2n})}{(1-2nfT_s)} \right\} \tag{2.13}$$

Hence

$$y_n(f) = \left| \frac{\sin(2\pi f T_s)}{2\pi f T_s} - \frac{n\sin(\pi f T_s)}{\sin(\frac{\pi}{2n})} \times \left\{ \frac{\sin(\pi f T_s + \frac{\pi}{2n})}{(1+2nfT_s)} + \frac{\sin(\pi f T_s - \frac{\pi}{2n})}{(1-2nfT_s)} \right\} \right| \tag{2.14}$$

Figure 2.7 shows the computer generated PSDs of TSI signals for $n = 1, 2, 3$, and $n \to \infty$. These PSDs exhibit sharper mainlobes and lower sidelobes than those of NRZ (Non Return to Zero) signals. The measured PSDs of TSI signals for $n = 1$ and $n \to \infty$ are also obtained and shown in Fig. 2.8. These measured results are in close agreement with our computer simulated results and can be served as an experimental confirmation of our theoretical results.

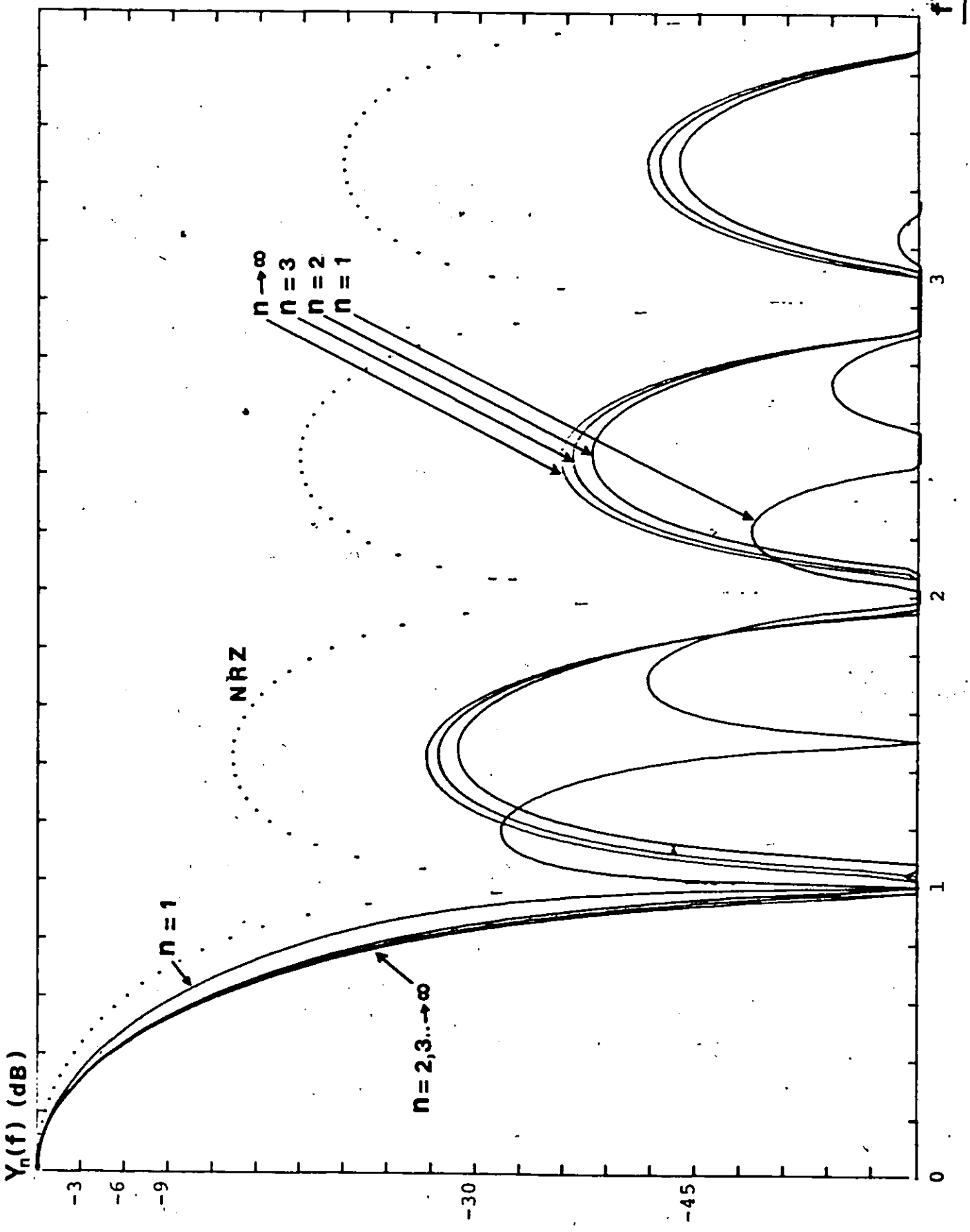

Fig2.7 : Power spectral density of TSI signals

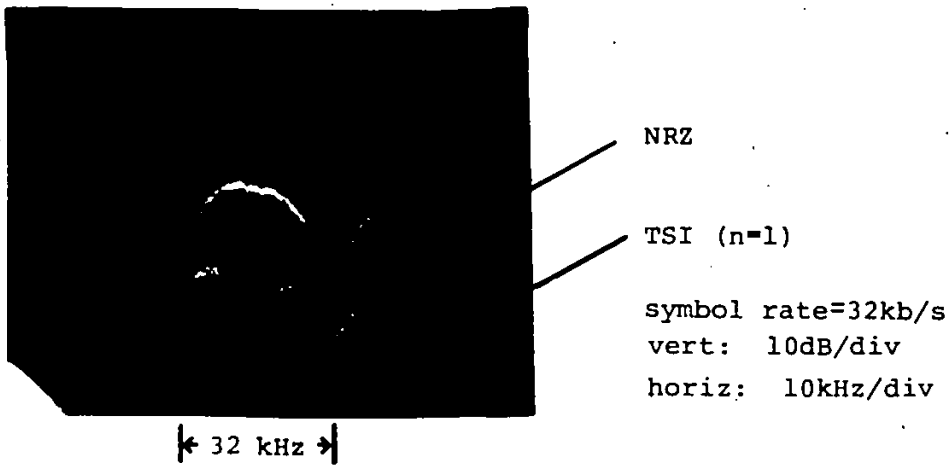

Fig 2.8a Measured PSD of NRZ and TSI (n=1) signals (Measurements performed on our hardware prototypes)

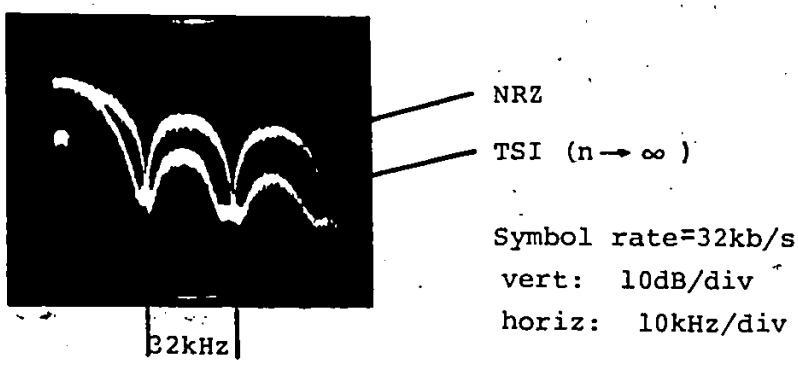

Fig 2.8b Measured PSD of NRZ and TSI (n → ∞) signals (Courtesy of Dr. J. Huang, Aydin, CA)

2.2.3 The Modulated TSI-OQPSK Signal

The modulated TSI-OQPSK signal at the output of the modulator (Fig. 2.3) is expressed as:

$$z_n(t) = y_{In}(t)\cos(w_c t) + y_{Qn}(t)\sin(w_c t) \qquad (2.15)$$

where $w_c = 2\pi f_c$ and f_c is the carrier frequency. Since both the PSD functions of $y_{In}(t)$ and $y_{Qn}(t)$ are equal to $Y_n(f)$, the combined normalized PSD of the TSI-OQPSK signal is

$$Z_n(f) = Y_n(f-f_c) \qquad (2.16)$$

We note that Austin [15, 35], Foster [16] and Divsalar [17], use the term staggered *Quadrature-Overlapped-Raised-Cosine Modulation* (SQORC) for the specific case of n=1. Thus SQORC modulation is a *subclass* of our more general TSI-OQPSK modulation techniques [26, 27, 47].

The modulted TSI-OQPSK signal at the output of the modulator can also be written as:

$$z_n(t) = A_n(t)\cos[w_c t + \phi_n(t)] \qquad (2.17)$$

where

$A_n(t)$ and $\phi_n(t)$ represent the envelope and phase of the modulated signals. The equations of $A_n(t)$ and $\phi_n(t)$ are as follows:

$$A_n(t) = [y_{In}(t)^2 + y_{Qn}(t)^2]^{\frac{1}{2}} \qquad (2.18)$$

and

$$\phi_n(t) = -\tan^{-1}\left\{\frac{y_{Qn}(t)}{y_{In}(t)}\right\} \mod \pi \qquad (2.19)$$

The maximum value of $A_n(t)$ is obtained when both the in-phase and quadrature channels ($y_{In}(t)$ and $y_{Qn}(t)$) of TSI-OQPSK signals equal 1. The maximum envelope-amplitudes of TSI-OQPSK signals for different values of n are the same and equal to $\sqrt{2}$.

The minimum envelope amplitudes of $A_n(t)$ are obtained during the time intervals when $y_{In}(t)$ and $y_{Qn}(t)$ of TSI-OQPSK signals are either $s_{on}(t)$ or $-s_{on}(t)$, for $0 \leq t \leq T_s/2$. From equation (2.18) and (2.2), the minimum envelope amplitude of the modulated TSI-OQPSK signals is the minimum of the following equation:

$$[C^2\sin^2(\frac{\pi t}{nT_s}) + C^2\sin^2((\frac{\pi t}{nT_s}) + \frac{\pi}{2n})]^{\frac{1}{2}} \qquad (2.20)$$

where $C = 1/\sin(\frac{\pi}{2n})$ & $0 \leq t \leq \frac{T_s}{2}$

By equating the first derivative of (2.20) to zero, we obtain the minimum value at $t = \frac{T_s}{4}$. Hence, the minimum envelope amplitude of TSI-OQPSK signals is

$$\frac{1}{\sin(\frac{\pi}{2n})} \times (2\sin^2\frac{\pi}{4n}).$$

Table 1 shows the computed maximum and minimum envelope fluctuations of TSI-OQPSK signals for $n = 1, 2, 3$ and $n \to \infty$. Phase transitions of TSI-OQPSK signals are also computed and shown in Fig. 2.9. We note that the phase paths of TSI-OQPSK signals for all values of n are smoother and shorter than those of MSK signals. The computed signal space constellations of TSI-OQPSK signals for $n = 1, 2, \to \infty$ are shown in Fig. 2.10a. The measured signal space constellation for n = 1 is in close agreement with the computer simulated result, shown in Fig. 2.10b.

n	Amplitude Maximum	Amplitude Minimum	Max Amplitude / Min Amplitude (dB)
1	1.4142	1	3.0
2	1.4142	.7653.	5.33
3	1.4142	.7320	5.72
$\rightarrow\infty$	1.4142	.7071	6.0

Table 1: Computed envelope fluctuations of TSI-OQPSK signals

Note that the TSI-OQPSK signal having the n=2 pulse shape , defined in equation(2.1), has an envelope fluctuation of 5.33 dB. Later in Fig. 2.14, we show that this signal has the sharpest mainlobe in a saturated channel.

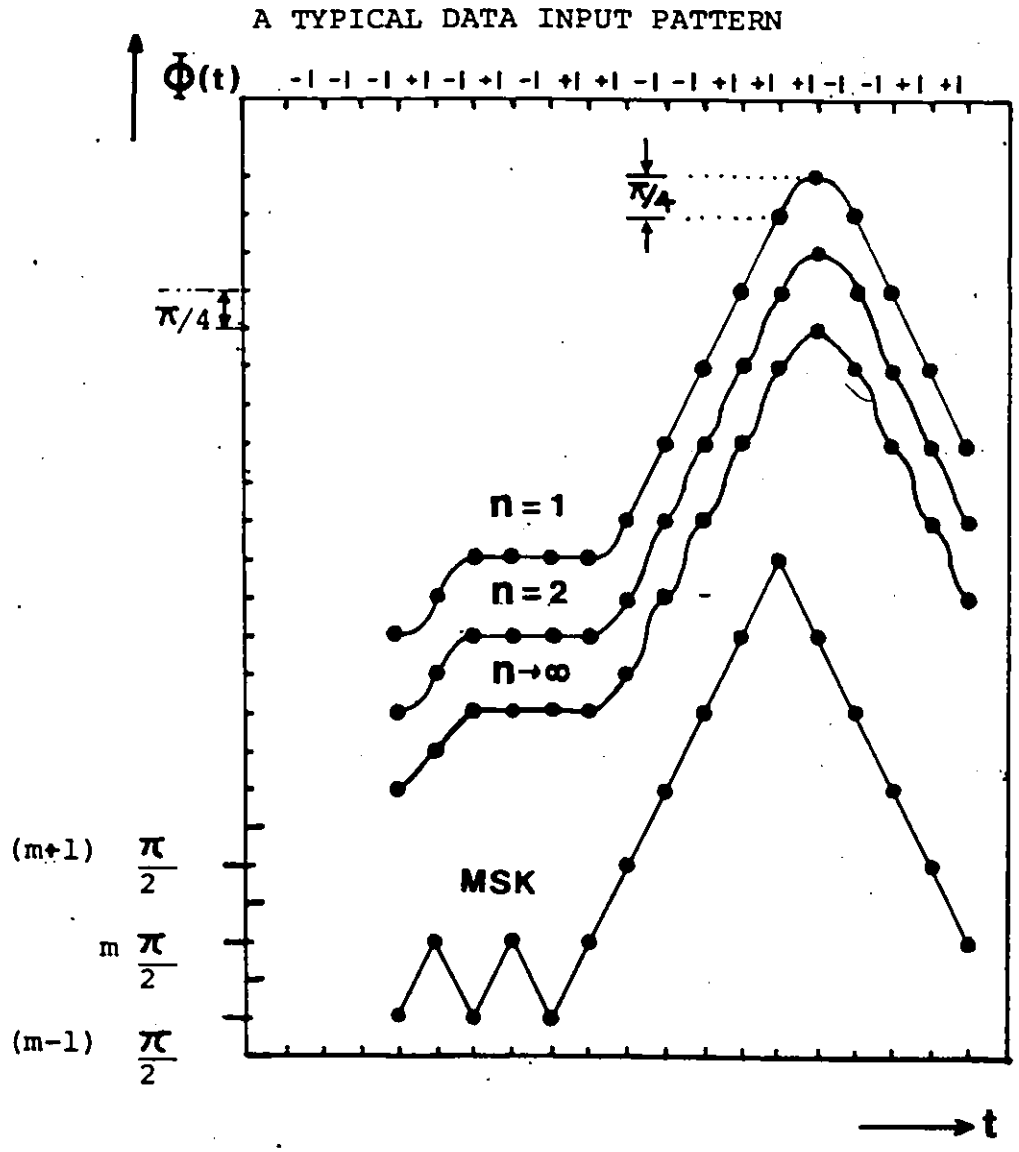

Fig. 2.9 : Phase transitions of TSI-OQPSK and MSK signals

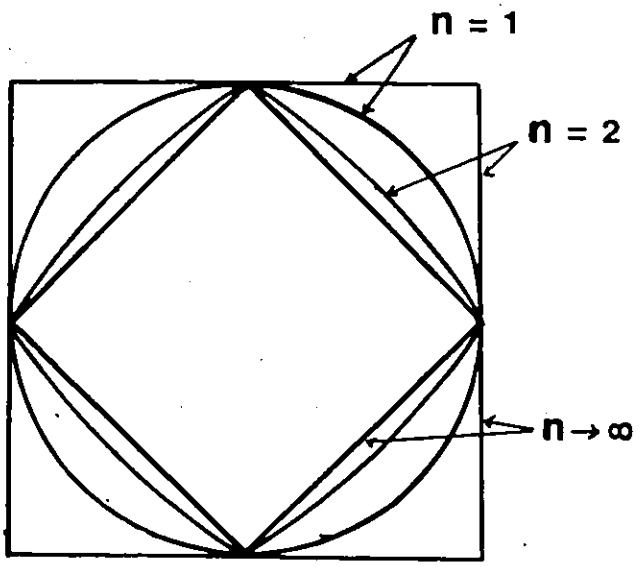

Fig 2.10a: Computed constellation diagram of TSI-OQPSK signals for different values of n

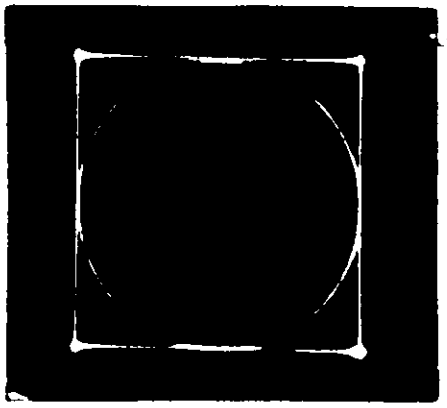

Fig. 2.10b: Measured constellation diagram of TSI-OQPSK signals for n = 1

2.3 Properties of TSI-OQPSK Signals in a Nonlinearly Amplified Channel

To maximize power efficiency, the HPA used in a transmitter typically operates in a saturated mode. In this section, we are going to examine the properties of TSI-OQPSK signals in a saturated INTELSAT V type HPA [10] and hard-limited channel.

2.3.1 Hardlimited Channel

In this seciton, a saturated HPA is modeled as an ideal hardlimiter to examine the effect of AM to AM conversion on the modulated signal. The hard-limited model has been shown to be a good first order approximation of typical earth station satellite transponder HPA's and terrestrial microwave amplifiers [4]. Fig. 2.11 shows the phase and amplitudes responses of an ideal hardlimiter. The hardlimited TSI-OQPSK signals, $z^1_n(t)$, of different pulse shapes described in equation (2.1), can be represented by:

$$z^1_n(t) = y^1_{In}(t)\cos(2\pi f_c t) + y^1_{Qn}(t) j \sin(2\pi f_c t) \qquad (2.21)$$

$$\text{where } y^1_{In}(t) = \frac{C\, Y_{In}(t)}{(y^2_{In}(t) + y^2_{Qn}(t))^{1/2}} \qquad (2.22)$$

$$y^1_{Qn}(t) = \frac{C\, Y_{Qn}(t)}{(y^2_{In}(t) + y^2_{Qn}(t))^{1/2}}$$

where c is a constant dependent on the output power of the hardlimiter and f_c is the carrier frequency.

A 16-state Markov chain model can be used to derive the PSDs of $y^1_{In}(t)$ and $y^1_{Qn}(t)$ [9]. Hence the PSD of *hardlimited* TSI-OQPSK signals for a selected pulse shape is:

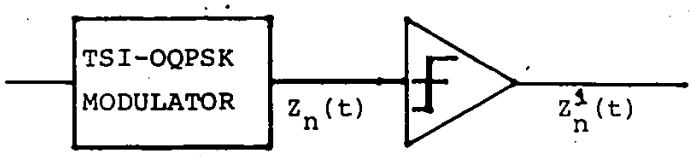

Model to examine hardlimited signals

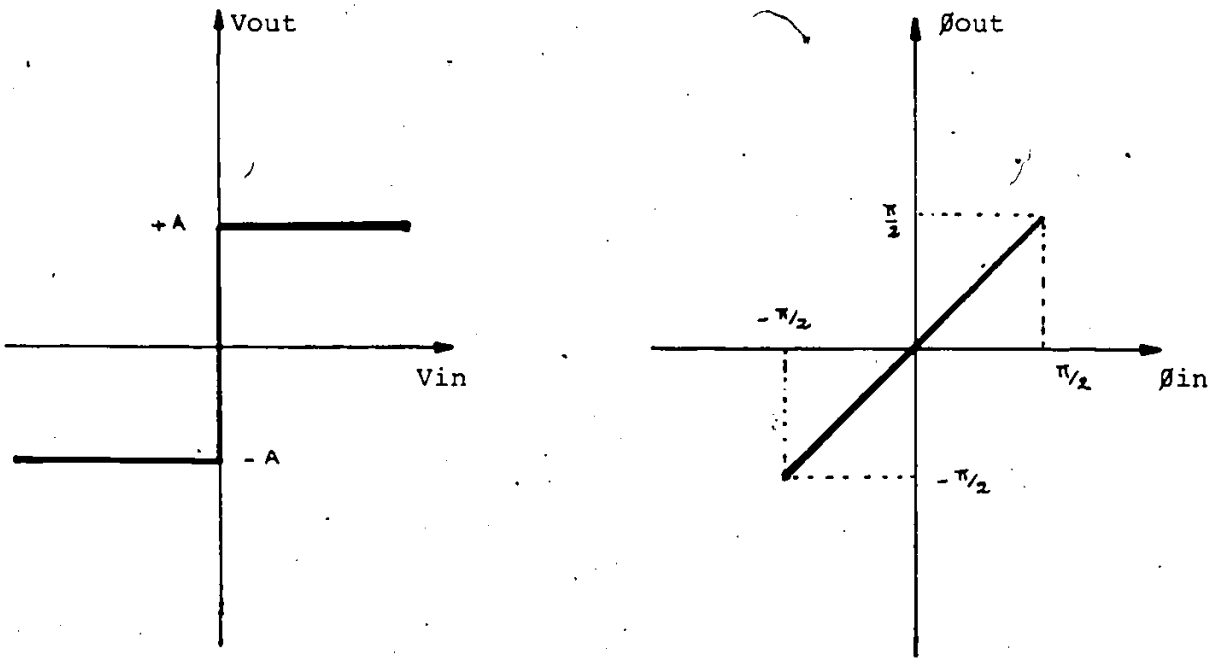

a/ Amplitude response

b/ phase response

Fig. 2.11 Characteristics of an ideal hardlimiter

$$Z^1(f) = \frac{1}{8T_s}\left\{\sum_{i=1}^{8}\left|V_i(f)\right|^2\right\} + \frac{1}{16}R_e\left\{\left\{V_1(f)+V_3(f)+V_5(f)+V_7(f)\right\}*\right.$$

$$X\left\{V_1(f)+V_4(f)-V_5(f)-V_8(f)+(V_2(f)+V_4(f)+V_6(f)+V_8(f))*\right\}$$

$$\left.X\left\{V_2(f)+V_3(f)-V_6(f)-V_7(f)\right\}e^{-j2\pi fT_s}\right\} \qquad (2.23)$$

where Re [....] is the real part of [....], a "*" means conjugation of that complex number, $V_i(f)$ is the Fourier transform of $v_i(t)$ which is given in Appendix I.3.

Using equation (2.23) and Appendix I.3, the PSDs of hardlimited TSI-OQPSK signals for n = 1, 2, 3 and n → ∞ are found and shown in Fig. 2.12. The measured PSD of a TSI-OQPSK signal, for n = 1, after the hardlimiter is shown in Fig. 2.13. It is also in close agreement with the computed result in Fig. 2.12a.

It is interesting to note that the PSDs of hardlimited TSI-OQPSK signals for n ≥ 2 in certain regions fall below those of the individual signal spectra, see Fig. 2.12b - 2.12d. By comparing the PSDs of hardlimited QPSK, OQPSK and TSI-OQPSK signals, Fig 2.14, we can see that the PSDs of hardlimited TSI-OQPSK signals are better than those of the others.

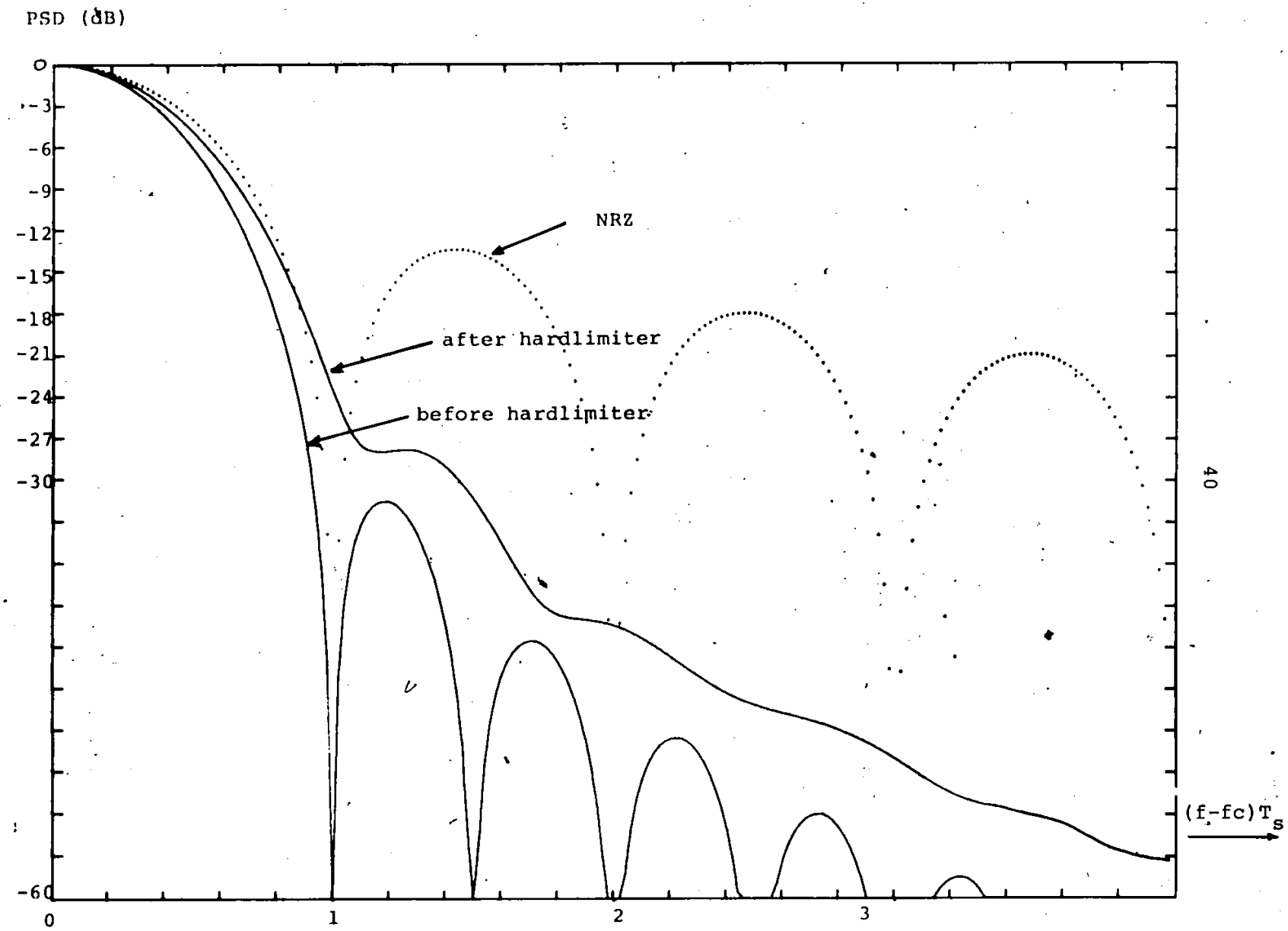

Fig. 2.12a Computer simulated PSDs of hardlimited TSI-OQPSK signal (n = 1)

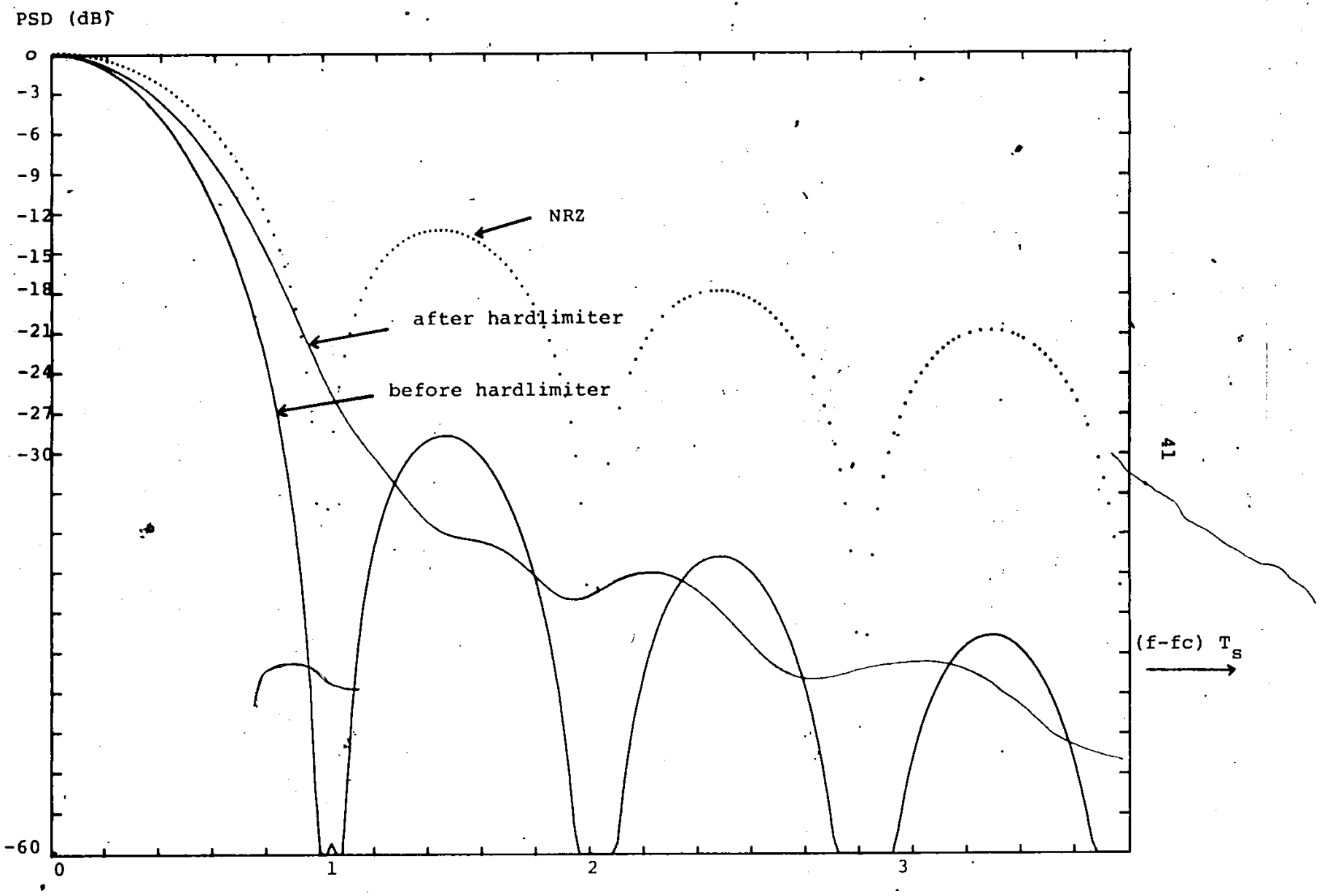

Fig. 2.12b Computer simulated PSDs of hardlimited TSI-OQPSK signal (n= 2)

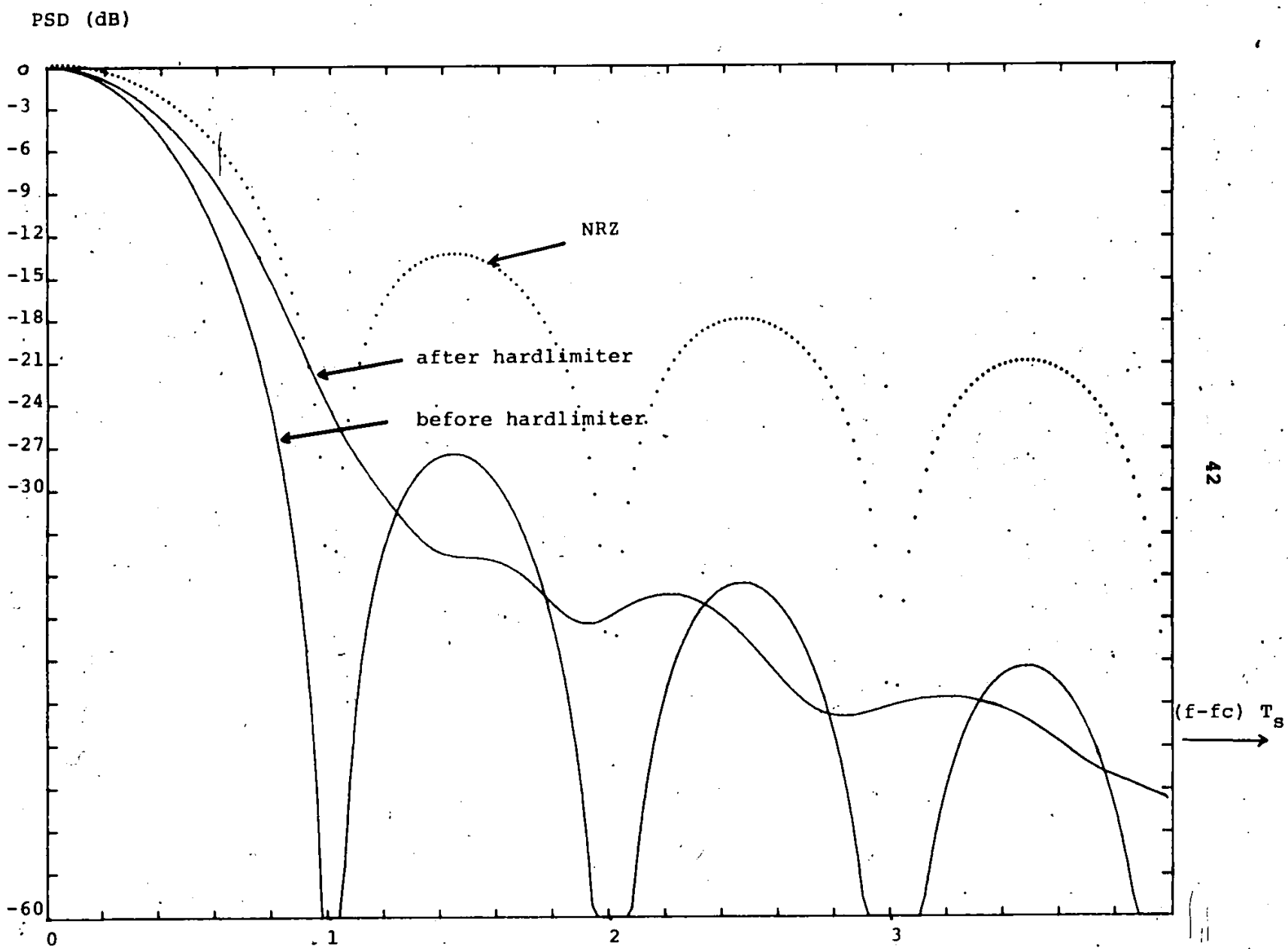

Fig 2.12c Computer simulated PSDs of hardlimited TSI-OQPSK signal (n = 3)

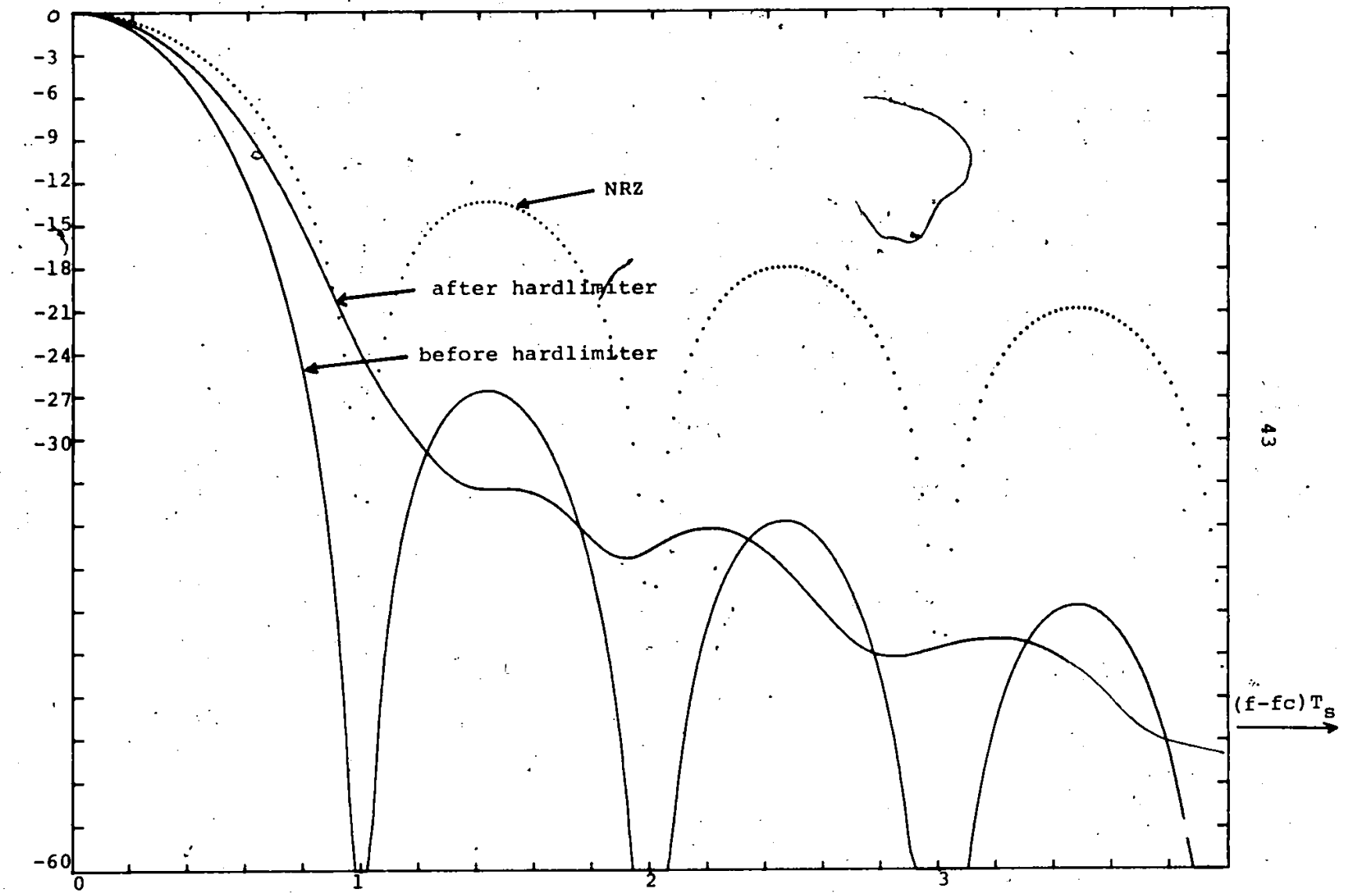

Fig. 2.12d Computer simulated PSDs of hardlimited TSI-OQPSK signal ($n \rightarrow \infty$)

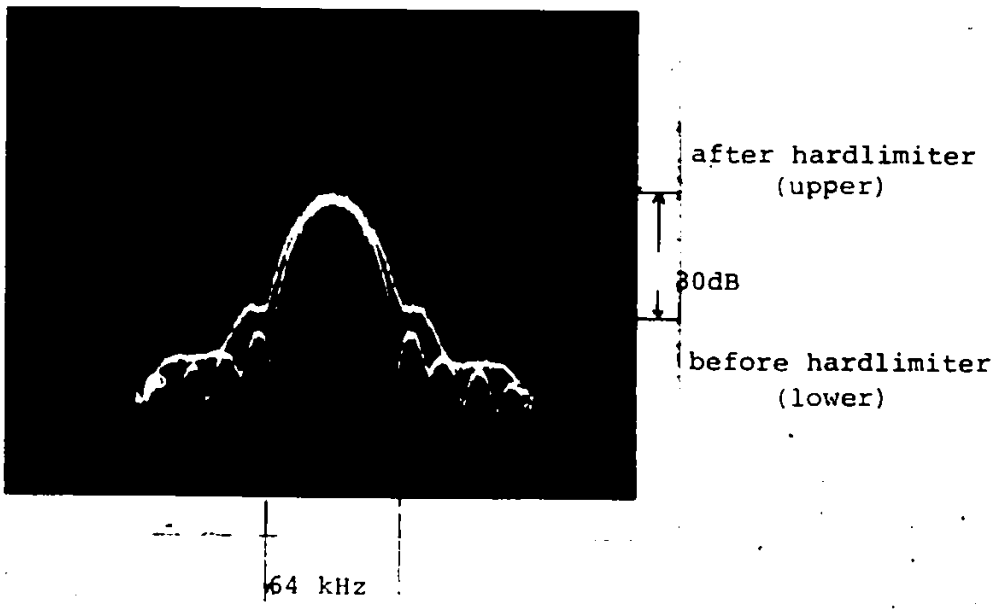

FIG. 2.13 MEASURED PSD OF HARDLIMITED TSI-OQPSK (n = 1)

f_b = 64 kb/s

f_c = 512 kHz

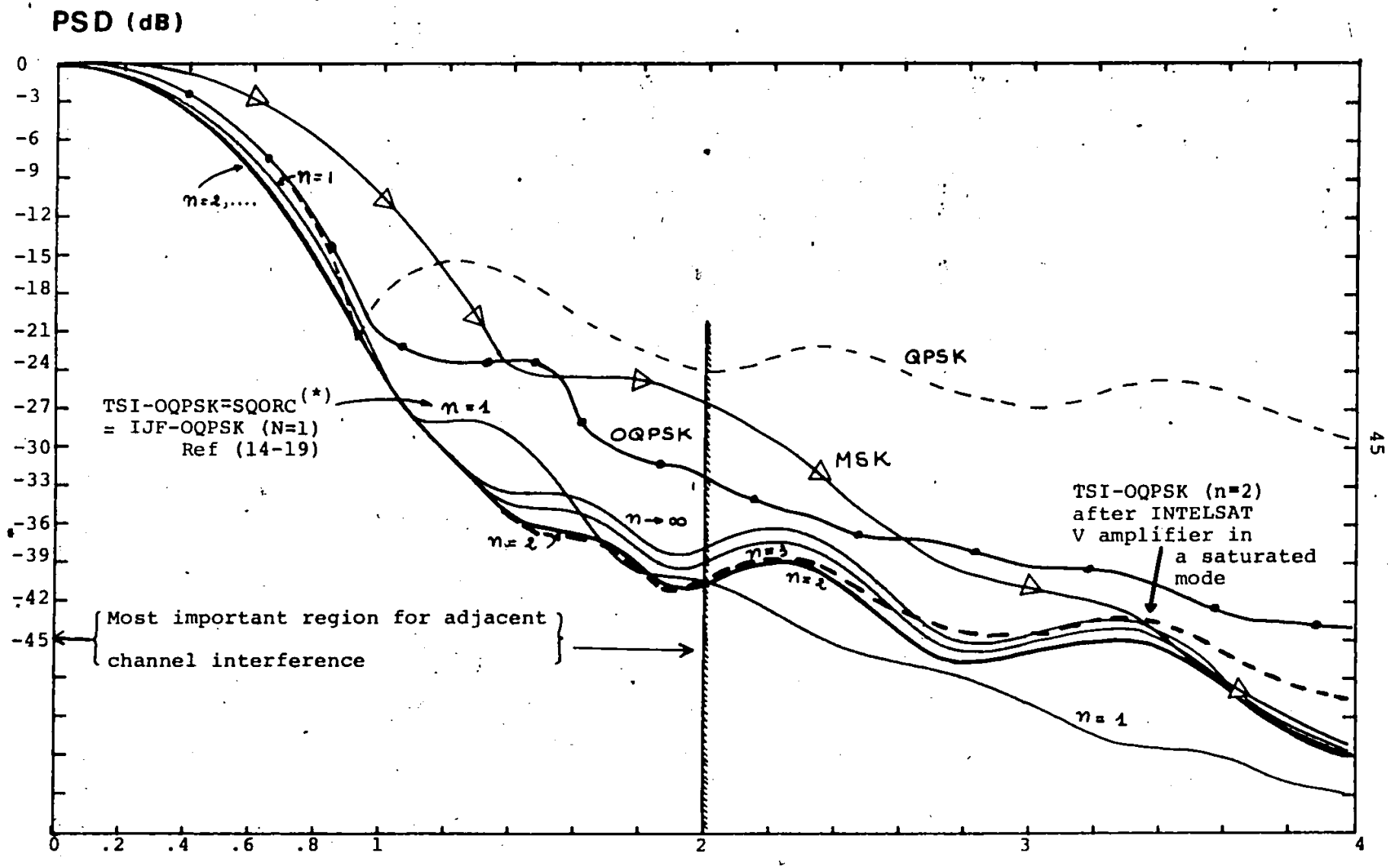

FIG.2.14 POWER SPECTRAL DENSITY (PSD) OF HARDLIMITED MSK, QPSK, OQPSK AND TSI-OQPSK SIGNALS

*NOTE THAT: THE n=1 - TSIOQPSK SIGNAL IS IDENTICAL TO THE N=1 - IJFOQPSK (14) AND TO THE SQORC SIGNALS (15-17)

Examining the characteristics of all the PSDs in Fig. 2.14, it can be shown that the tails of these PSDs fall off gradually and their levels tend to be lower as the distances from the carrier frequency (f_c) increase. As indicated in Chapter One (Fig. 1), the regenerated sidelobes (these tails) caused adjacent channel interference and degraded the P_e performance of the system. The lower level the tails are, the better performance the system is. We also note that in Fig. 2.14, the regenerated sidelobes in the regions of $(f-f_c)T_s \geq 2$ are much lower than those in the regions of $(f-f_c)T_s \leq 1$ (at least 10 dB). Due to these characteristics the regions most affected by adjacent channel interference are within $(f-f_c)T_s \leq 2$. Examining the PSDs of hardlimited TSI-OQPSK signals in this region (Fig. 2.14), the case of $n = 2$ is found to be the best of this class, even though the PSD of the $n=1$ case is the lowest when $(f-f_c)$. $T_s \geq 2$. Further investigation in the next section will show that the performance of the TSI-OQPSK system with $n = 2$ is the best of this class, in a multiple-carrier adjacent channel environment, having a carrier frequency spacing of Δf, where $\Delta f.T_s \leq 1.35$.

Due to the effect of hardlimiting, the envelope of the modulated signals is constant. Therefore, the signal space constellations of hardlimited TSI-OQPSK signals for all values of n are the same and shown in Fig. 2.15a. The measured signal space constellation of TSI-OQPSK signal for $n = 1$ is also shown in Fig. 2.15b.

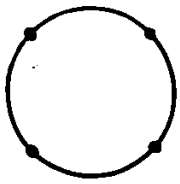

a/ Computer simulated result (for all values of n)

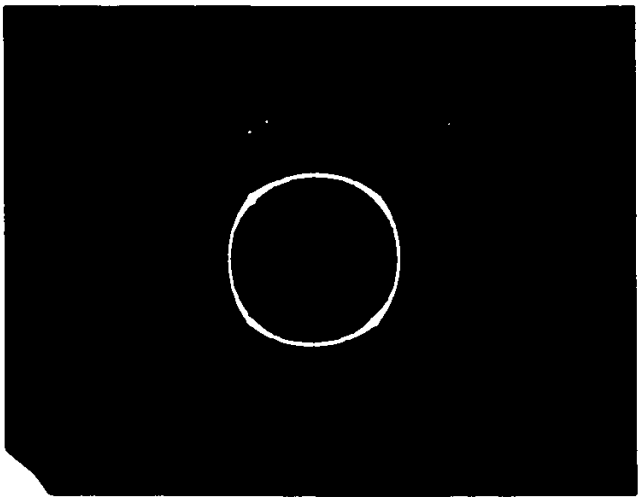

b/ Measured result (n = 1)

Fig. 2.15 Signal Space Constellations of hardlimited TSI-OQPSK Signal

2.3.2 Saturated INTELSAT V Type HPA Channel

In this section, the saturated INTELSAT V type HPA is used as the nonlinear amplifier. An Intelsat earth station transmit type HPA is chosen to be used as our nonlinear amplifier model because of its popularity and its high speed (120 Mb/s) application in the Intelsat network. The AM/AM and AM/PM characteristics of this HPA are obtained from Intelsat Specification [10] and shown in Fig. 2.16. Details of our computer simulated HPA will be discussed in Chapter 4. The computer simulation results show that the power spectral densities of TSI-OQPSK signals, after passing through the saturated HPA operating at 0 dB input backoff, are better than those of QPSK and OQPSK signals (Fig. 2.17). The results also indicate that the spectral regrowths of the TSI-OQPSK signals after the ideal hardlimiter and saturated HPA operating at 0 dB backoff are practically identical. These results confirm that an ideal hardlimiter can be used as a first order approximation of a saturated HPA (operated at 0 dB input back off).

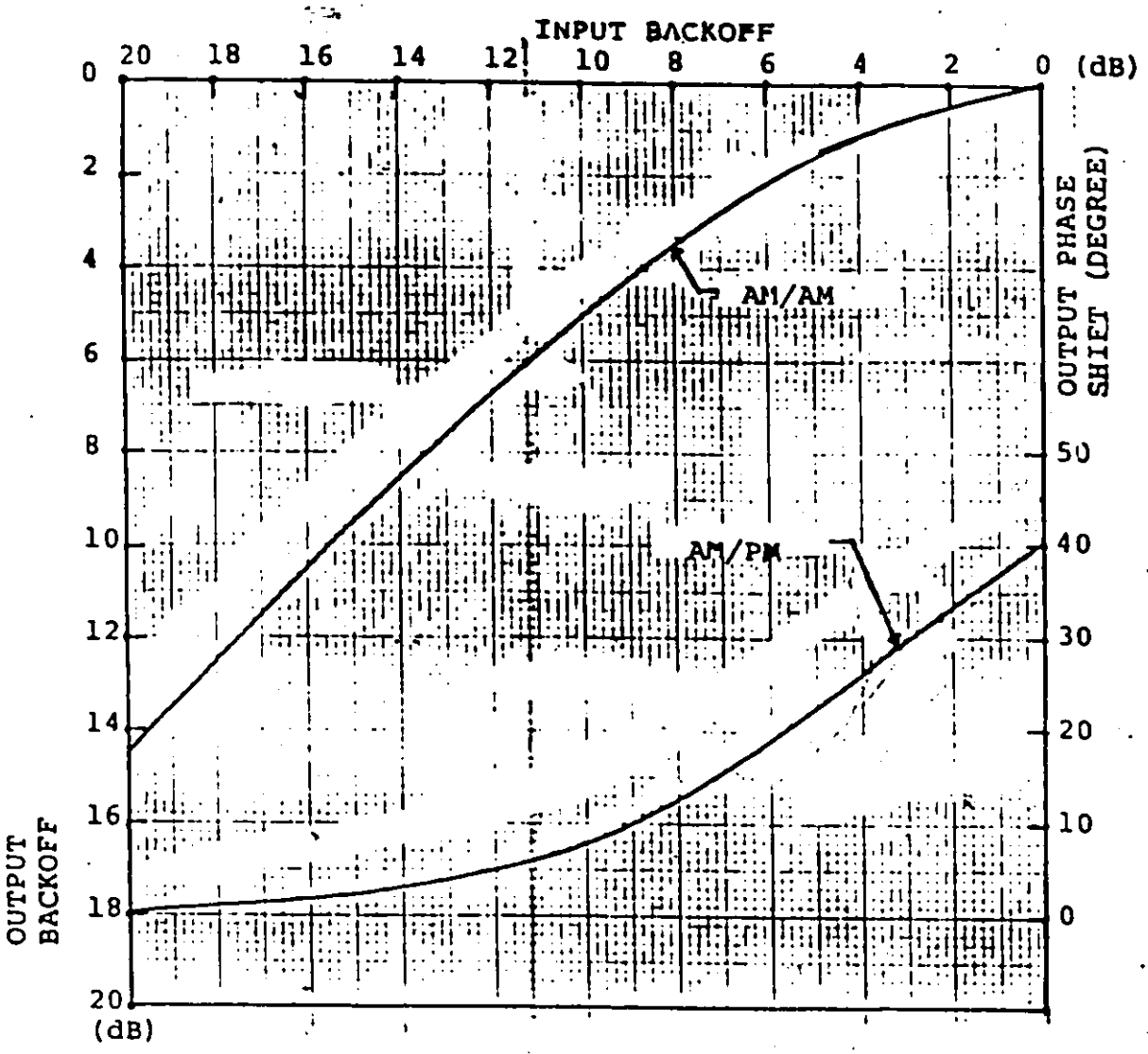

FIG.2.16 NONLINEAR CHARACTERISTICS OF INTELSAT V TYPE HPA 10

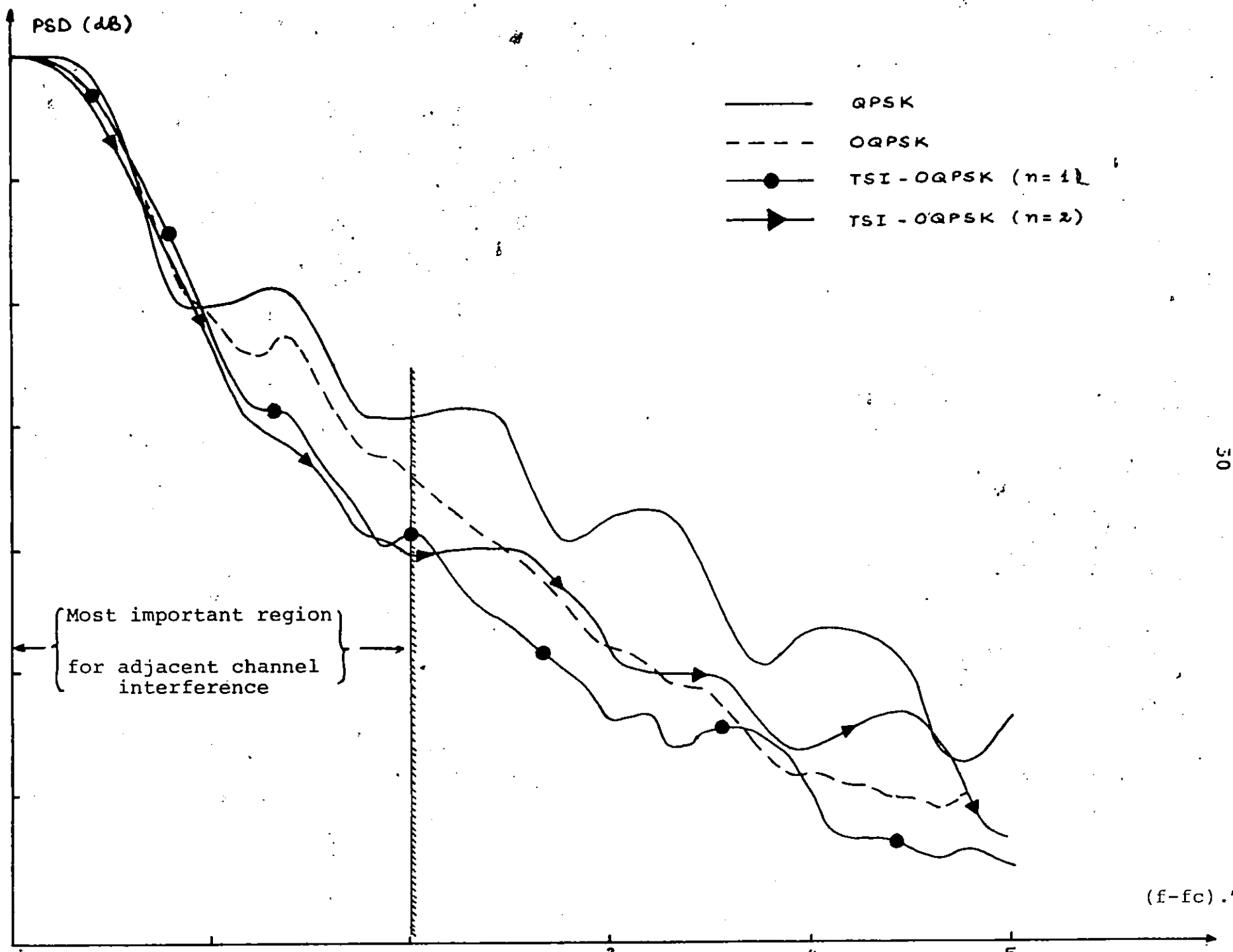

FIG. 2.17 PSDs of DIFFERENT MODULATED SIGNALS AT THE OUTPUT OF A SATURATED HPA (0dB INPUT BACKOFF)

2.4 TSI-OQPSK Receiver

The block diagram of the TSI-OQPSK demodulator is shown in Fig. 2.18. This model may be the same as the conventional receiver's model of OQPSK system [3-5, 23, 36]. The received signal is passed through a bandpass filter (BPF) (*) and split into the in-phase and quadrature components. These two components are multiplied by $\cos(w_c t)$ and $\sin(w_c t)$ respectively and passed through two lowpass filters. The two lowpass filters prior to the threshold comparators are used solely to eliminate high frequency components. Two threshold comparators are used to convert the received analog signals into digital signals. Then the in-phase and quadrature channel signals are converted back into serial data.

If the 3-dB bandwidth of the receive bandpass filter (shown in Fig. 2.18) is much greater than the bit rate (at least twice the bit rate), then the received in-phase and quadrature components of hardlimited TSI-OQPSK signals at the threshold comparator inputs are approximately equal to $Y^1_{I_n}(t)$ and $Y^1_{Q_n}(t)$ respectively. The computer generated signal eye diagrams of $Y^1_{I_n}(t)$ or $Y^1_{Q_n}(t)$ are shown in Fig. 2.19.

The measured signal eye diagram of hardlimited TSI-OQPSK $\eta = 1$ is also obtained and shown in Fig. 2.20. The two results in Fig. 2.20 and 2.19a are in close agreement.

Based on these results a new filtering strategy called Sum of Approximate Eye is introduced and will be discussed in the next chapter.

* The BPF may represent conventional Linear Zero Forcing filters or our new class of Sum of Approximate Eye filters, which will be discussed in the next chapter.

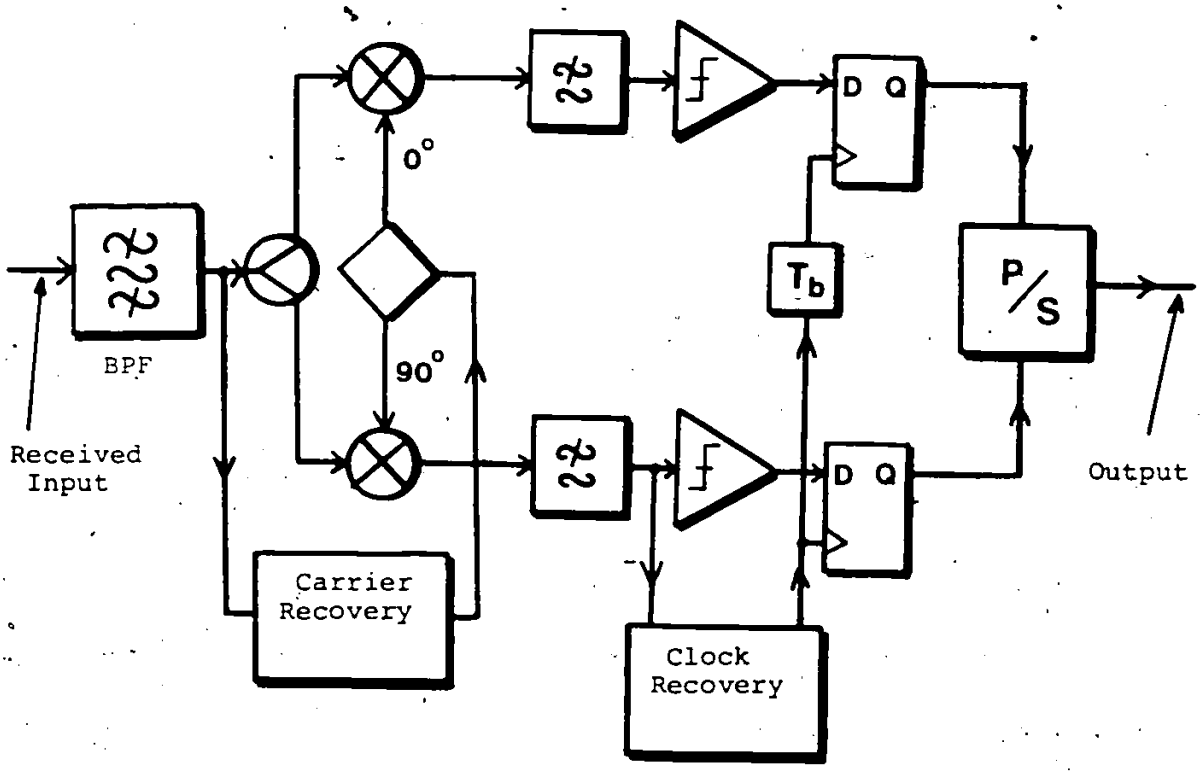

Fig. 2.18 :Block diagram of Two-Symbol-Interval-OQPSK demodulator

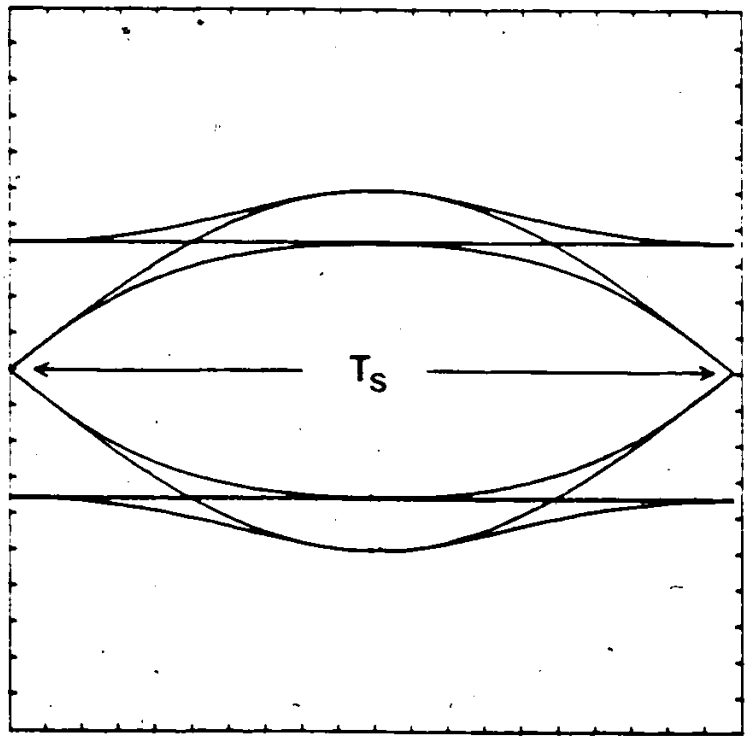

Fig.2.19: Received signal eye diagrams of hardlimited TSI-OQPSK systems (with a wideband BPF)

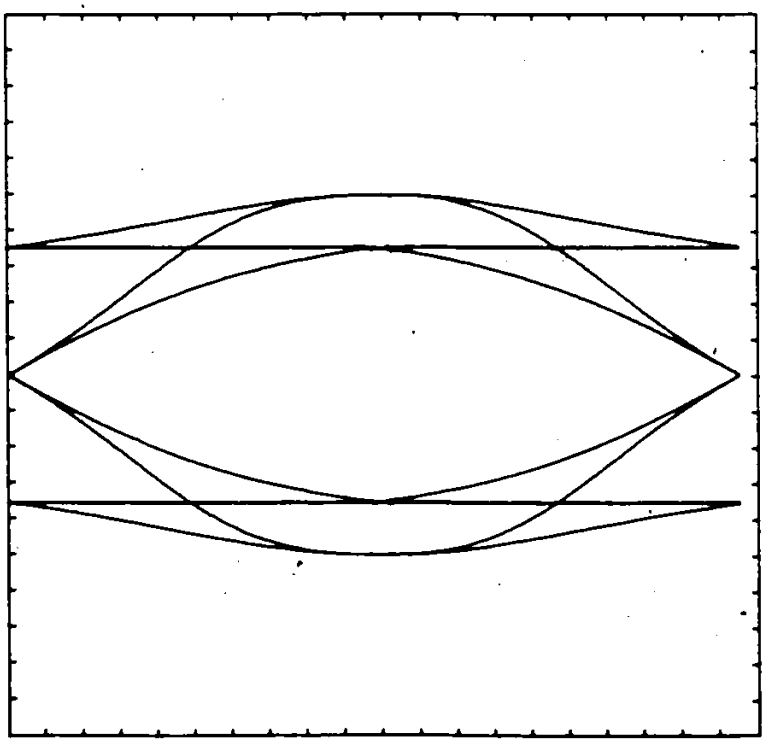

b/ n = 2

Fig.2.19: Received signal eye diagrams of hardlimited TSI-OQPSK systems (with a wideband BPF)

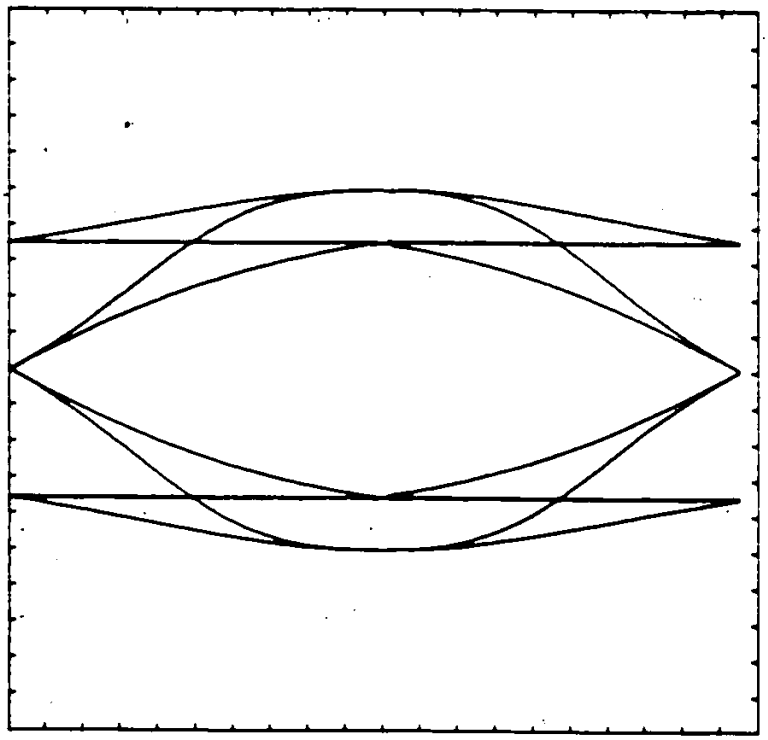

Fig.2.19: Received signal eye diagrams of hardlimited TSI-OQPSK systems (with a wideband BPF)

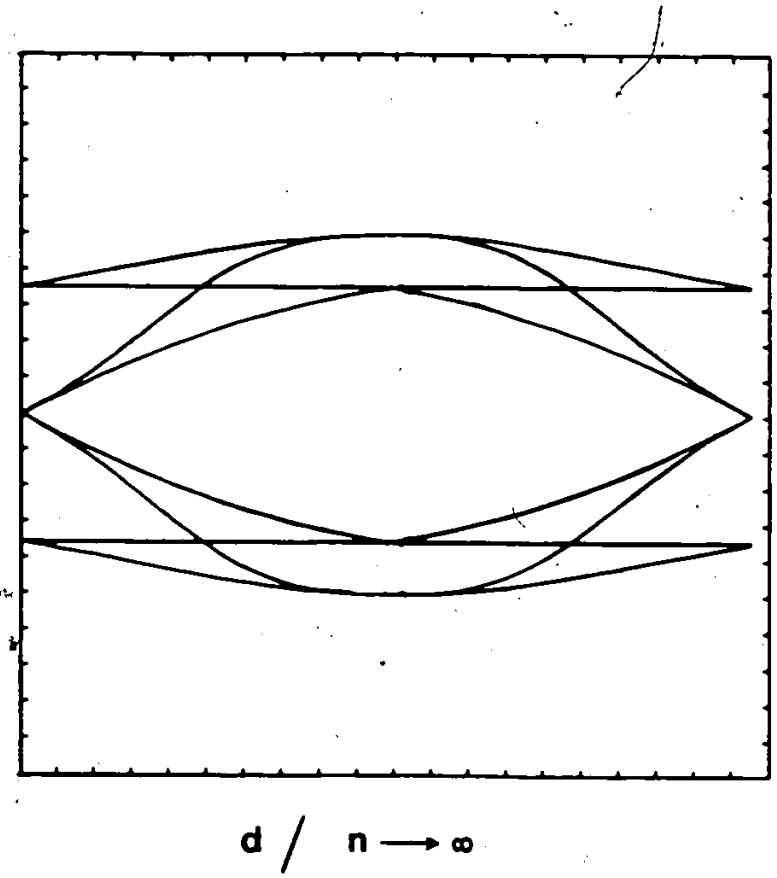

Fig. 2.19: Received signal eye diagrams of hardlimited TSI-OQPSK systems (with a wideband BPF)

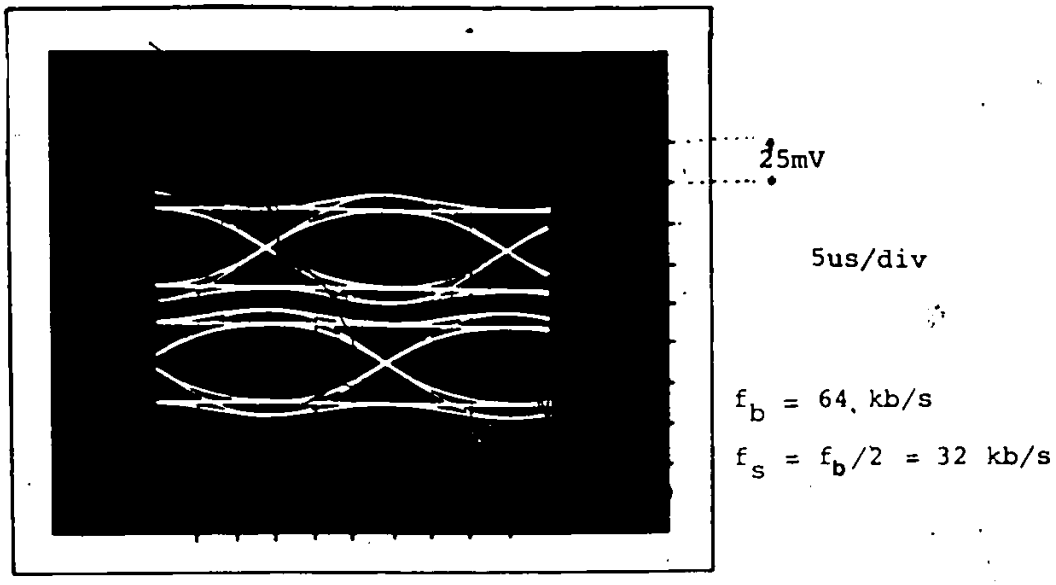

Fig. 2.20: **Measured signal eye diagram for n=1. The in-phase and quadrature channels (the later delayed by T_b-** seconds) are obtained prior to the threshold comparator.

CHAPTER THREE

FILTERING STRATEGIES FOR TSI-OQPSK SIGNALS

Filters have many important functions in a digital multi-carrier communication system. They can be used to shape the signals and to reduce the noise and the adjacent channel interference. In our system a relatively narrow BPF is placed at the input of the demodulator (Fig. 2.18) in order to minimize adjacent channel interference (ACI) and noise variance σ^2 and to ease the carrier recovery design problem without introducing ISI. In this Chapter, two types of filters, zero forcing filter and SAE filter are used to examine the P_e performance of TSI-OQPSK systems in a multiple-carrier and hardlimited channel environment.

3.1 Zero Forcing Filter

The first type of filter, called a zero-forcing-filter [12-13, 20, 24-25], is defined by:

$$H_{1n}(f) = \frac{H(f)}{[Y_n(f)]^{\frac{1}{2}}} \tag{3.1}$$

where $Y_n(f)$ is the PSD of the TSI-OQPSK signal prior to hardlimiting (eq. 2.14) and $H(f)$ is the

transfer function of the raised cosine filter is [12-13, 20, 24, 25] defined by:

$$H(f) = \begin{cases} 1 & 0 \le f \le \frac{1}{2T}(1-\alpha) \\ 0.5\left\{1 - \sin\left(\frac{\pi T}{2\alpha}\left(2f-\frac{1}{T}\right)\right)\right\} & \frac{1}{2T}(1-\alpha) \le f \le \frac{1}{2T}(1+\alpha) \\ 0 & \text{otherwise} \end{cases} \quad (3.2)$$

α is the roll-off factor of the filter.

Figure 3.1a and 3.1b show the zero-forcing-filters of TSI-OQPSK systems for n = 1, 2, for linear channels. We note that zero-forcing filters are match filters for linear channels and have been used extensively [8, 10, 11, 14, 22-25, 46]. To justify the matching characteristics let us assume that there is no nonlinear amplifier between the transmitter and the receiver. The PSD of TSI-OQPSK signals after passing through the receive zero forcing filter will be:

$$R_n(f) = Y_n(f) \times H_{ln}^2(f)$$

$$= Y_n(f) \times \frac{H^2(f)}{Y_n(f)} = H^2(f) \quad (3.3)$$

Hence, the received signal $r_n(t)$ is equal to the summation of the impulse response of an ideal raised cosine filter [12, 13, 22, 24].

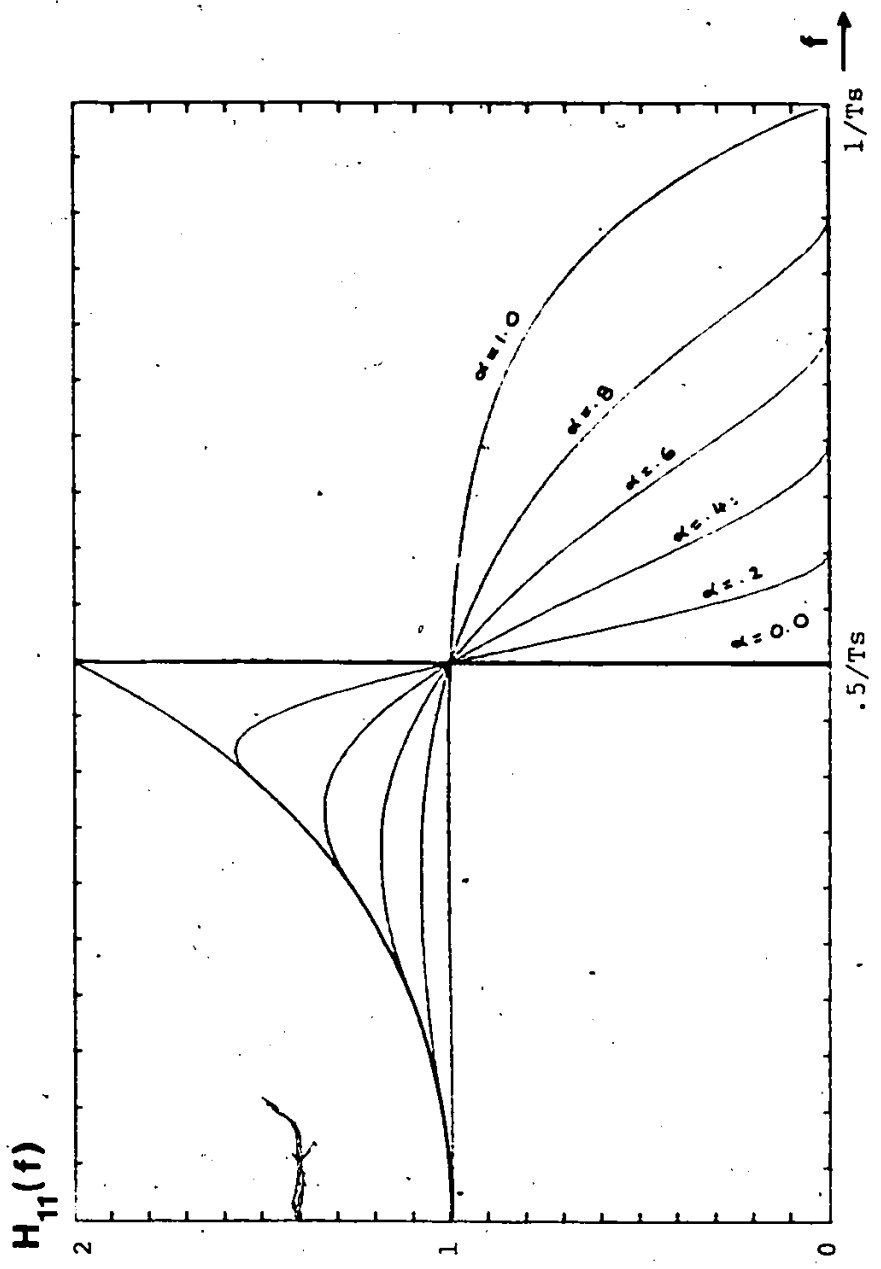

Fig. 3.1a: Zero-forcing filter for n=1 (for linear channels)

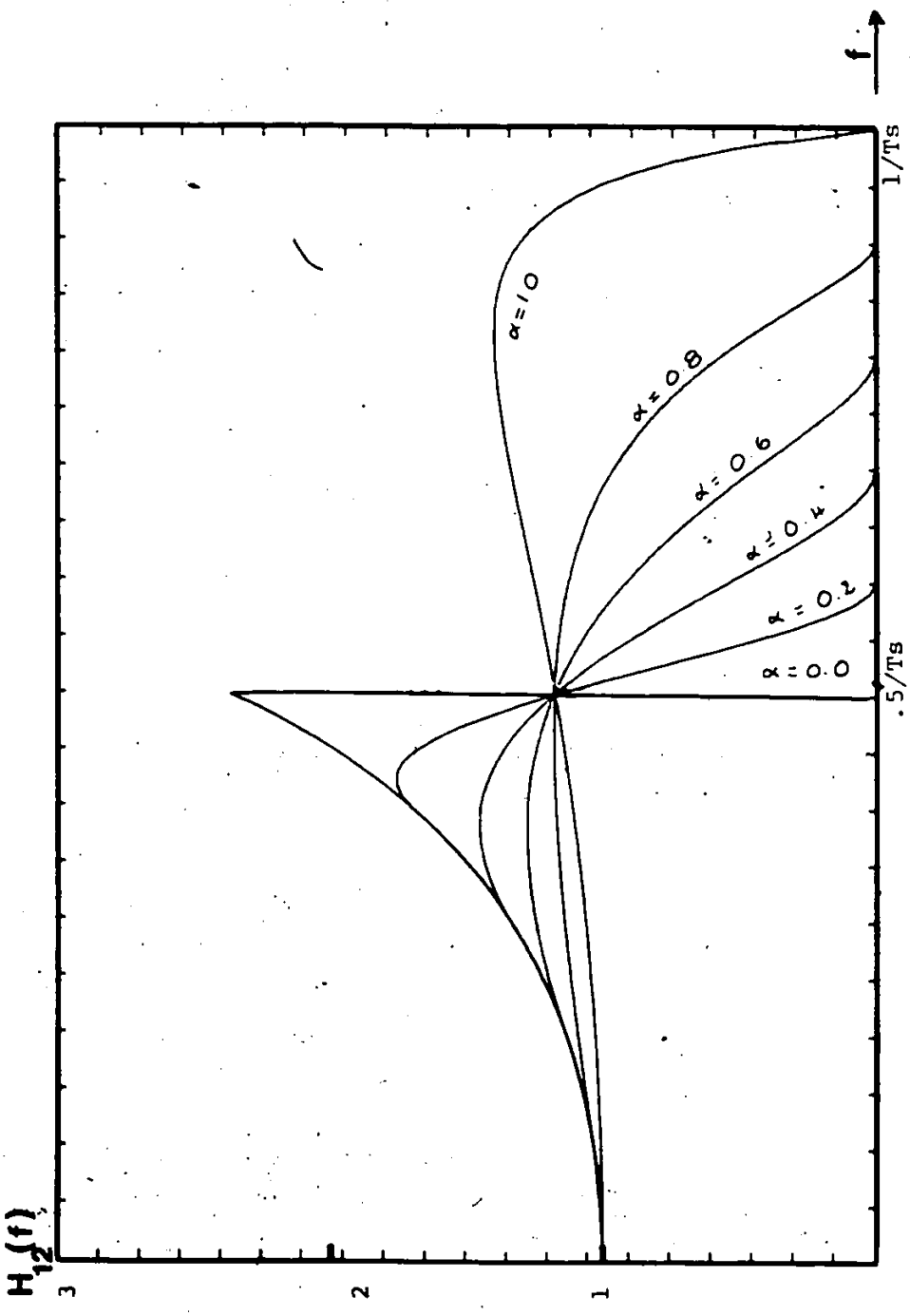

Fig. 3.1b : Zero-forcing-filter for n=2 (for linear channels)

$$r_n(t) = \sum_{k=-\infty}^{+\infty} x \left\{ \frac{\sin \pi t/T}{\pi t/T} \cdot \frac{\cos \alpha \pi t/T}{1-4\alpha^2 t^2/T^2} \right\} \cdot \delta\,(t-kT)(*) \qquad (3.4)$$

Because of this property (equation 3.4), the received signal eye diagram $r_n(t)$ will have no ISI at the sampling point.

Fig. 3.2 shows the received signal eye diagram of a TSI-OQPSK signal prior to the threshold detector, when a zero-forcing filter is used, in a linear channel environment. The roll-off factor, α, of the received filter used in Fig. 3.2 is equal to 0.4. From Fig. 3.2 we can see that the received eye diagram has no intersymbol interference at the sampling point.

(*) x is equal to +A if the input data at the time (t-kT) is high and x is equal to -A if the input data is low.

k = 0, 1, 2, 3,....

T is equal to T_s: symbol duration

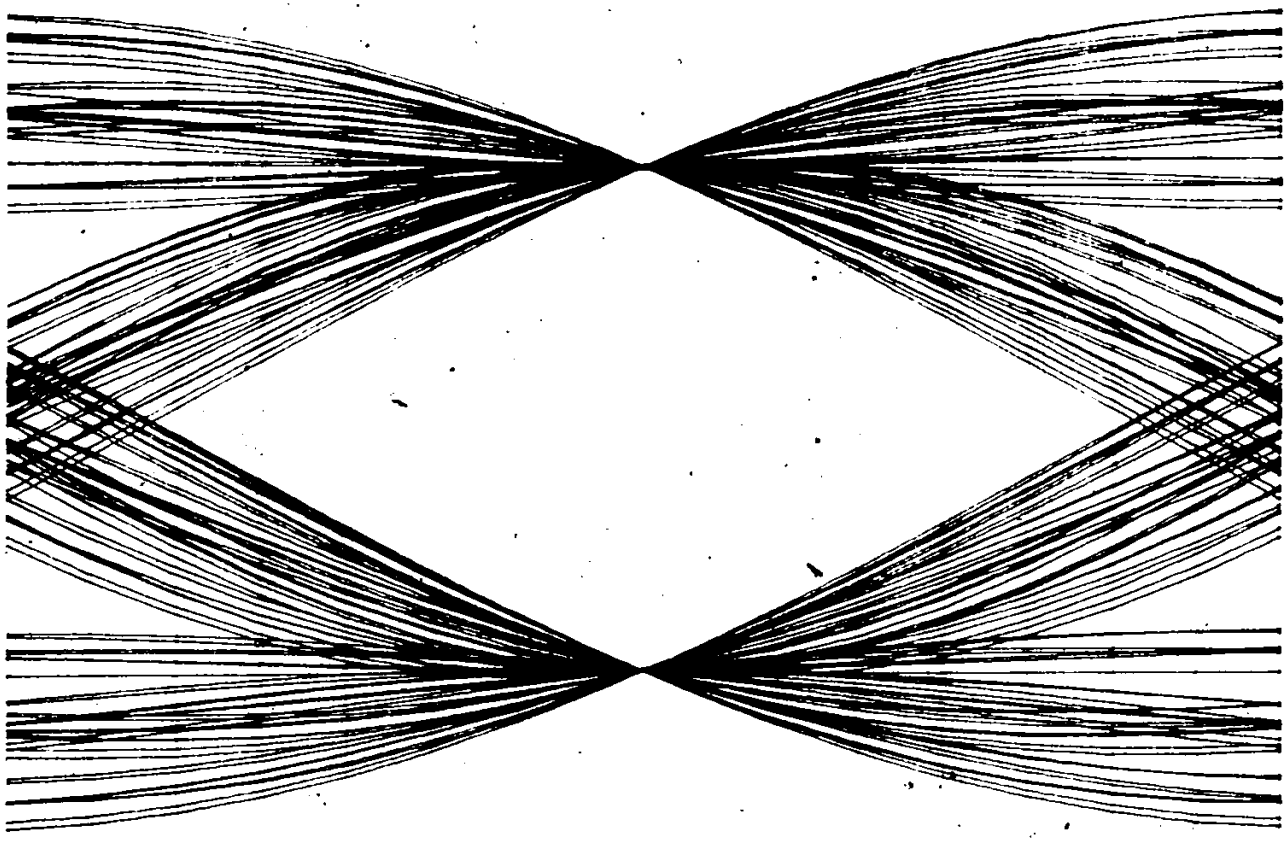

Fig. 3.2 Received signal eye diagram of TSI-OQPSK signal prior to the threshold detector (using Zero-Forcing-filter α = .4 and in a linear channel environment)

3.2 Sum of Approximate Eye filter

In this section we are going to introduce a new type of filtering strategy called Sum of Approximate Eye (SAE). The invention of this filtering strategy is based on the results found in Chapter Two (Fig. 2.19 and Fig. 2.20). This strategy is described as follows:

Examine the received signal eye diagrams (Fig. 2.19 and Fig. 2.20). We can separate these signals into two overlapping eye diagrams, namely the continued and dotted eye diagrams as shown in Fig. 3.3.

The odd and even elements of the continued eye diagram $v(t)$ and the dotted eye diagram $u(t)$ can be approximated as:

$$v_o(t) = \sin\left(\frac{\pi t}{T_s}\right) \qquad |t| \le \frac{T_s}{2}$$

$$v_e(t) = \left(\frac{1}{2}+\frac{\sqrt{2}}{4}\right) - \left(\frac{1}{2}-\frac{\sqrt{2}}{4}\right)\cos\left(\frac{2\pi t}{T_s}\right) \quad |t| \le \frac{T_s}{2}$$

$$u_o(t) = \frac{\sqrt{2}}{2}\sin\left(\frac{\pi t}{T_s}\right) \quad |t| \le \frac{T_s}{2}$$

$$u_e(t) = \frac{\sqrt{2}}{2} \qquad |t| \le \frac{T_s}{2}$$

Using equation (2.11), the PSDs of $v(t)$ and $u(t)$ are found to be

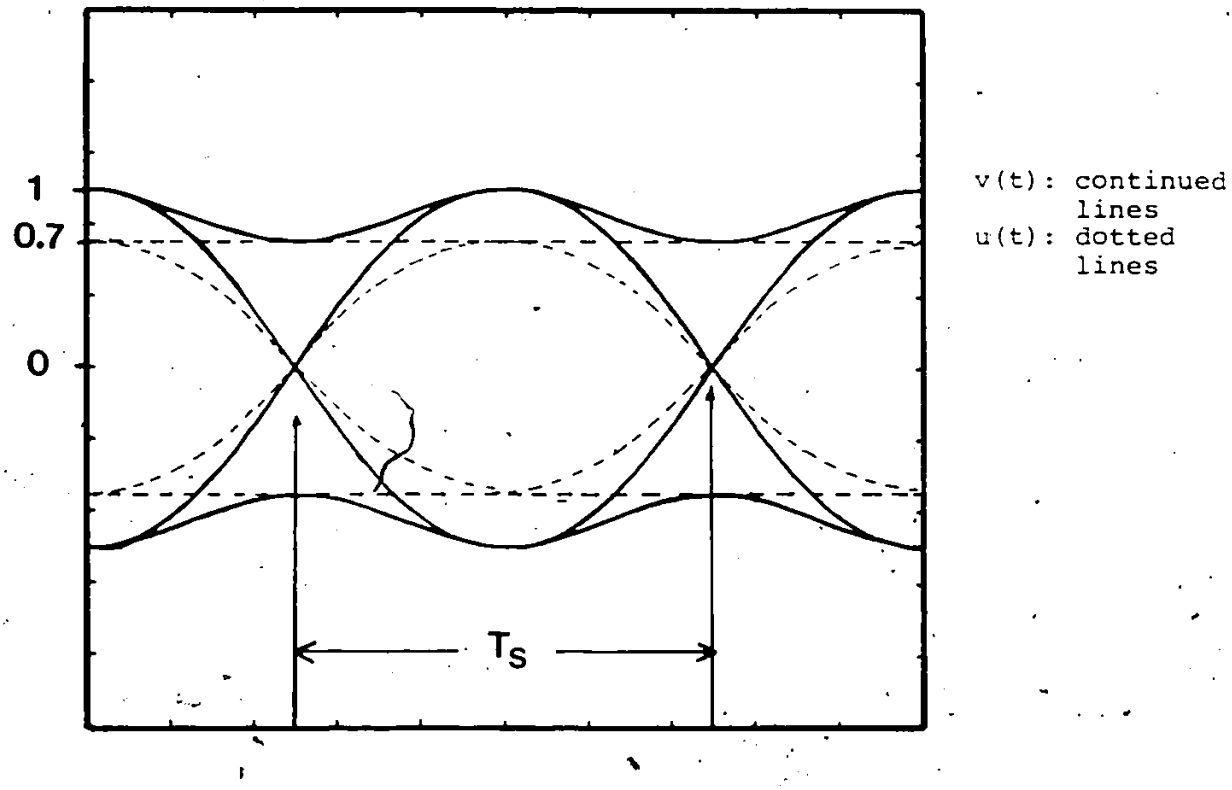

Fig. 3.3: Sum of Approximate Eye (SAE) construction concept:

Two overlapping eye diagrams can be separated from a received eye diagram of a hardlimited-TSI-OQPSK signal

$$|V(f)|^2 = \left\{ \frac{\sin(2\pi fT_s)}{2\pi fT_s} \left\{ \frac{1}{1-4f^2T_s^2} + .85 \right\} -.15\, fT_s \cdot \frac{\sin(2\pi fT_s)}{2\pi(1-f^2T^2_s)} \right\}^2 \tag{3.5}$$

$$|U(f)|^2 = \frac{1}{2}\left\{ \frac{\sin(2\pi fT_s)}{2\pi fT_s} \times \frac{1}{1-4f^2T^2_s} \right\}^2 \tag{3.6}$$

Since the probability of occurrence for a "+A" or a "-A" in the transmitted data stream are the same and equal to 0.5, therefore, the probability of occurrence for v(t) and u(t) are the same and equal to 0.5. Based on this assumption, the PSD of the sum of approximate eye signal is defined by

$$|W(f)|^2 = |V(f)|^2 + |U(f)|^2 \tag{3.7}$$

The normalized PSD of the SAE eye signal, $|W(f)|^2_N$, is

$$|W(f)|^2_N = \frac{W(f)^2}{W(0)^2} \tag{3.8}$$

Where W(0) is the value of W(f) at f = 0.

The receive filter, which is formed by the ratio of the raised-cosine-filter-transfer-function (H(f)) and the square root of SAE-PSD, is called the *Sum of Approximate Eye* filter. It is expressed as:

$$H_2(f) = \frac{H(f)}{|W(f)|_N}$$

The shapes of $H_2(f)$ for different values of α are shown in Fig. 3.4.

For the cases investigated, the implementation of the SAE filter is simpler than that of the zero-forcing filter because the attenuation of the zero-forcing filter is sharper than that of the SAE filter. To demonstrate the advantages of the SAE filter over the zero-forcing filter, we will examine the resulting ISI and the carrier to interference power ratio (C/I) caused by these filters in the next section.

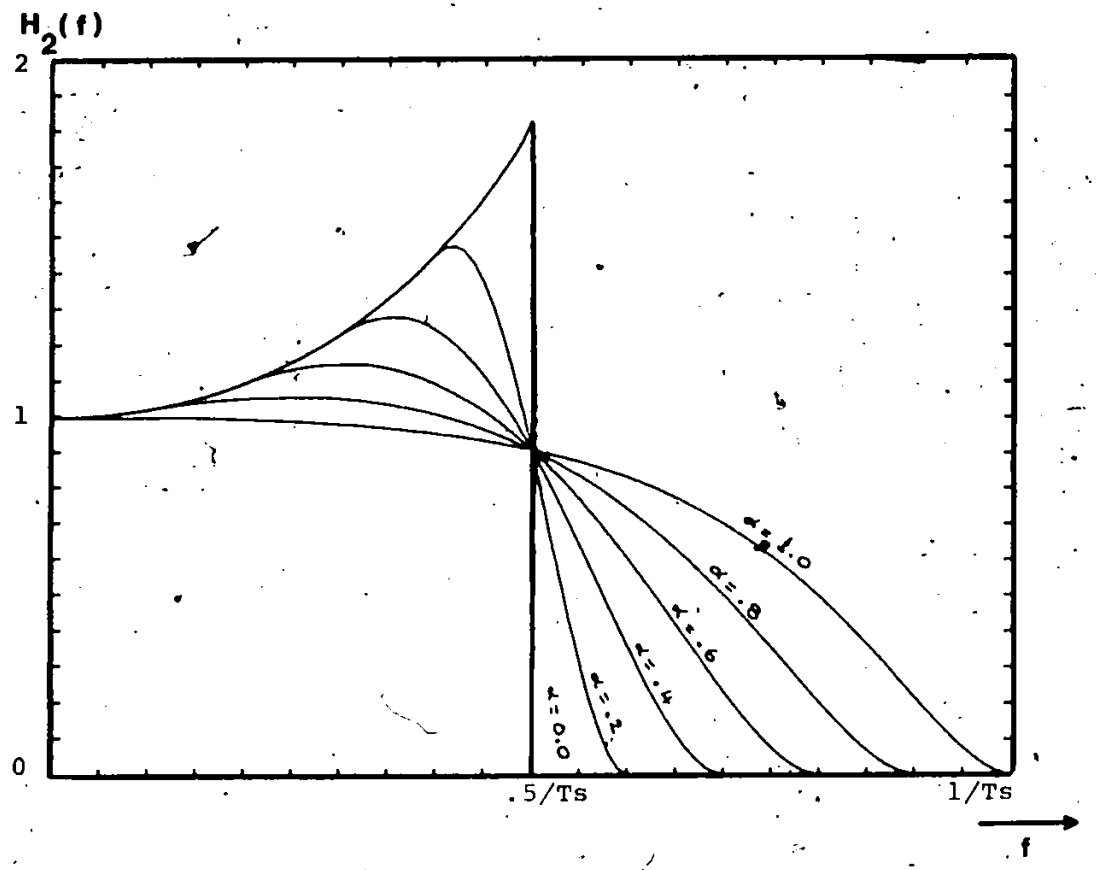

Fig. 3.4 : SUM OF APPROXIMATE EYE filter with different values of roll-off, α

3.3 Advantages of the SAE filter over the Zero Forcing Filter

3.3.1 P_e Performance

To examine the ISI generated as a result of a selected filtering strategy, we use our single channel model as shown in Fig. 3.5. The TSI-OQPSK modems were discussed in Chapter Two and the hardlimiter is used as our nonlinear amplifier. The computer simulated signal eye diagrams of TSI-OQPSK signals in a noise free channel are shown in Fig. 3.6 (for n = 1) and Fig. 3.7 (for n = 2). From Fig. 3.6a and Fig. 3.7a we can see that the SAE filters introduce less ISI than the zero forcing filter.

We note that the roll off factor α also affects the performance of the system. Fig. 3.8 shows the required E_b/N_o of TSI-OQPSK system (n = 1, 2), for different values of α, to obtain a P_e performance of 10^{-4}. The best P_e performance is obtained when α is in the region of 0.4 to 0.8. We also notice that the E_b/N_o requirements for zero forcing filtered systems is larger than for the SAE filtered system.

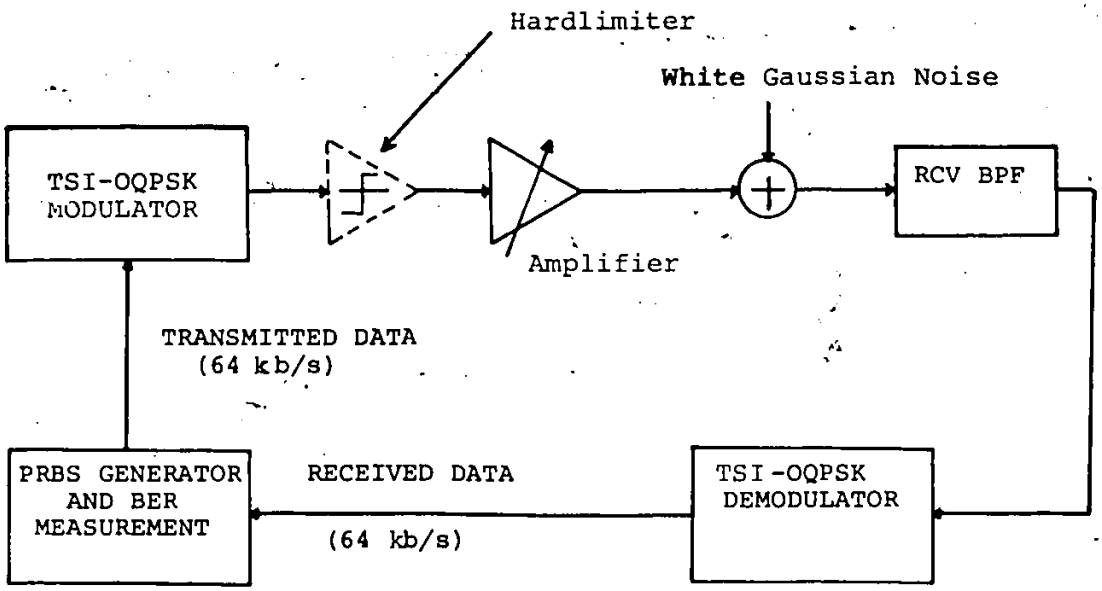

FIG. 3.5 P_e MEASUREMENT AND SIMULATION SET-UP FOR A SINGLE CHANNEL TSI-OQPSK SYSTEM

* RCV BPF: Receive BPF: Linear-Zero-Forcing-Filter or SAE Filter
* Carrier Frequency = 512 kHz
* Bit Rate = 64 kb/s

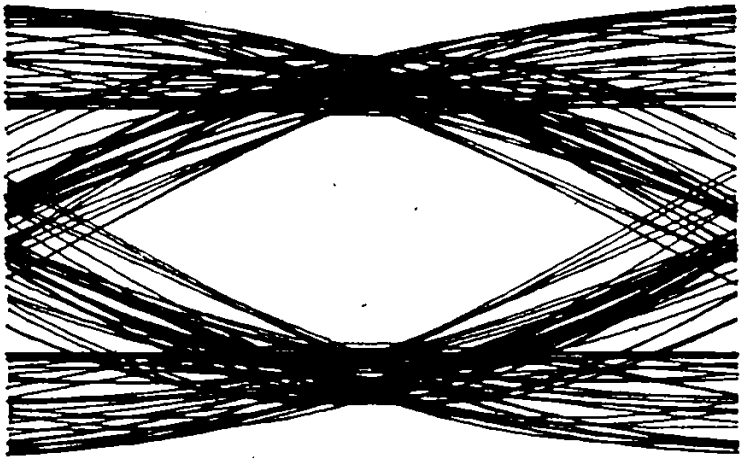

a/ Zero Forcing filter is used as received BPF

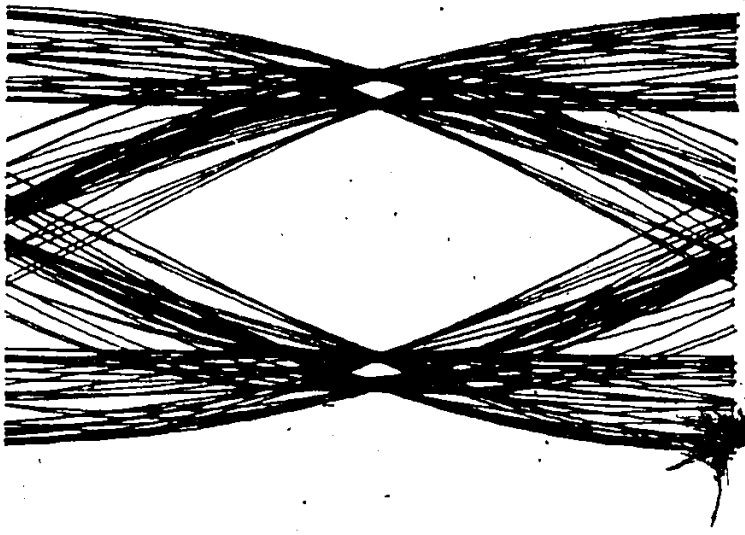

b/. SAE filter is used as received BPF

Fig. 3.6 Computer simulated eye diagram of hardlimited TSI-OQPSK (n = 1) signal (at the threshold detector input)

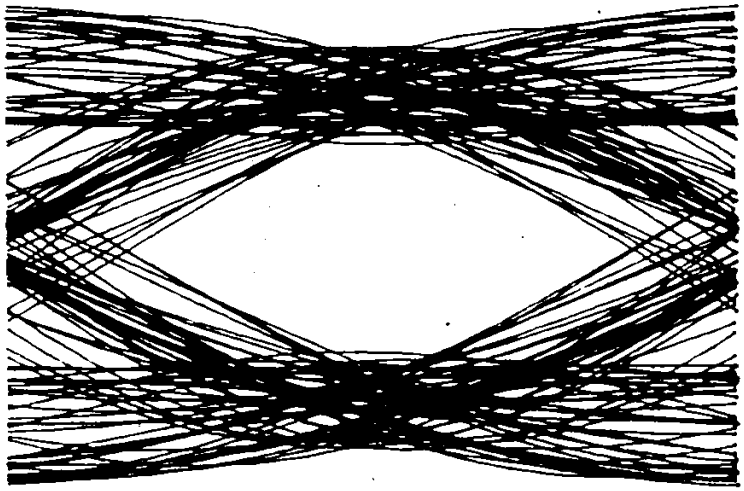

a/ Zero forcing filter is used as received BPF

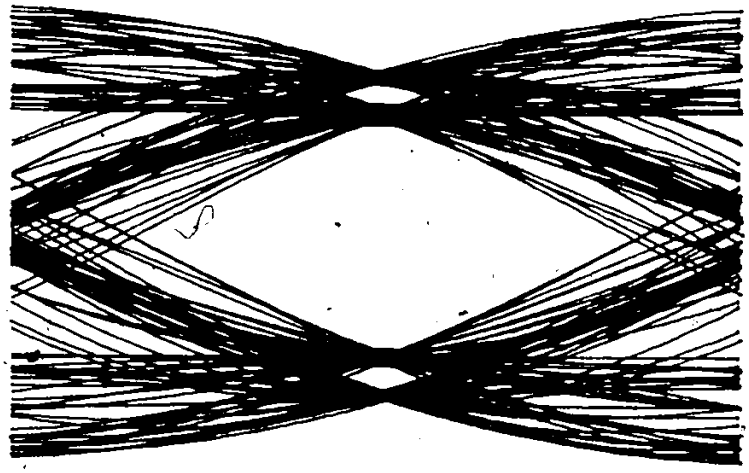

b/ SAE filter is used as received BPF

Fig. 3.7 Computer simulated eye diagram of hardlimited TSI-OQPSK (n = 2) signal (at the threshold detector input)

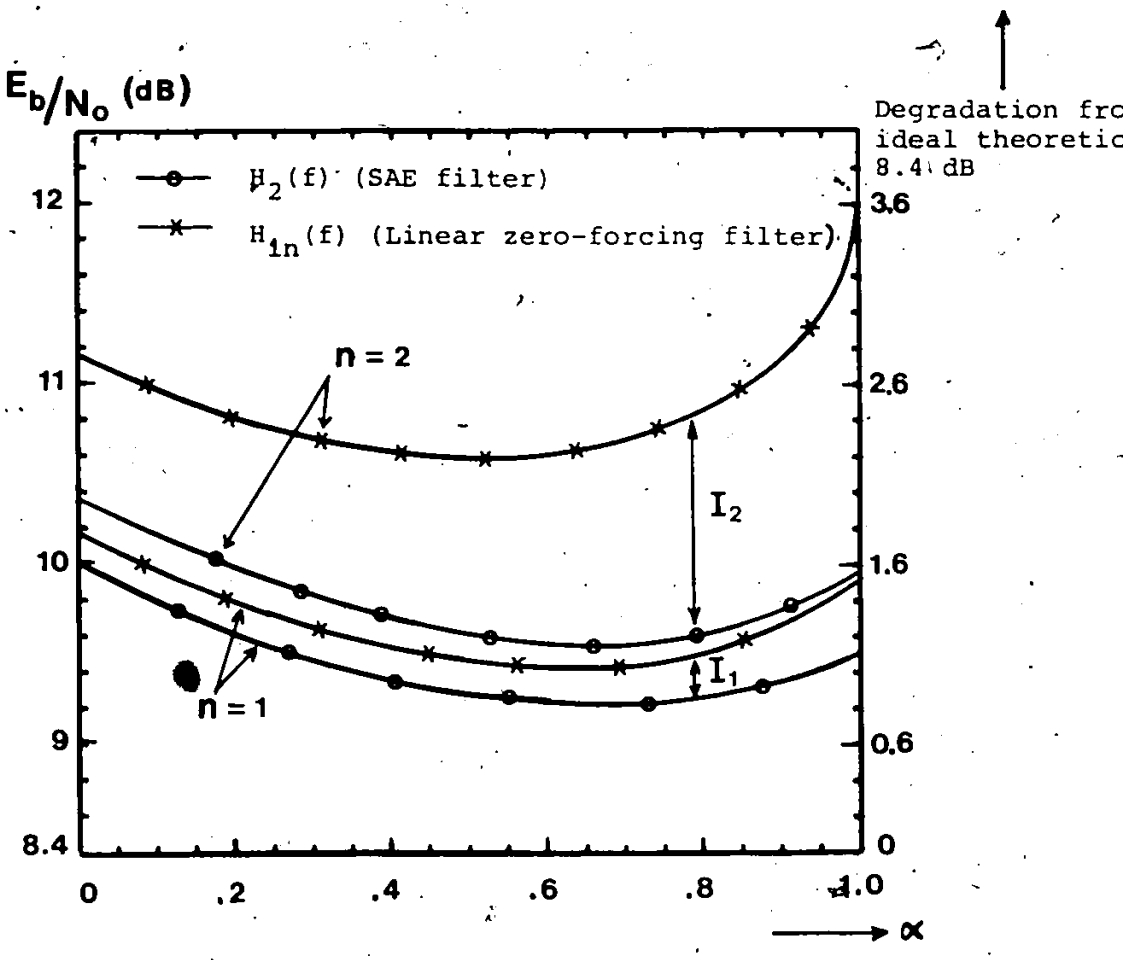

Fig. 3.8 E_b/N_o requirements of hardlimited TSI-OQPSK systems at $P_e = 10^{-4}$ in a single channel and additive white gaussian noise environment. α is the roll-off factor of the receive raised cosine filters. I_1 and I_2 represent the SAE filter improvement for the n=1 and n=2 cases respectively.

3.3.2 C/I power ratio

In the previous section (3.3.1), we demonstrated that the SAE filter improved the P_e performance of our TSI-OQPSK signals in a single channel environment. In this section we use the model shown in Fig. 1.a to examine how the C/I power ratio is affected by different types of filters. In this model three hardlimited TSI-OQPSK signals having different carrier frequencies, namely f_1, f_2, f_3 with equal power are added and filtered by the bandpass filter (BPF) centered at f_2 (Fig. 3.9). The channel spacing Δf is defined by $\Delta f = f_2 - f_1$ (also equal to $f_3 - f_2$).

The signal power after passing through the filter is

$$C = \int_{-\infty}^{+\infty} S_2(f) \cdot |H_R(f)|^2 \, df$$

and the total interference due to the two adjacent channels is

$$I = \int_{-\infty}^{+\infty} \{S_1(f) \cdot |H_R(f)|^2 + S_3(f) \cdot |H_R(f)|^2\} \, df$$

Therefore the C/I ratio is

$$C/I = \frac{\int_{-\infty}^{\infty} S_2(f) \cdot |H_R(f)|^2 \, df}{\int_{-\infty}^{\infty} \left\{ S_1(f) \cdot |H_R(f)|^2 + S_3(f) \cdot |H_R(f)|^2 \right\} df} \qquad (3.9)$$

where $S_i(f)$ is the PSD of the modulated signal ($i = 1, 2, 3$) at the input of the filter.

Using equation (3.9) and the two types of filters mentioned in the previous sections, the C/I ratio for TSI-OQPSK signals n = 1 and n = 2 is found and shown in Fig. 3.10. From these results, we can see that by using the SAE filter ($H_2(f)$) as the receive filter for hardlimited TSI-OQPSK signals, the ratio C/I has been improved significantly. This improvement is obtained because of the attenuation of the SAE filter is much greater than the zero-forcing filter in the interval $.5 \leq \Delta f . T_s \leq 1$.

Fig. 3.11 shows a comparison of the C/I power ratios of hardlimited TSI-OQPSK signals for the cases n = 1 and n = 2. For both types of filter, the C/I ratio of the n = 2 case is better than that of the n = 1 case.

From the P_e and C/I power ratio results, we can conclude that the SAE filter improves the performance of hardlimited TSI-OQPSK modems more than the zero forcing filter.

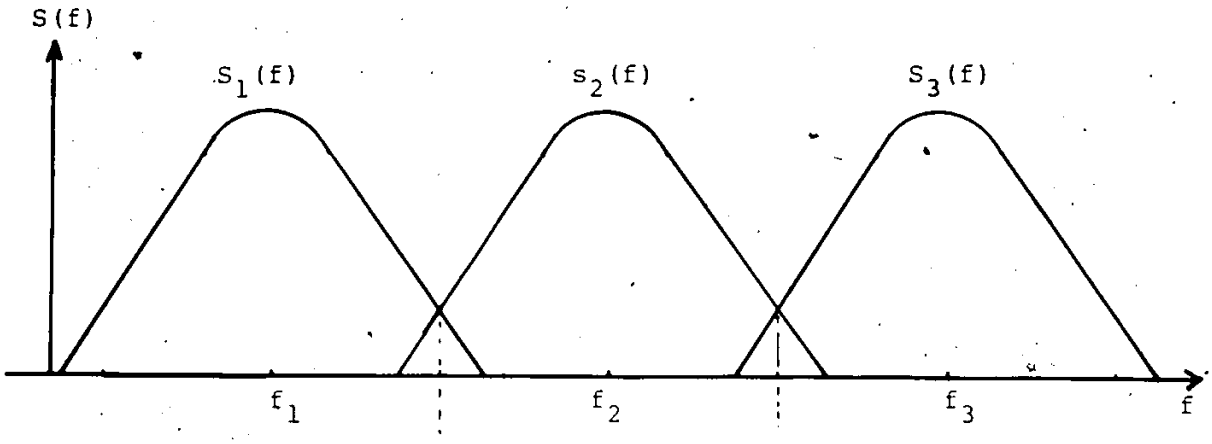

a/ PSDs before the receive filter

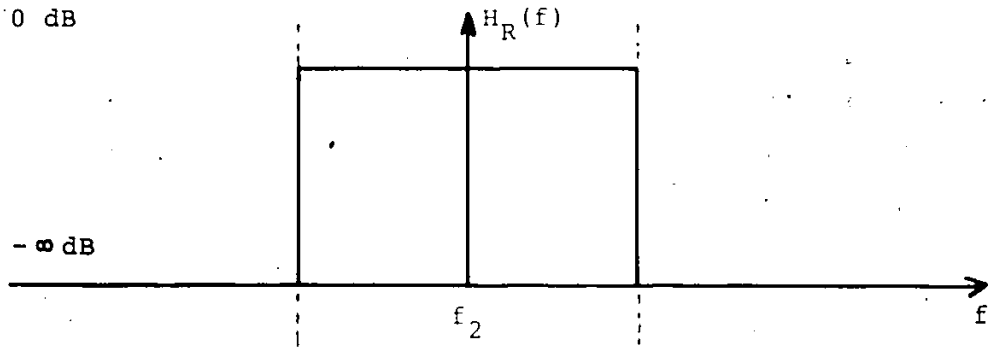

b/ Receive filter (SAE filter or Zero Forcing Filter)

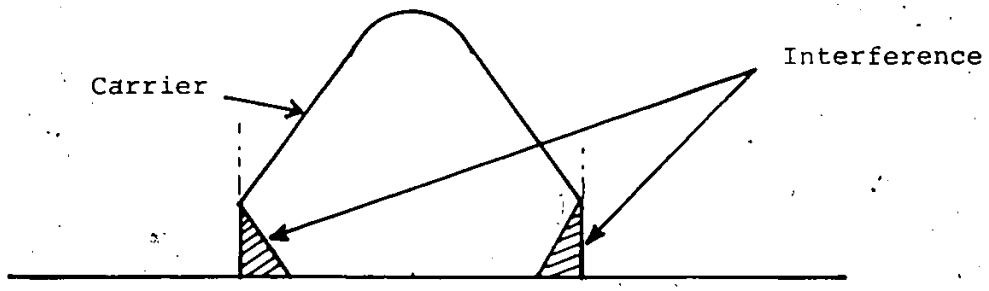

c/ Adjacent channel interference after the receive filter

Fig. 3.9 Model to examine the C/I power ratio

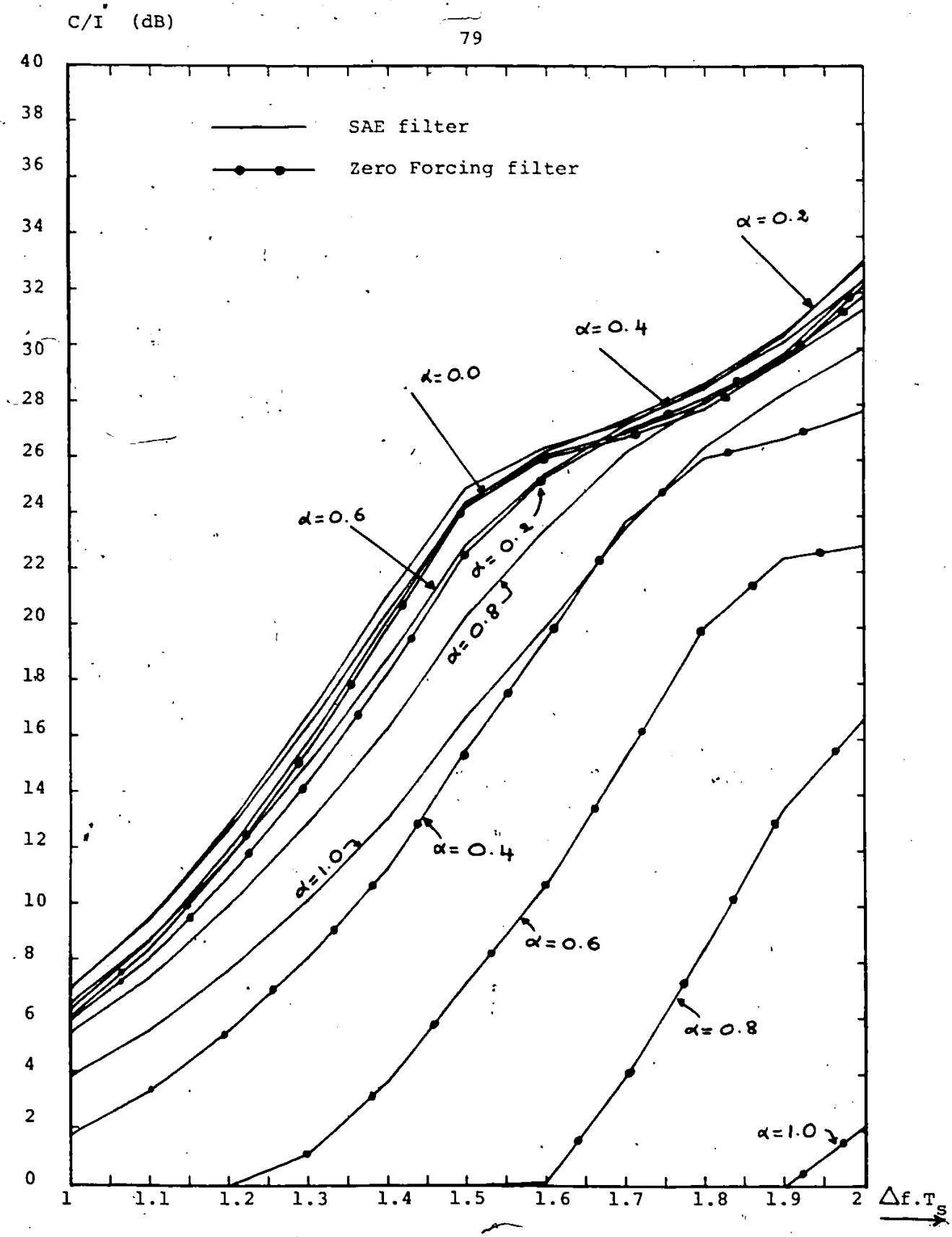

Fig. 3.10a C/I versus Δf for TSI-OQPSK (n = 1) signal using the model shown in Fig. 3.9

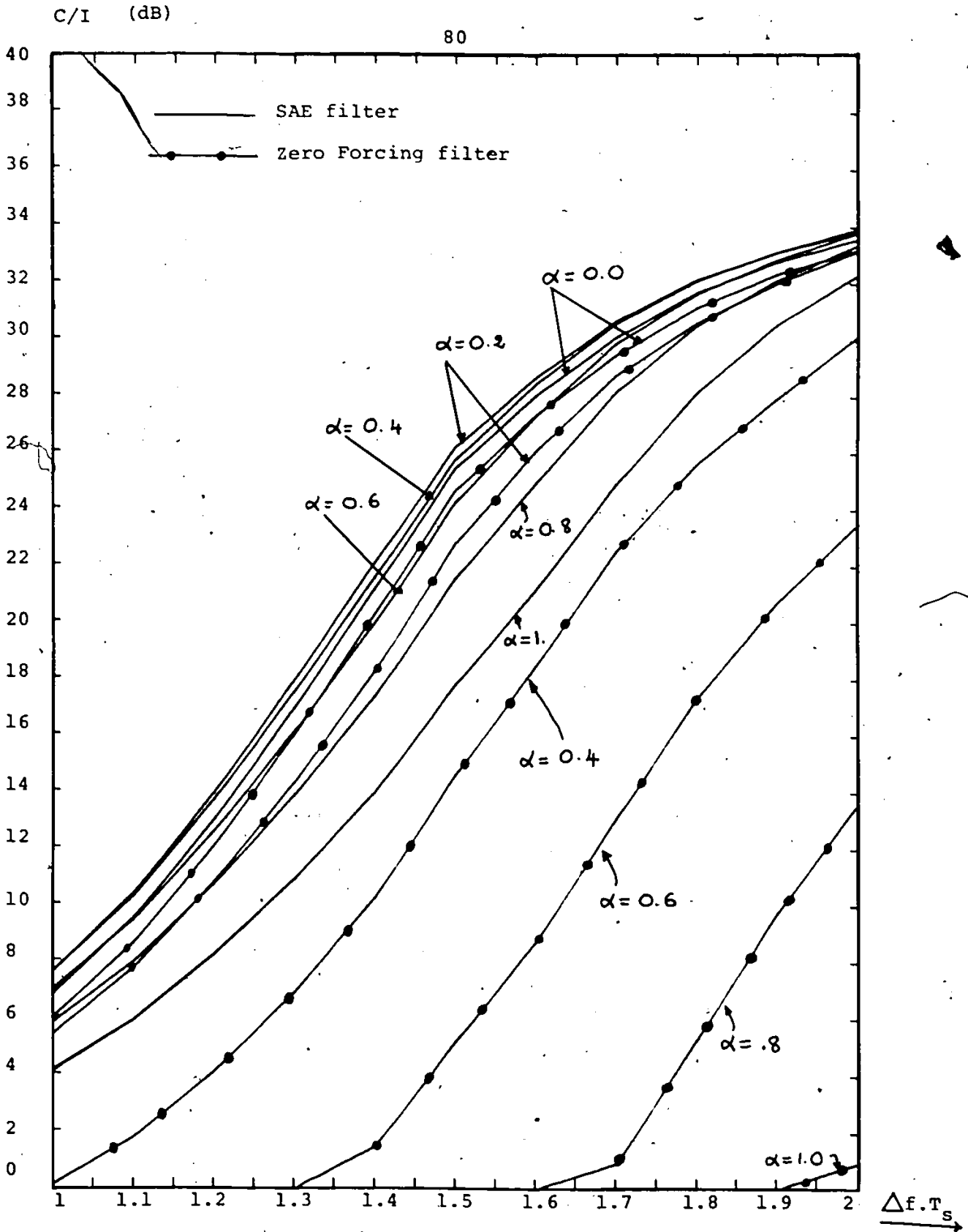

Fig. 3.10b C/I versus Δf for TSI-OQPSK (n = 2) signal using the model shown in Fig. 3.9

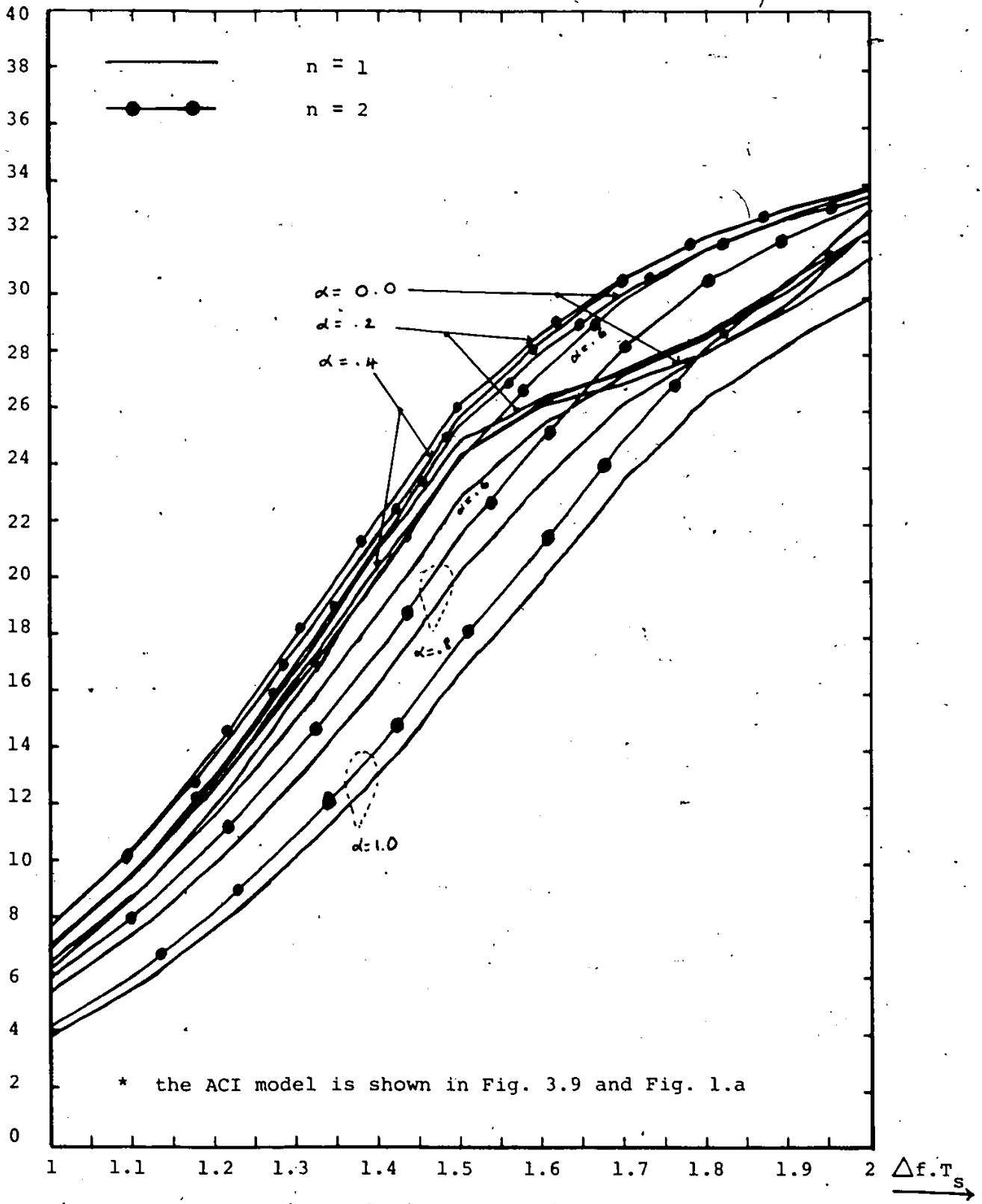

Fig. 3.11a Comparison of C/I power ratio between TSI-OQPSK n = 1 and n = 2 when SAE filter is used as Received BPF

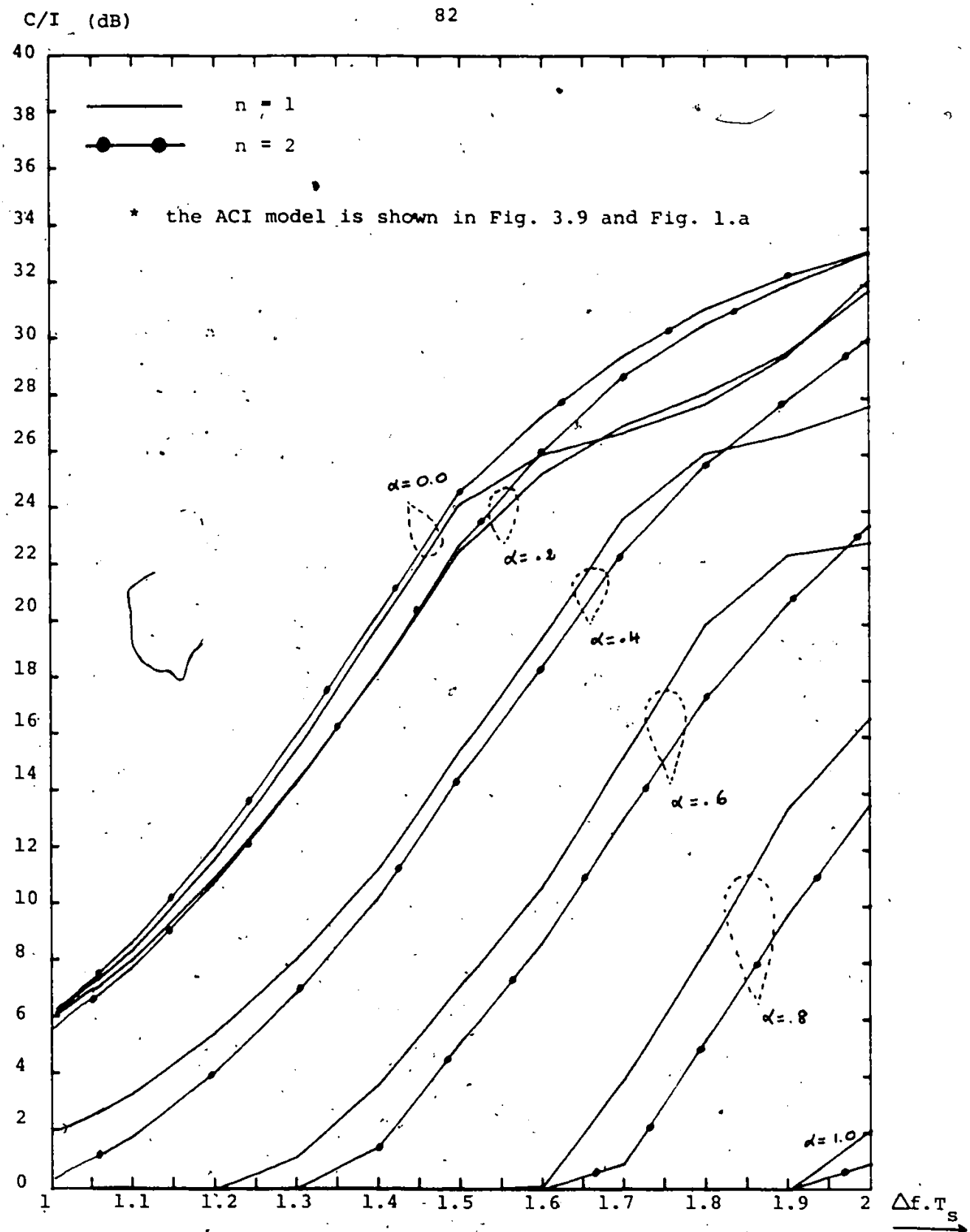

Fig. 3.11b Comparison of C/I power ratio between TSI-OQPSK n = 1 and n = 2 when zero forcing filter is used as Received BPF

CHAPTER FOUR

P_e PERFORMANCE OF TSI-OQPSK MODEMS

In this chapter the performance of TSI-OQPSK modems in an adjacent channel interference, additive white Gaussian noise and nonlinear amplifier channel environment is investigated.

We use computer simulations to evaluate the probability of error (P_e) performance of different systems (TSI-OQPSK, QPSK and OQPSK). The accuracy of our computer simulations was verified by comparing the computer generated $P_e = f(E_b/N_o)$ results with our measurement results.

In this chapter we assume that the carrier and symbol timing recovery circuit degradations are negligible and that the channel filters are equalized. In the last section of this chapter, we will show the P_e performance of QPSK, OQPSK, IJF-OQPSK (N=1) and TSI-OQPSK (n=2) resulted from different values of fade depth and channel spacings.

4.1 Simulation Model

The system model used in our adjacent channel satellite system simulation is shown in Fig. 4.1. The modulated signals in our system can be represented by complex baseband signals [4,13, 24,25]. Filtering is processed in the frequency domain with the aid of Fast Fourier Transform (FFT) techniques. The receive bandpass filter of the main (desired) channel is represented by its lowpass equivalent transfer function $H_R(f)$. The Fourier transform of the desired received signal, $R_o(f)$, is:

$$R_o(f) = H_R(f) \cdot F\{x_o(t)\} \tag{4.1}$$

and the Fourier transform of the received interference signal is:

$$R_i(f) = H_R(f) \cdot X_i(f \pm \Delta f) \tag{4.2}$$

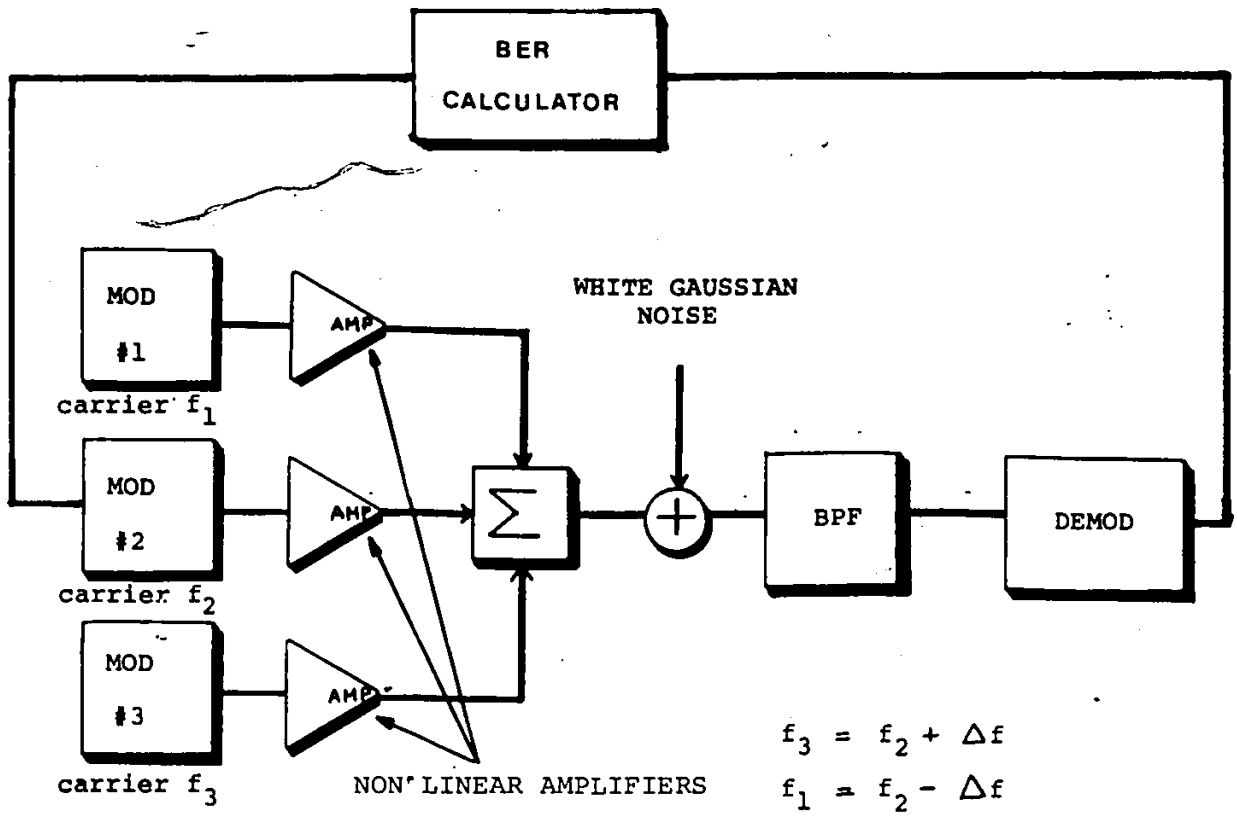

$f_b = \frac{1}{T_b}$ = bit rate of individual modulators.

Note: $T_s = 2\ T_b$ = Symbol duration.

NON-LINEAR AMPLIFIER MODELS USED IN THIS STUDY

a) Ideal hardlimiter (low power hardlimiter)

b) Saturated earth station HPA. AM/AM and AM/PM coefficients are specified by INTELSAT [10]

c) Low power hardlimiter in cascade with an INTELSAT type of HPA.

Fig. 4.1 Simulation model for probability of error computation and measurements

where $X_i(f) = F\left\{ x_i(t) \right\}$

$x_o(t)$ is the complex baseband signal of the main channel at the input of the receive BPF, and $x_i(t)$ is the complex baseband signal of the adjacent channel at the input of the receive BPF.

Carrier incoherence between the interfering channels and the desired channel is assured by the multiplication of $R_i(f)$ by $e^{j\Phi_i}$ where Φ_i is a random variable uniformly distributed over $(0, 2\pi)$. The lack of bit synchronization between the interfering channels and the desired channel is introduced by rotating the interfering complex baseband signal $r_i(t)$ by Π_i where Π_i is a random variable uniformly distributed over $(0, T_s)$ and where T_s is the symbol interval ($T_s = 2T_b$).

The interferring complex baseband signal is given by

$$r_i(t) = F^{-1}\left\{ R_i(f)\ e^{j\Phi_i} \right\} \qquad (4.3)$$

The noise free received signal is given by

$$r(t) = r_o(t) + \sum_{i=-M}^{M} r_i(t) \qquad (4.4)$$

where $r_o(t)$ is the receive signal of the desired channel.

As mentioned in Chapter Two, adjacent channel degradation is due primarily to the immediate adjacent channels. For this reason we use M = 1, that is, only two adjacent channels are considered.

In our model Fig. 4.1, the transmit sources are composed of six shift register arrays which generate variable length pseudo-random sequences. One sequence pair is used as the desired channel. The other two are used as the upper and lower adjacent channel interferences respectively. The filtering process is performed by multiplying the Fourier transform of the complex baseband signal by the lowpass equivalent transfer function of the filter and then transforming the result of the multiplication process back to the time domain [13, 19].

We note that no conventional transmit filter is used for TSI-OQPSK signals, as the equivalent filtering is achieved by the Two-Symbol-Interval encoder [26-27].

For the adjacent channel interference, the Fourier transform of the complex interfering baseband signal is shifted by +/- Δf ($\Delta f = f_2 - f_1 = f_3 - f_2$). The complex output of the receiver filter is converted into time domain original desired sequences; distorted by the effects of inter-symbol-interference.

The average signal power at the input to the decision threshold unit is computed and for each symbol, the amplitude at the sampling instant relative to its decision threshold is determined. For a specified power of Gaussian noise at the detector input, the individual symbol P_e is calculated according to theory [12-13, 19-20, 22, 24, 25]. The average of these calculated P_e's over the total transmitted symbol sequence is calculated to give the estimate of P_e for the given simulated system. This average P_e is associated with the ratio of the average signal power to the specified rms noise at the decision threshold input and is given by [52]:

$$P_e = \frac{1}{2M} \sum_{k=1}^{M} \left\{ P(e/r_I(kT_s)) + P(e/r_Q((k+1/2)T_s) \right\}$$

where M is the length of the transmitted pseudo-random sequence. $P(e/r_I(kT_x))$ and $P(e/r_Q((k+1/2)T_s)$ are the conditional error probabilities in an AWGN environment of the received in-phase ($r_I(kT_s)$) and quadrature ($r_Q((k+1/2)T_s)$) signals respectively [52].

The validity of the simulation results was carefully tested by running and averaging several simulations with different values of Φ_i and Π_i and by comparing some of these results to our

measured results reported in [9, 11, 14] and chapter 5.

The saturated amplifier shown in Figure 4.1 was modeled as an ideal hardlimiter and also as a saturated INTELSAT V TDMA earth station type of High Power Amplifier (HPA) [10]. For an ideal hardlimiter, the equations of the equivalent complex baseband components of a hardlimited signals were given in chapter 2 (eq. 2.22).

For the saturated INTELSAT V earth station HPA, the equivalent complex baseband components are represented by [28].

$$y^1_{IN}(t) = y_{IN}(t)\, p(r(t)) - y_{QN}(t)\, q(r(t)) \qquad (4.5)$$

$$y^1_{QN}(t) = y_{IN}(t)\, q(r(t)) + y_{QN}(t)\, p(r(t)) \qquad (4.6)$$

where $r(t) = \left\{ y^2_{IN}(t) + y^2_{QN}(t) \right\}^{1/2}$ is the envelope of the input signal and the polynominals $rp(r)$ and $rq(r)$ are expressed as

$$rp(r) = \sum_{i=1}^{M} a_{2i-1}\, r^{2i-1} \qquad (4.7)$$

$$rq(r) = \sum_{i=1}^{M} b_{2i-1}\, r^{2i-1} \qquad (4.8)$$

where M is the order of the polynominal and all even coefficients are zero. The coefficients (a_i, b_i) are determined by using polynominal fitting.

In the following sections, computer simulation results are presented that are based on the following filtering strategy:

FILTERING STRATEGY

TSI-OQPSK

No conventional transmit filter is used, as the equivalent filtering is achieved by the TSI processor. Receive filter: SAE filter ($\alpha = 0.4$) and linear zero forcing filter ($\alpha = 0.4$).

QPSK and OQPSK (*)

Transmit filter: $\sqrt{\alpha = .4}$ square root of raised-cosine filter with $\frac{x}{\sin x}$ amplitude compensation.

Receive filter: $\sqrt{\alpha = .4}$ raised cosine.

(*) This filtering strategy was selected as an illustrative example as it is identical with the INTELSAT V TDMA/DSI filtering requirements [10].

4.2 Performance of TSI-OQPSK Modems in a Hardlimited Channel

In this section, ideal hardlimiters are used as simplified models of the saturated amplifier shown in Figure 4.1. The computer simulated eye diagrams of hardlimited TSI-OQPSK, QPSK and OQPSK, signals in a noise free, equal power, adjacent channel interference environment and prior to the decision threshold are shown in Figure 4.2 (Channel Spacing $\Delta f = .67\ T_b$). The E_b/N_o improvement at $P_e = 10^{-6}$, of the SAE filter, over the Linear-Zero-Forcing filter operated in the AWGN and equal power adjacent-channel environment is shown in Figure 4.3. The equation of E_b/N_o *improvement* (I_1) is:

$$I_1 = D_{LZF} - D_{SAE} \tag{4.9}$$

where D_{LZF} = degradation (in dB) from the theoretical linear channel model with a linear zero forcing filter

D_{SAE} = degradation (in dB) from the theoretical linear channel model with a sum of approximate eye filter

We define degradation as:

$$D_x = (E_b/N_o)_p - (E_b/N_o)_t \qquad (4.10)$$

where x is the type of filter or the type of non-linear amplifier.

$(E_b/N_o)_p$ is the E_b/N_o required for the practical system in dB.

$(E_b/N_o)_t$ is the E_b/N_o of a theoretically ideal linear system in dB.

From Figure 4.3, it is evident that the SAE filter improves the P_e performance of both the n = 1 and n = 2 hardlimited TSI-OQPSK systems.

A comparison of the computer simulated P_e performance of hardlimited TSI-OQPSK, QPSK and OQPSK modems in an AWGN and equal power adjacent channel environment is shown in Figure 4.4. The results indicate the TSI-OQPSK modems have the best P_e performance in a hardlimited and narrow bandwidth system ($\Delta f \leq 1/T_b$). These results are in good agreement with the hardware measurement results reported in [11]. Among TSI-OQPSK modems, the case n = 2 has the best P_e performance when $\Delta f \leq 0.67/T_b$.

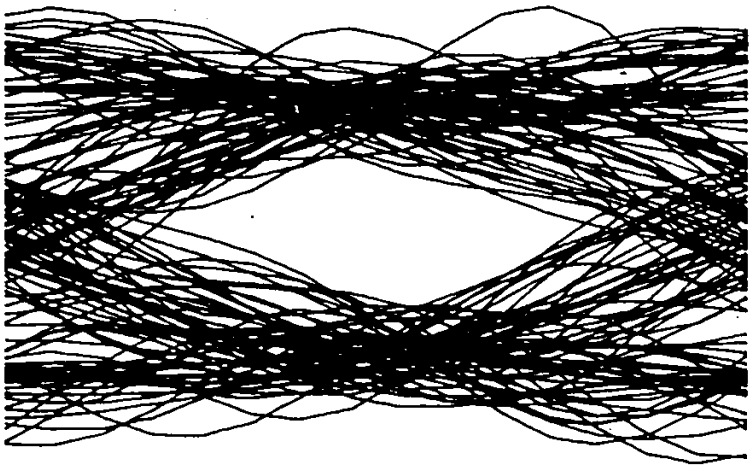

FIG. 4.2a EYE DIAGRAMS OF HARDLIMITED QPSK IN AN ADJACENT CHANNEL ENVIRONMENT ($\Delta f = .67/T_b$)
(Tx filter: $\sqrt{\alpha=.4}$ Raised cosine $\frac{\pi}{\sin \pi}$ compensation
(Rx filter: $\sqrt{\alpha=.4}$ Raised cosine

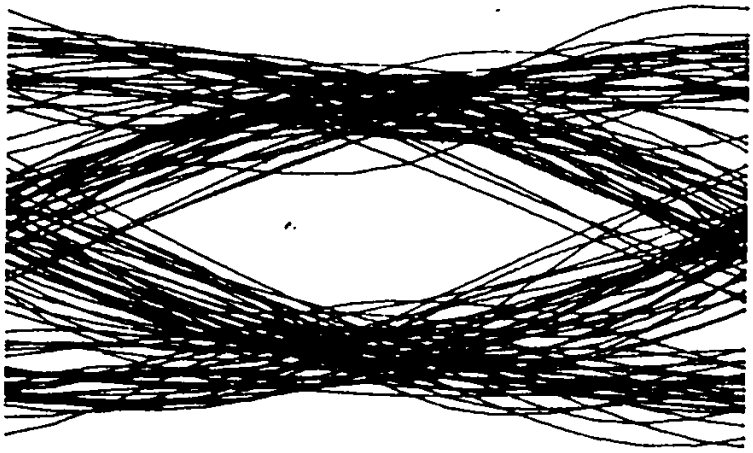

FIG. 4.2b EYE DIAGRAMS OF HARDLIMITED OQPSK IN AN ADJACENT CHANNEL ENVIRONMENT ($\Delta f = .67/T_b$)
(SAME FILTERS AS IN FIGURE 4.2a)

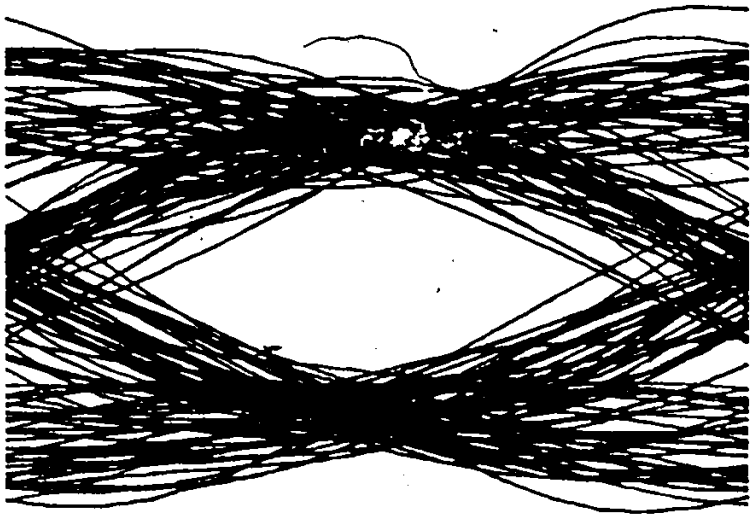

FIG. 4.2c EYE DIAGRAMS OF HARDLIMITED TSI-OQPSK (n = 1) IN AN ADJACENT CHANNEL ENVIRONMENT (SAE FILTER IS USED AS RECEIVE FILTER) ($\Delta f = .67/T_b$)

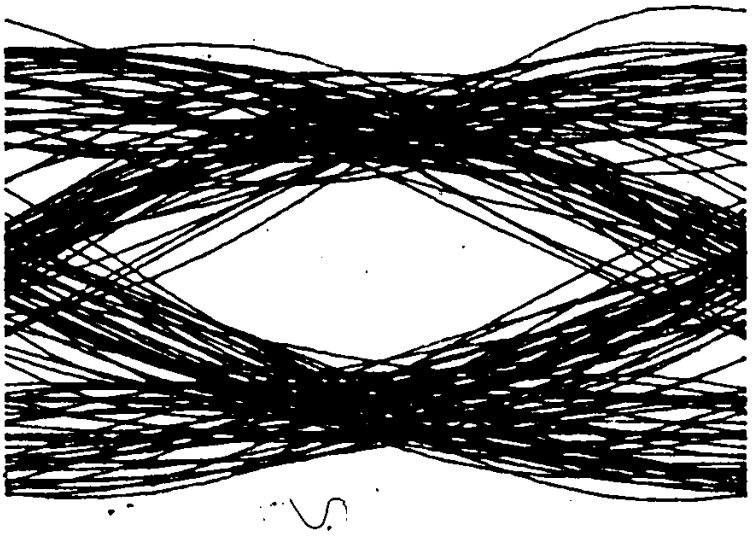

FIG. 4.2d EYE DIAGRAMS OF HARDLIMITED TSI-OQPSK (n = 2) IN AN ADJACENT CHANNEL ENVIRONMENT (SAE FILTER IS USED AS RECEIVE FILTER) ($\Delta f = .67/T_b$)

FIG. 4.3 E_b/N_o IMPROVEMENT OF A SAE FILTER OVER A LINEAR ZERO FORCING FILTER (AT $P_e = 10^{-6}$) FOR A HARDLIMITED TSI-OQPSK MODEM OPERATED IN AN AWGN AND ADJACENT CHANNEL ENVIRONMENT. (*)

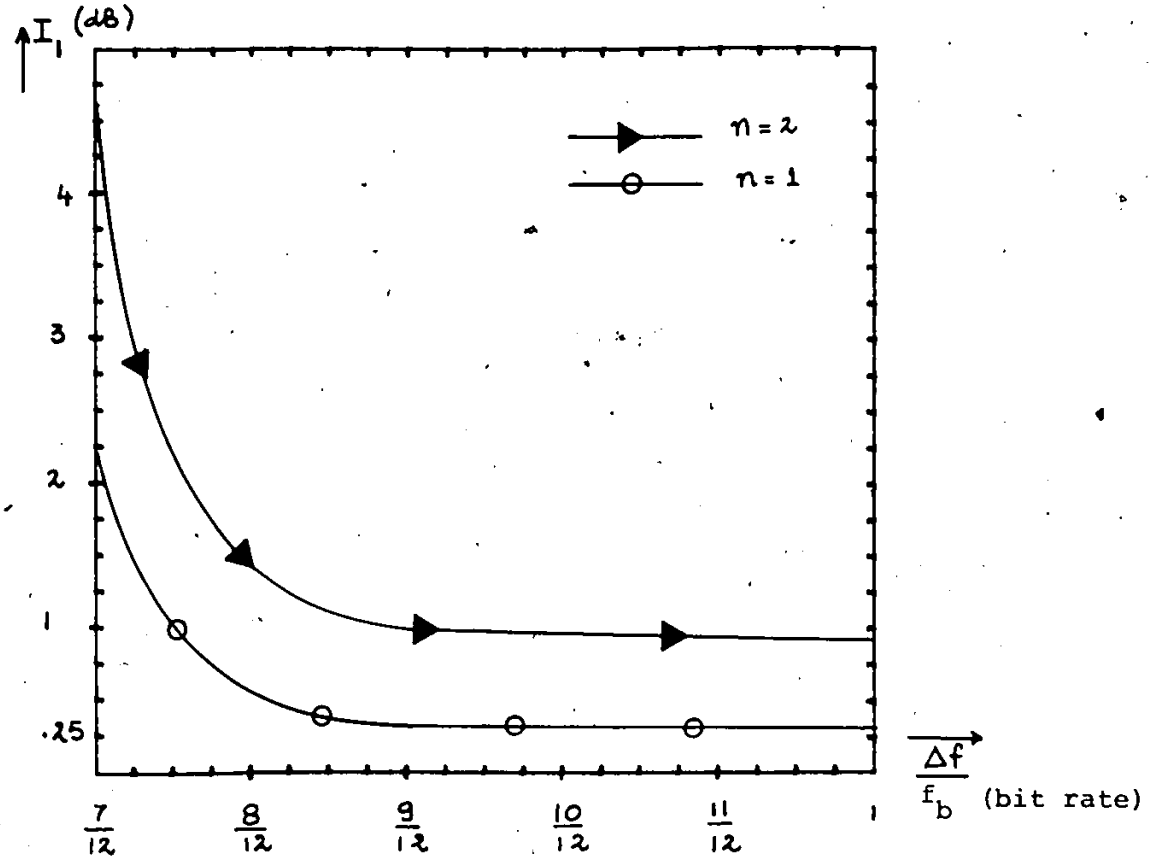

* (E_b/N_o IMPROVEMENT) dB = (DEGRADATION IF A LINEAR ZERO FORCING FILTER IS USED) dB - (DEGRADATION IF A SAE FILTER IS USED) dB

FIG. 4.4 E_b/N_o DEGRADATION (AT $P_e = 10^{-6}$) OF HARDLIMITED QPSK, OQPSK AND TSI-OQPSK MODEMS IN AN ADJACENT CHANNEL INTERFERENCE AND AWGN ENVIRONMENT. (SAE FILTER IS USED AS RECEIVE FILTER FOR TSI-OQPSK MODEMS) (*)

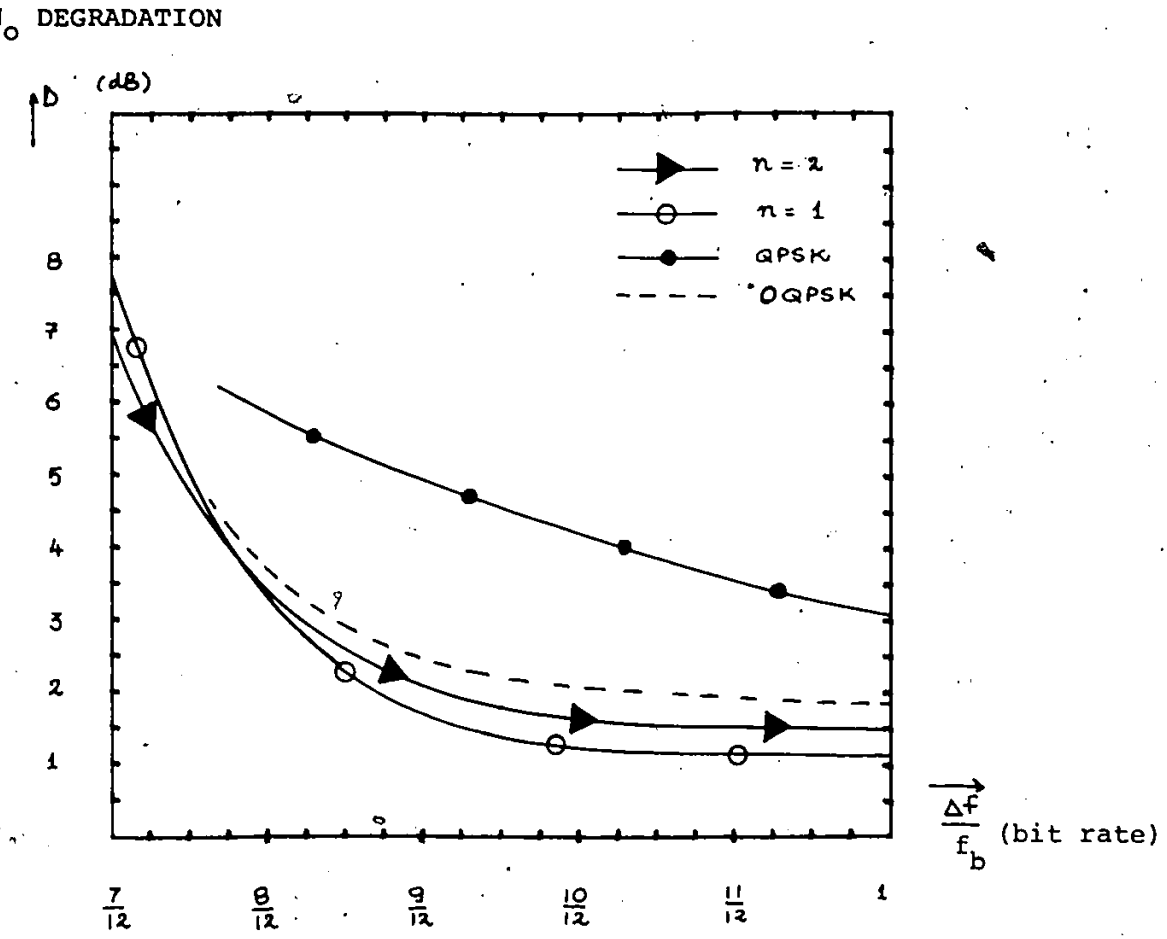

* (E_b/N_o DEGRADATION) dB = (E_b/N_o REQUIRED FOR THE PRACTICAL SYSTEM) dB - (E_b/N_o OF THEORETICAL IDEAL LINEAR SYSTEM) dB

This means that TSI-OQPSK n = 2 has a better P_e performance than SQORC [15-17] or IJF-OQPSK N = 1 [11 & 14, 46] (equivalent to TSI-OQPSK n = 1) in a narrow-bandwidth and hardlimited channel ($\Delta f \leq 0.67/T_b$). However, we should note that in this region, the E_b/N_o degradation caused by the spectral spreading of the *equal power*-saturated adjacent channels is very significant, i.e. more than 3 dB. If the permissible system degradation is in the order of 1 dB, then the n = 1 case *with* SAE *filters* leads to the most spectral efficient system design.

If one or both adjacent channels are higher than the desired channel, then the n = 2 system has the best performance. This is a realistic situation if the uplink of the desired channel is faded. An illustration of different values of fade depth is shown in section 4.4

4.3 Performance of TSI-OQPSK Modems in a Saturated INTELSAT V Type HPA Channel

In this section, the simulated INTELSAT V type earth station HPA [10] is operated at 0 dB input backoff and used as the saturated amplifier shown in Figure 4.1. The PSDs of TSI-OQPSK, pre-filtered QPSK and OQPSK, after passing through the saturated HPA INTELSAT V were shown in Figure 2.17. As in the case of hardlimiter, the PSDs of the saturated HPA - TSI-OQPSK modems show a significant spectral density advantage over saturated HPA - QPSK and OQPSK. Figure 2.17 also indicates that TSI-OQPSK n = 2 has a lower spectral restoration than SQORC or IJF-OQPSK N = 1 (TSI-OQPSK n = 1) in the most significant PSD region, $((f-f_c).\ T_b) \leq 1$. The SAE filter also improves the P_e performance of saturated HPA TSI-OQPSK modems compared with that of the Linear-Zero-Forcing filter. The E_b/N_o improvement at $P_e = 10^{-6}$ is shown in Figure 4.5.

Figure 4.6 shows the P_e performance of the saturated HPA TSI-OQPSK, QPSK and OQPSK modems in an AWGN and equal power-adjacent channel interference environment. The results indicate

that TSI-OQPSK modems have the best P_e performance in a narrow bandwidth channel ($\Delta f \leq 1/T_b$). TSI-OQPSK n = 2 has the best P_e performance when $\Delta f \leq 0.67/T_b$ and TSI-OQPSK n = 1 has the best P_e performance when $\frac{0.67}{T_b} \leq \Delta f \leq 1/T_b$.

FIG. 4.5 E_b/N_o IMPROVEMENT OF A SAE FILTER OVER A LINEAR ZERO FORCING FILTER (AT $P_e = 10^{-6}$) IN A SATURATED HPA-TSI-OQPSK MODEM OPERATED IN AN AWGN AND ADJACENT CHANNEL ENVIRONMENT. (*)

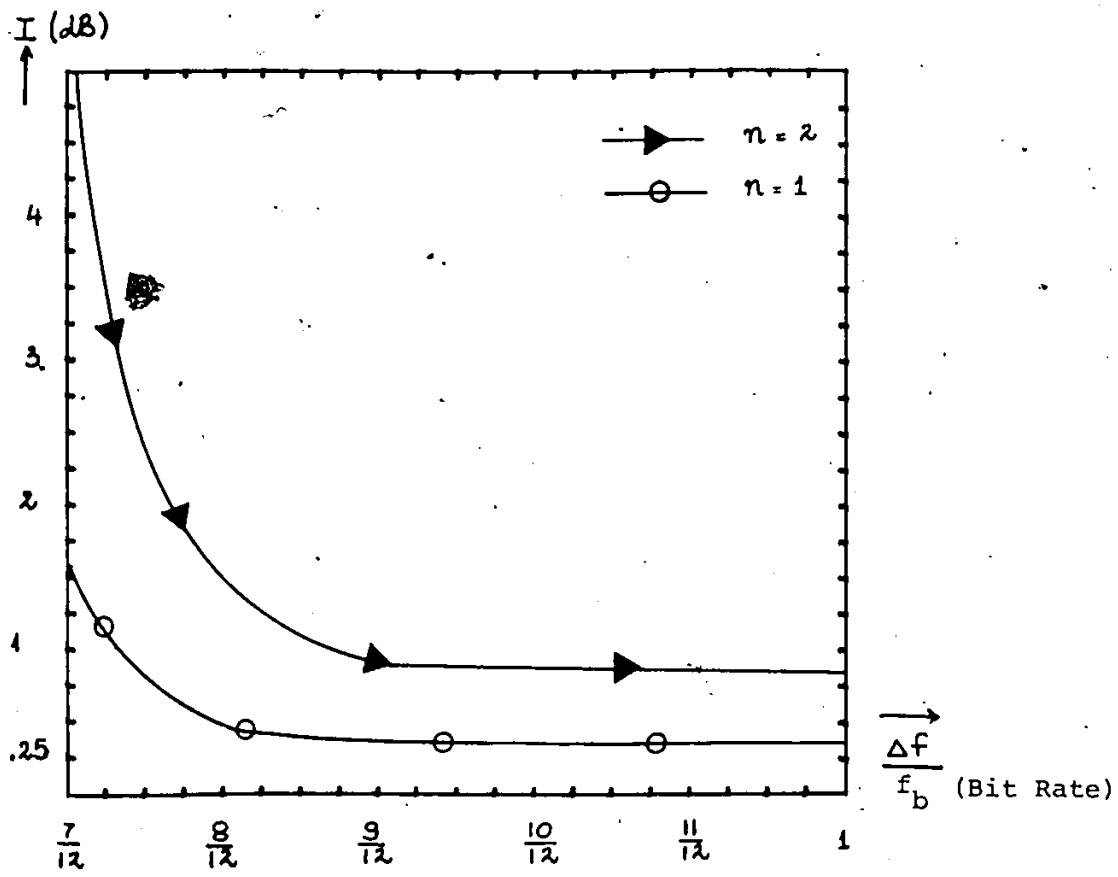

* (E_b/N_o IMPROVEMENT) dB = (DEGRADATION IF A LINEAR ZERO FORCING FILTER IS USED) dB - (DEGRADATION IF A SAE FILTER IS USED) dB

FIG. 4.6 E_b/N_o DEGRADATION OF SATURATED HPA-QPSK, OQPSK AND TSI-OQPSK MODEMS (AT $P_e = 10^{-6}$) IN AN ADJACENT CHANNEL WITH AWGN ENVIRONMENT. (SAE FILTER IS USED AS RECEIVE FILTER FOR TSI-OQPSK MODEMS). (*)

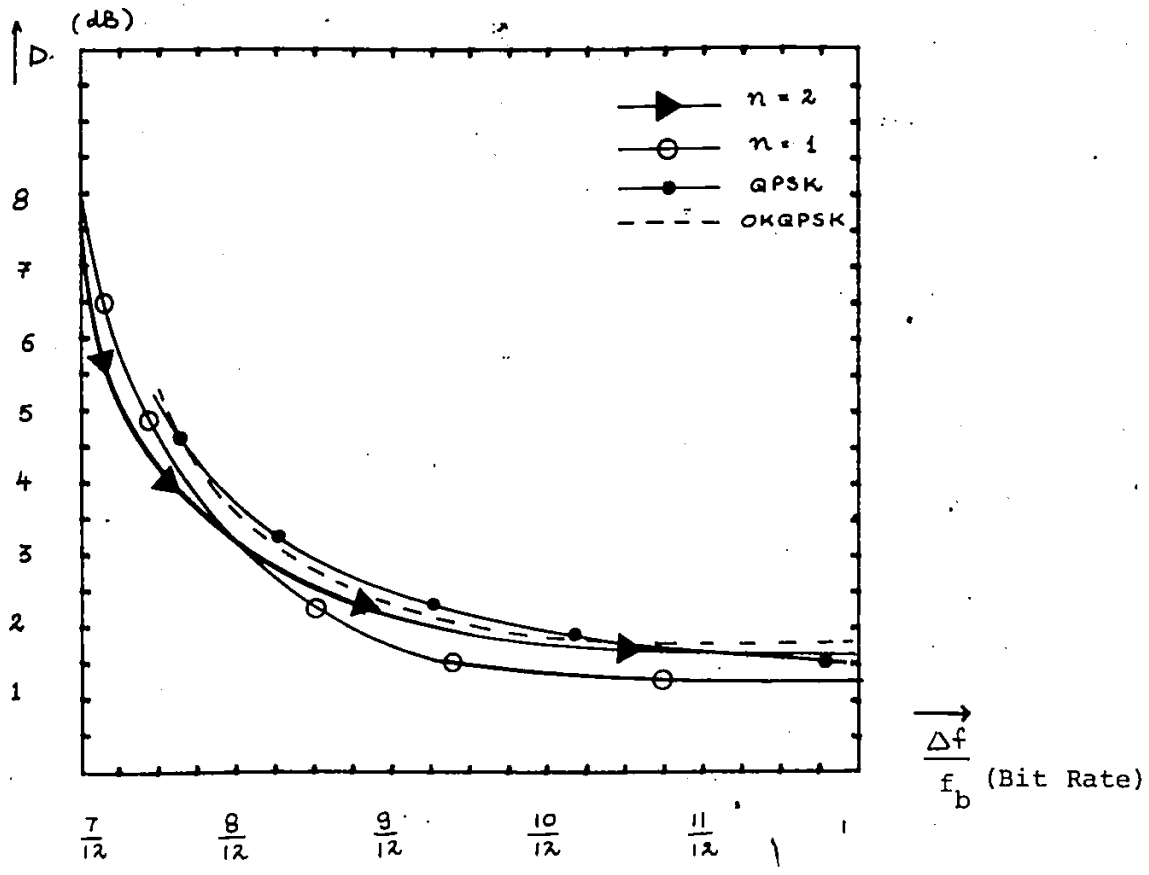

* (E_b/N_o DEGRADATION) dB = (E_b/N_o REQUIRED FOR THE PRACTICAL SYSTEM) dB - (E_b/N_o OF THEORETICAL IDEAL LINEAR SYSTEM) dB

4.4 Performance of TSI-OQPSK Modems in a Cascaded-Hardlimited and Saturated HPA System

In this section we show, that by introducing a low-power hardlimiter (having a negligible AM/PM) prior to the input of the saturated earth station HPA, the P_e performance of TSI-OQPSK modems *improves significantly*. However, this improvement *does not* occur for QPSK and OQPSK modems. The E_b/N_o improvement at $P_e = 10^{-6}$ of TSI-OQPSK modems, when a hardlimiter is placed prior to the input of the saturated HPA is shown in Figure 4.7. The E_b/N_o improvement (I_2) due to the hardlimiter is given by:

$$I_2 = {}^{D}\text{saturated HPA} - {}^{D}\text{hardlimited-saturated HPA}$$

where the definition of the term "Degradation" D_x has been given in eq. (4.10).

The SAE filter also improves the P_e performance of TSI-OQPSK Modems compared with Linear-Zero-Forcing filters, when a hardlimiter is placed prior to the HPA input. However, this improvement is almost the same as the improvement in the hardlimited case given in Figure 4.3. A comparison of the P_e performance between saturated HPA-QPSK and OQPSK

FIG. 4.7 E_b/N_o IMPROVEMENT OF SATURATED HPA-TSI-OQPSK MODEMS WHEN A HARDLIMITER IS PLACED PRIOR TO THE HPA INPUT (AT $P_e = 10^{-6}$) IN AN AWGN AND ADJACENT CHANNEL INTERFERENCE ENVIRONMENT (SAE FILTER IS USED AS RECEIVE FILTER) (*)

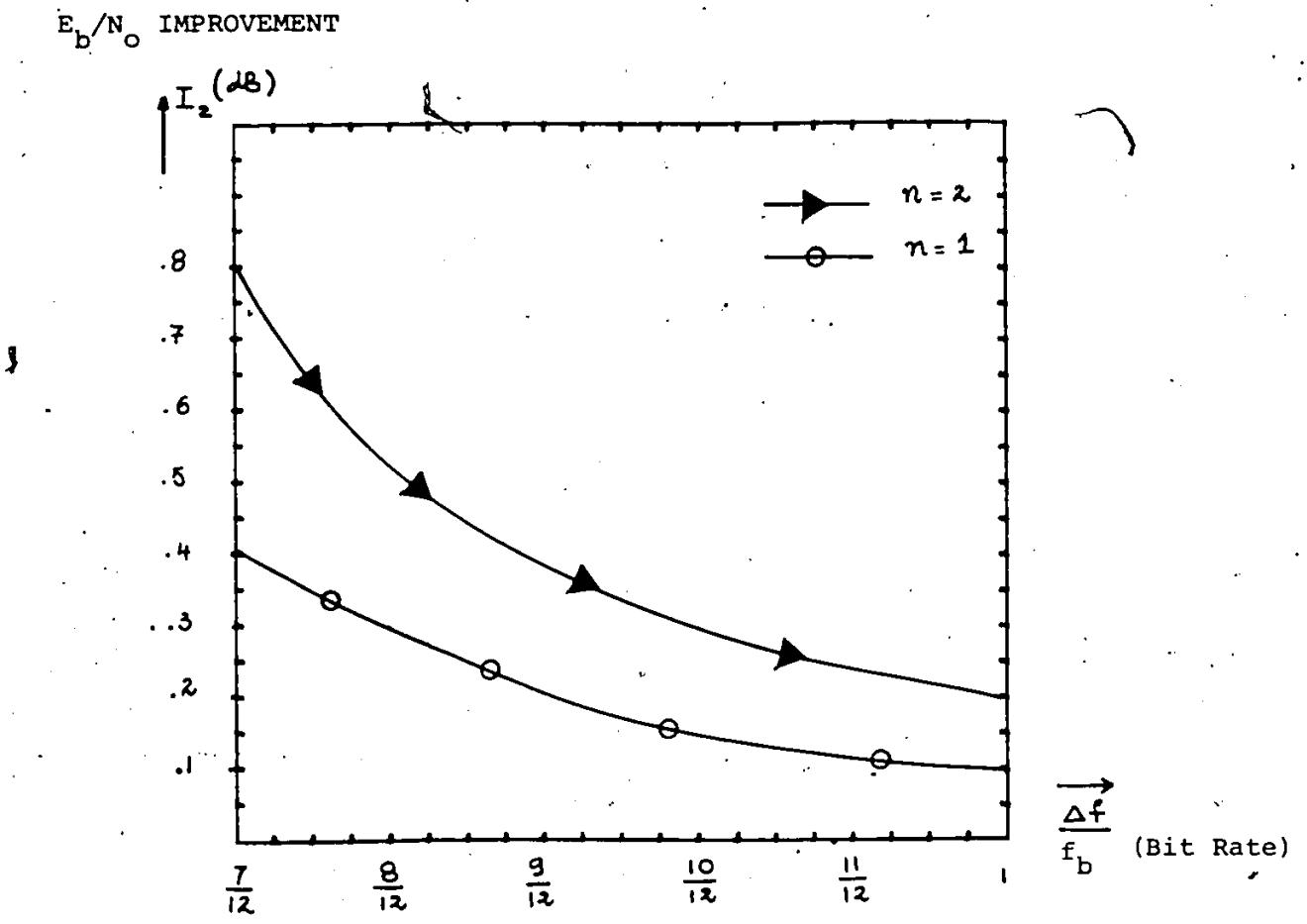

* $(E_b/N_o$ IMPROVEMENT) dB = (DEGRADATION OBTAINED FROM AN HPA-TSI-OQPSK MODEM) dB - (DEGRADATION OBTAINED FROM A HARD-LIMITED - HPA-TSI-OQPSK MODEM) dB

FIG.4.8 E_b/N_o DEGRADATION OF A SATURATED HPA-QPSK, OQPSK AND CASCADED HARDLIMITER - HPA-TSI-OQPSK MODEMS IN AN ADJACENT CHANNEL AND AWGN INTERFERENCE ENVIRONMENT. (SAE FILTER IS USED AS RECEIVE FILTER FOR TSI-OQPSK MODEMS). (*) (AT $P_e = 10^{-6}$)

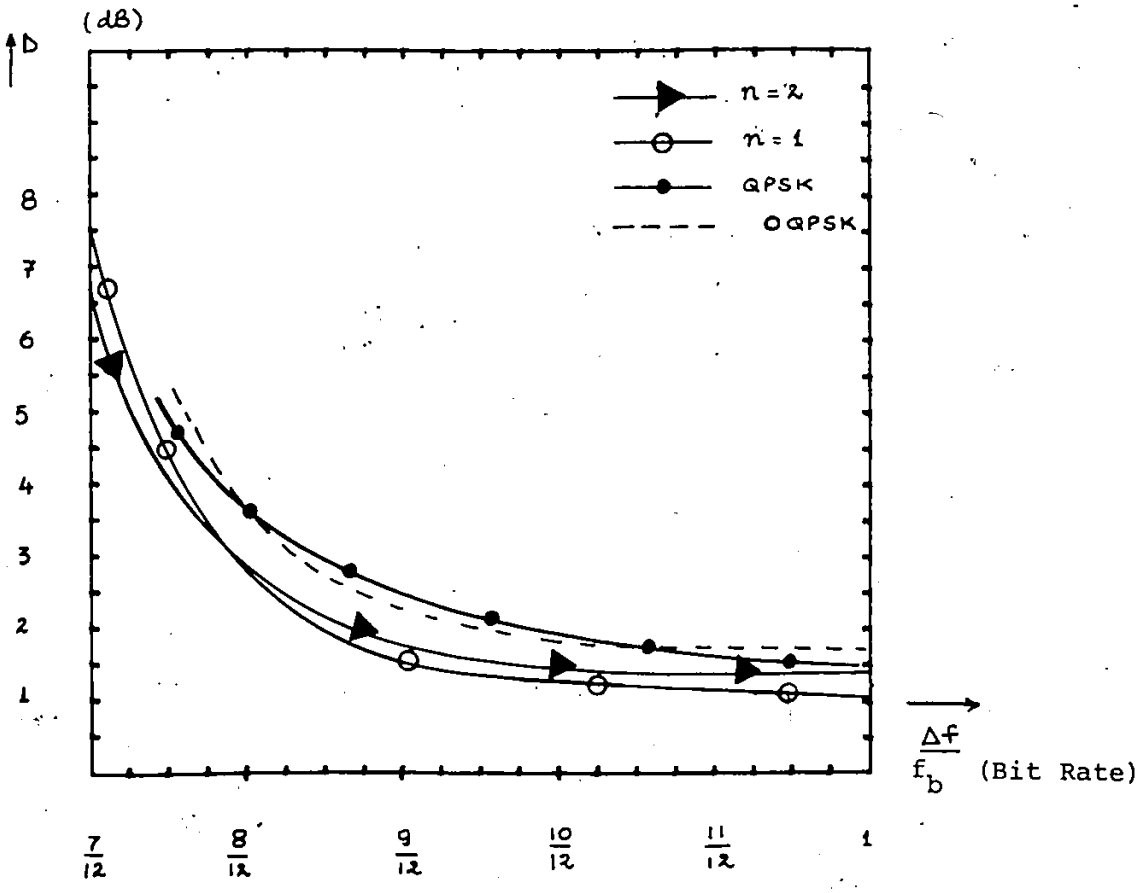

* (E_b/N_o DEGRADATION) dB = (E_b/N_o REQUIRED FOR THE PRACTICAL SYSTEM) dB - (E_b/N_o OF THEORETICAL IDEAL LINEAR SYSTEM) dB

modems with cascaded hardlimiter and saturated HPA TSI-OQPSK modems is shown in Figure 4.8. The results indicate that TSI-OQPSK modems have the best P_e performance in a narrow bandwidth channel ($\Delta f.T_b \leq 1$). Among the TSI-OQPSK modems, TSI-OQPSK n = 2 has the best P_e performance in this class when $\Delta f\ T_b \leq 0.67$, TSI-OQPSK n = 1 has the best P_e performance when $0.67/T_b \leq \Delta f \leq 1/T_b$.

In chapter 3, we showed that the C/I power ratio of TSI-OQPSK (n = 2) is greater than for TSI-OQPSK (n = 1). The higher C/I advantages of the n = 2 case become more evident when the received modulated carrier power of the main channel is below that of the adjacent channels. This situation may occur in the case of an *up-link fade* of the desired channel. Figure 4.9 presents the E_b/N_o degradation as a function of the fade depth of the desired channel. As the main channel is attenuated, the adjacent channel interference becomes predominant and for this reason the modulation technique which creates less ACI provides better performance. As an example, for a fade depth of 12 dB of the desired channel, the TSI-OQPSK modems exhibit only 2 dB degradation; the performance degradation of QPSK modem is more than 7 dB (see

Figure 4.9.b). These results indicate a significant performance improvement of the saturated HPA-SCPC system with TSI-OQPSK modems.

Also from Fig. 4.9, the P_e performance of TSI-OQPSK ($n=2$) modem is improving and better than that of the other modems as the channel spacing is smaller.

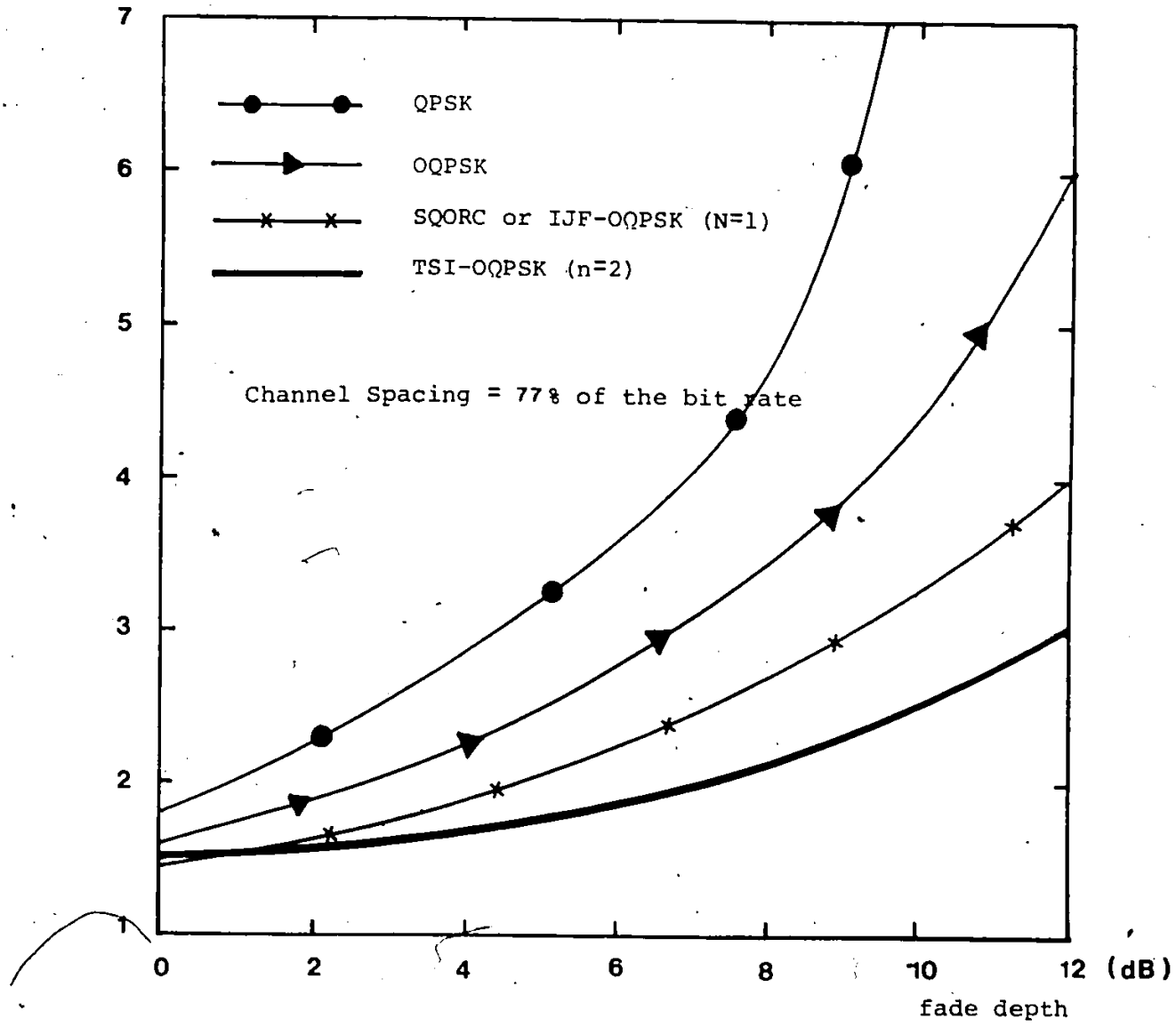

Fig. 4.9.a Eb/No degradation versus fade depth of the desired channel (spacing of 77 percent of the bit rate, compared to Eb/No = 8.4 dB for $P_e = 10^{-4}$)

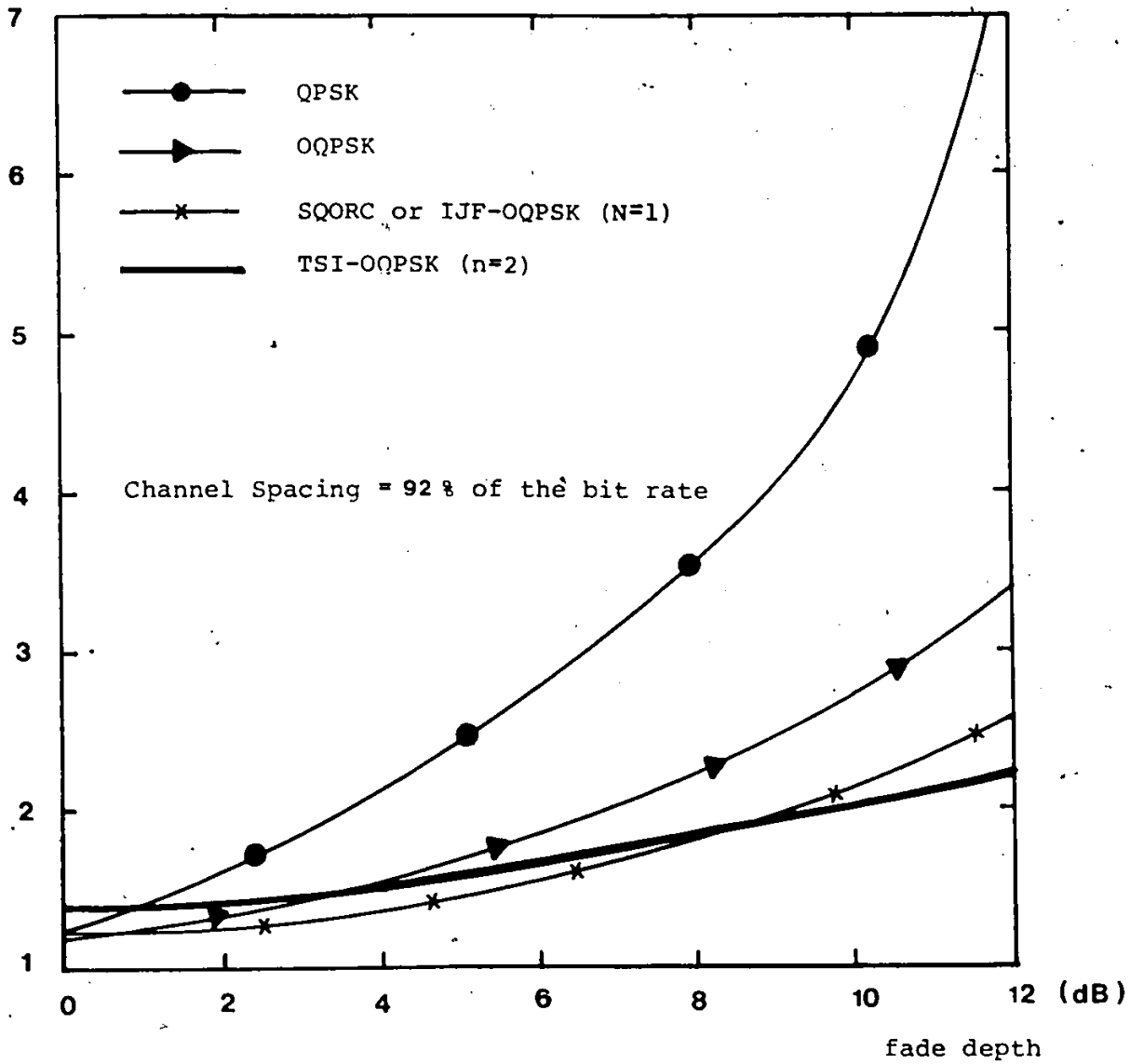

Fig. 4.9 b Eb/No degradation versus fade depth of the desired channel (spacing of 92 percent of the bit rate, compared to Eb/No = 8.4 dB for $P_e = 10^{-4}$)

CHAPTER FIVE

DESIGN AND EVALUATION OF A TSI-OQPSK MODEM

This Chapter highlights the design and the basic operating principles of the TSI-OQPSK modem. One may find it useful to refer to Chapters 2, 3 and 4 occasionally to help in understanding the modem and its operation.

The TSI-OQPSK modem enables the user to transmit and receive digital signals over a nonlinearly amplified channel without significant degradation. The modem uses a type of phase modulation: Offset-Quadrature Phase Shift Keying, and the digital signals are encoded by TSI encoders prior to modulation. It is the aim of this chapter to verify the computer simulated results and describe the philosophy of the design.

5.1 TSI-OQPSK Modulator

The block diagram of a TSI-OQPSK Modulator was presented in Chapter 2 (Fig. 2.3). The input data is converted into two data streams I and Q which represent the in-phase and quadrature channel respectively. The data stream of the Q channel is

delayed by T_b. Two TSI encoders are used to shape the binary data of the I and Q channels. The TSI signals can be generated using the Non-linear Switching Filter [7, 9, 18] or Pulse Overlapping concepts [7, 15, 35]. The second concept has more advantages because it can be used in a flexible rate mode.(*)

5.1.1 Nonlinear Switching Filter Concept (NLSF)

Fig. 5.1 shows the block diagram of the TSI signal encoder using the NLSF concept.

The input to the encoder is a Non-Return-to-Zero data (NRZ) stream and the output of the TSI encoder is the encoded TSI stream.

As we described in Chapter Two, the encoded signals are the combinations of two DC signals and two sinusoidal signals. From Fig. 5.1, the data input signals are synchronized with the sinusoidal signals by referencing to the "CLOCK". Some delay may be

---

* Note that there are some other hardware implementation techniques such as in Ref.[29].

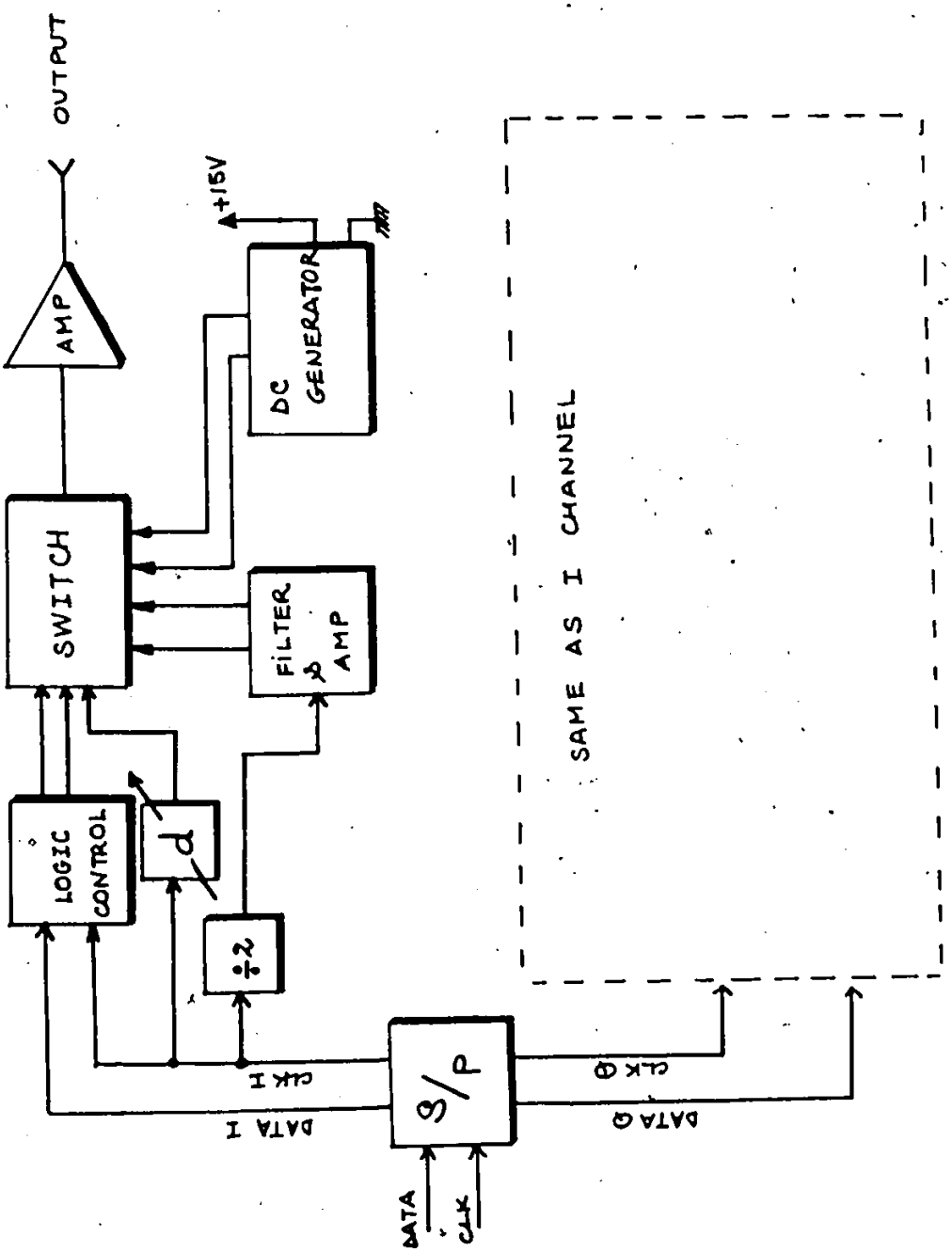

Fig. 5.1 Block Diagram of the TSI baseband encoder using NLSF concept

added so that the transitions of the data stream are exactly at the maximum or minimum of the sinusoidal signal. Two digital signals controlled the analog switch to select one of the four input signals. The output signals of the TSI encoder are amplified to meet the input level requirements of the modulator.

An example of TSI (n = 1) signal generation using the NLSF concept is described in Fig. 5.2. In this example the four switching signals are:

$$S_1 = -S_2 = A$$

$$S_3 = -S_4 = A \sin \frac{\pi t}{T_s} \qquad |t| \leq \frac{T_s}{2}$$

We can see that the maximum and the minimum of the TSI encoded signals occur at the transition points of the input data. By triggering the encoded signals with the synchronized CLOCK, the measured TSI signal eye diagram is obtained and shown in Fig. 5.2b.

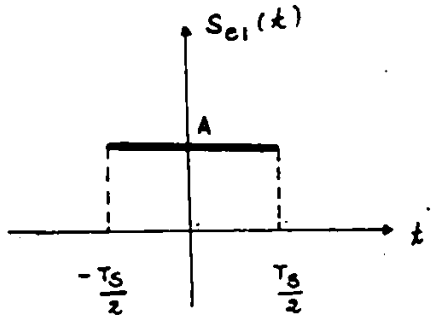

$$s_{el}(t) = \begin{cases} A, & |t| \leq \frac{T_s}{2} \\ 0 & \text{elsewhere} \end{cases}$$

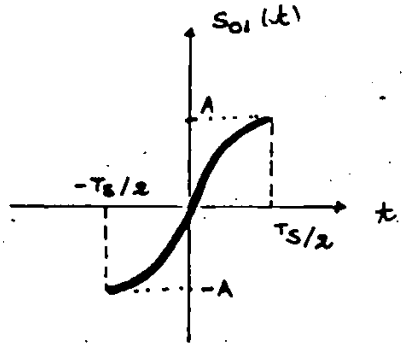

$$s_{o1}(t) = \begin{cases} A\sin\frac{\pi t}{T_s} & |t| \leq \frac{T_s}{2} \\ 0 & \text{elsewhere} \end{cases}$$

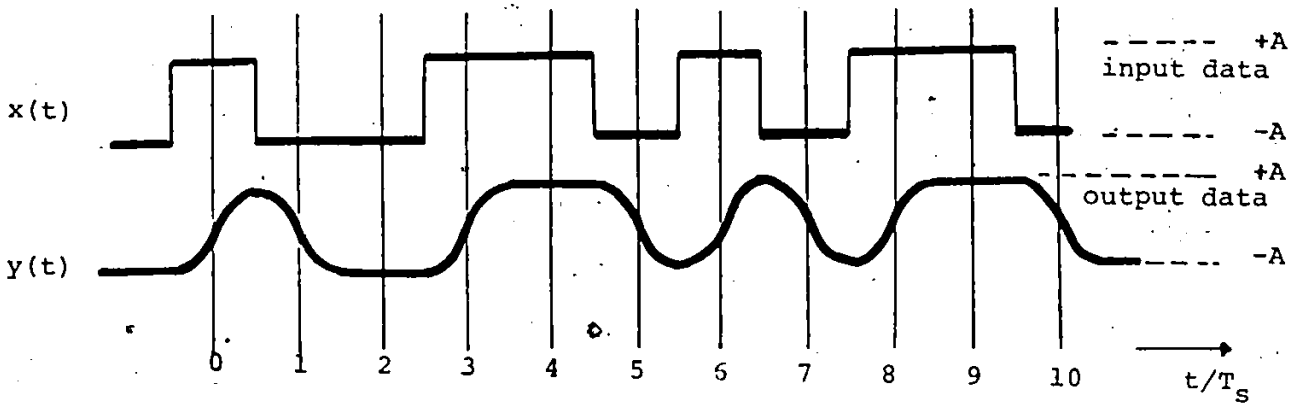

a/ example of NLSF concept

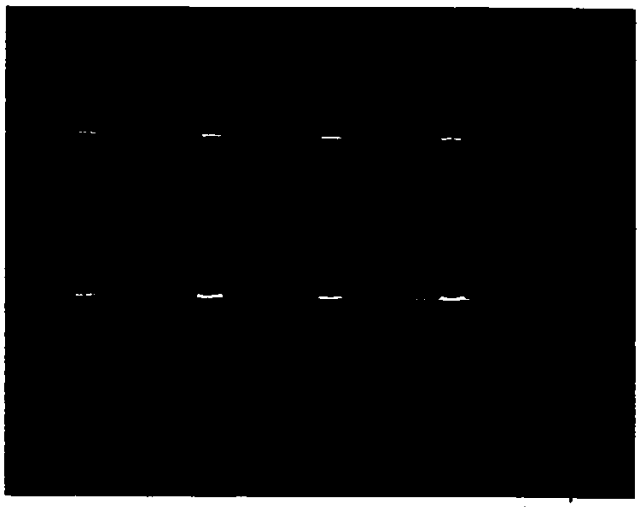

b/ measured eye diagram of y(t) for the n = 1 case

300m volts

Fig. 5.2 An example of a TSI signal encoding using the NLSF concept

The schematic diagram of a TSI encoder (n = 1) using the NLSF concept is shown in Fig. 5.3. U1, U2 and U8 are used to synchronize the input data and the CLOCK. Both the input data and the CLK must satisfy the TTL level definitions. U3, U6, U9, U11 are used to generate two control signals. These control signals are dependent on the present and previous input data signals (pin 5 U3). In order to synchronize the input data stream with the sinusoidal signal, the Filter and Amplifier circuit (Fig. 5.3) uses the reference CLK signal as the input signal (pin 3 U9). U22 are used to buffer the sinusoidal signals and DC signals prior to the analog switch (U16). U7 and U14 adjust the positions of the control signals so that the maximum and minimum of the encoded signals occur at the data transition points. U18 eliminates the harmonic signals and buffers the output signals.

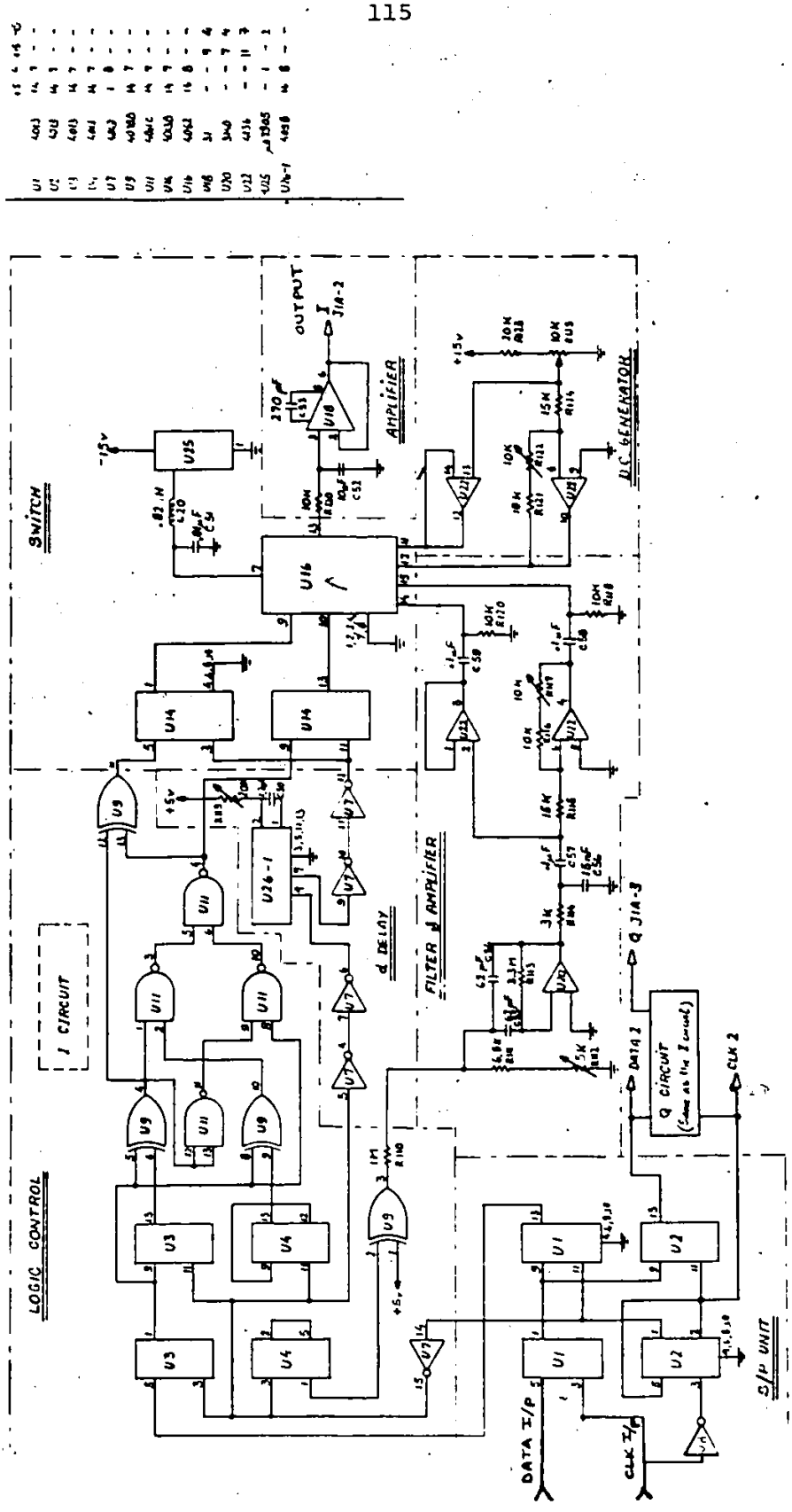

Fig. 5.3. TSI signal encoder (n = 1) using NLSF concept

5.1.2 Pulse Overlapping Concept

The block diagram of a practical implementation of a TSI signal encoder, using the double interval pulse overlapping concept is shown in Fig. 5.4. The input data is converted into a Bipolar waveform (BIP), delayed and multiplied by the weighting coefficients b_m and then added together. The total delay time (d) for each step and the total (2N+1) delay elements must satisfy the equation $dN=T_s$. The output signal prior to the lowpass filter is

$$S'(t) = \sum_{m=-N}^{N} b_m x'(t_m)$$

where b_m is the weighting coefficients of S(t) at time t_m and t_m is the sampling time. Fig. 5.5 shows an example of a TSI signal encoder (n = 1) using pulse overlapping concept.

Due to the sampling and adding of the delayed signals, the harmonic signals are generated. These harmonic signals can be eliminated by using a simple low pass filter called "REJECT FILTER". Note that the 3 dB cut off frequency of those filters must be smaller than the sampling rate. The schematic

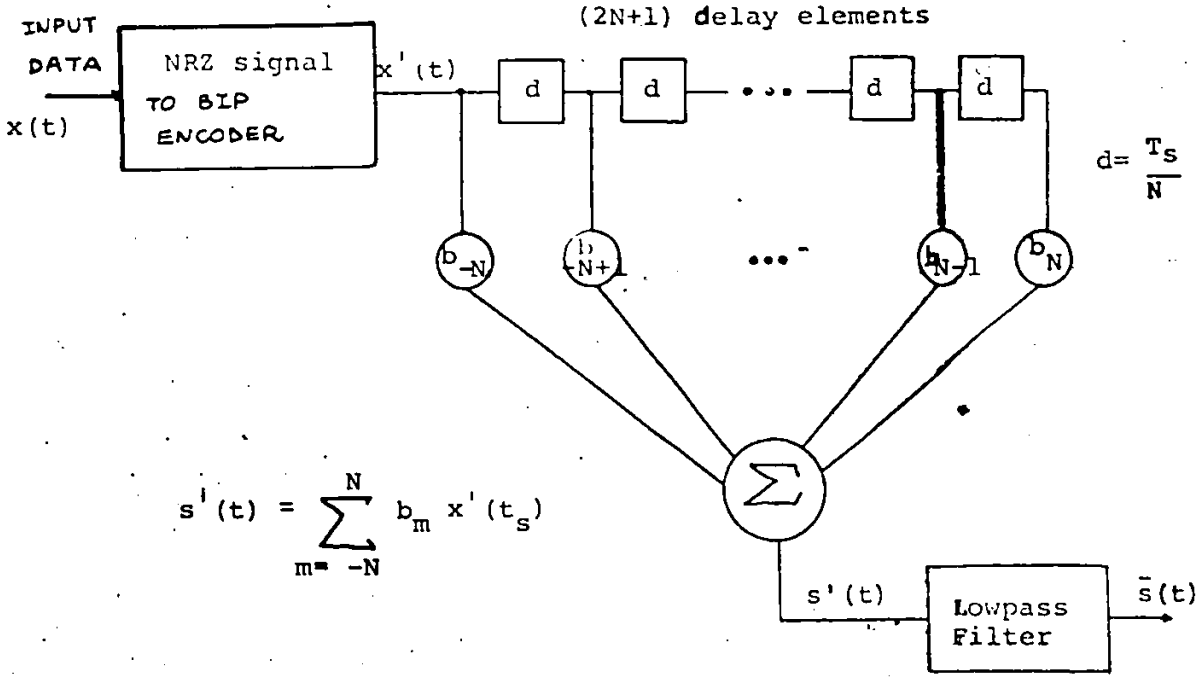

Fig. 5.4 Block diagram of a TSI signal encoder using the pulse overlapping concept

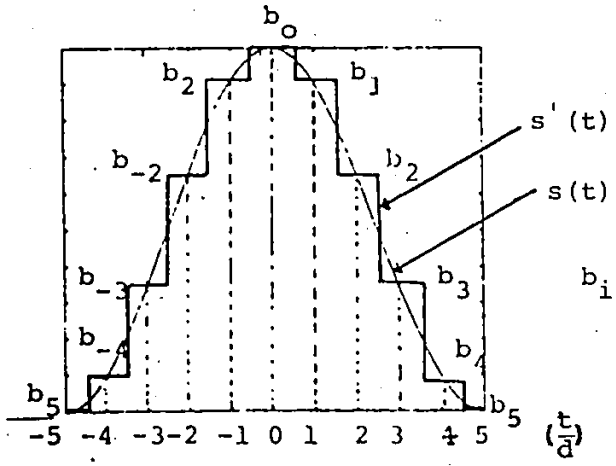

Fig. 5.5 An example of the encoder pulse response

$N = 5$

$s_1(t) = \frac{1}{2}(1 + \cos\frac{\pi t}{T_s})$ $\quad (n = 1)$

diagram of a TSI signal encoder (n = 1) using Pulse overlapping concept is shown in Fig. 5.6. The value of N in this circuit is equal to 8 and the sampling CLK is 8 times larger than the data rate. U9 to U12 are used to generate the BIP signals. U1 to U4 and U5 to U8 are used to generate the delayed pulses. U13 is used to overlap (add up) the positive and negative TSI pulses to generate TSI signals. The circuit shown in Fig. 5.6 is designed for 32 kb/s data rate and the coefficients b_m are the ratios between R_m (m = 0, 2, 4, 6,...) and R(105 Ω).

We note that by changing the values of R_m in Fig. 5.6, (m = 0, 2, 4, ...) the output pulse shape will vary. Fig. 5.7 shows the measured TSI pulse shapes before and after the "reject" filter (LPF) for the n = 1 and n = 2 case (N = 8). The input of the TSI encoder is a single pulse with duration T_s.

Fig. 5.8 shows the encoded waveforms before and after the "reject" filter for TSI signals (n = 1 and n = 2) (N = 8). The input of the TSI encoder is a pseudo random data stream, T_s = 1/32 (msec).

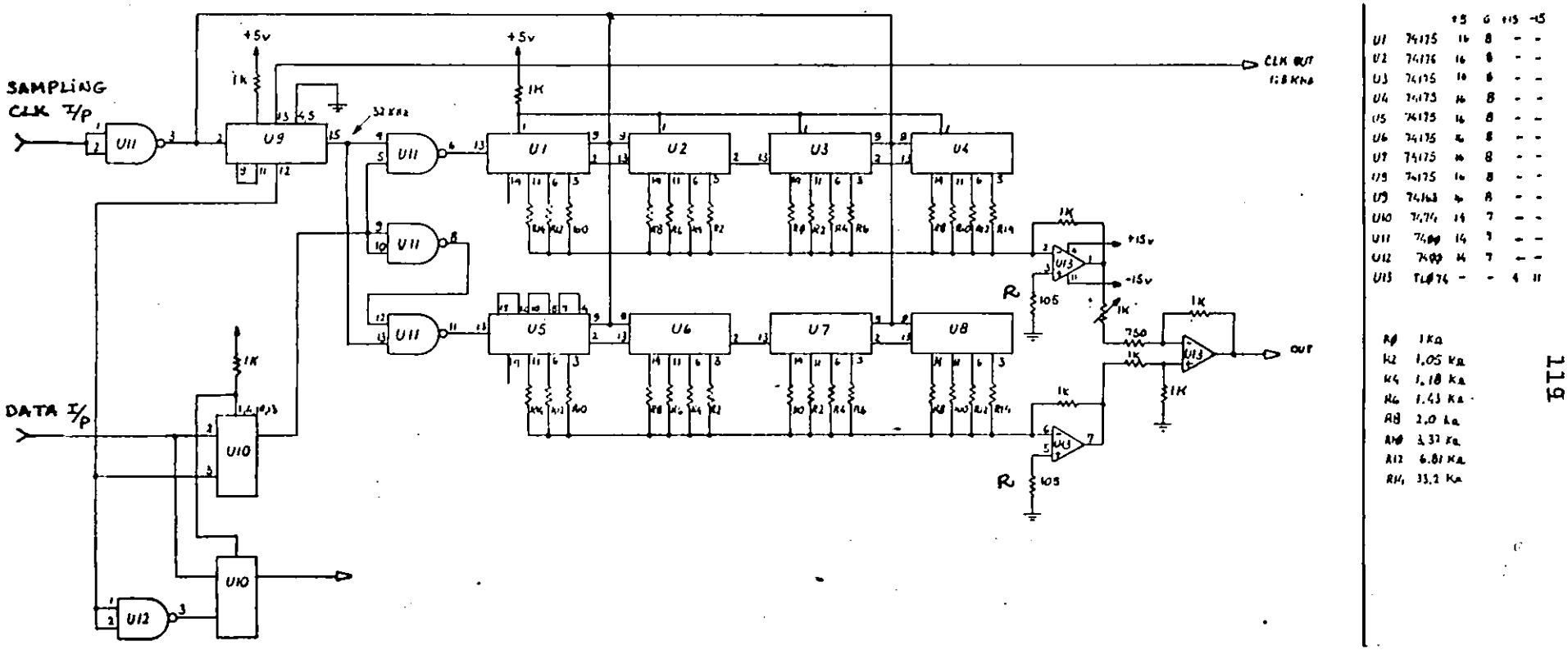

		+5	G	+15	-15
U1	74175	16	8	-	-
U2	74175	16	8	-	-
U3	74175	16	8	-	-
U4	74175	16	8	-	-
U5	74175	16	8	-	-
U6	74175	16	8	-	-
U7	74175	16	8	-	-
U8	74175	16	8	-	-
U9	74163	16	8	-	-
U10	7474	14	7	-	-
U11	7409	14	7	-	-
U12	7409	14	7	-	-
U13	TL074	-	-	4	11

R0	1 KΩ
R2	1.05 KΩ
R4	1.18 KΩ
R6	1.43 KΩ
R8	2.0 KΩ
R10	3.32 KΩ
R12	6.81 KΩ
R14	33.2 KΩ

Fig. 5.6. Pulse overlapping generator

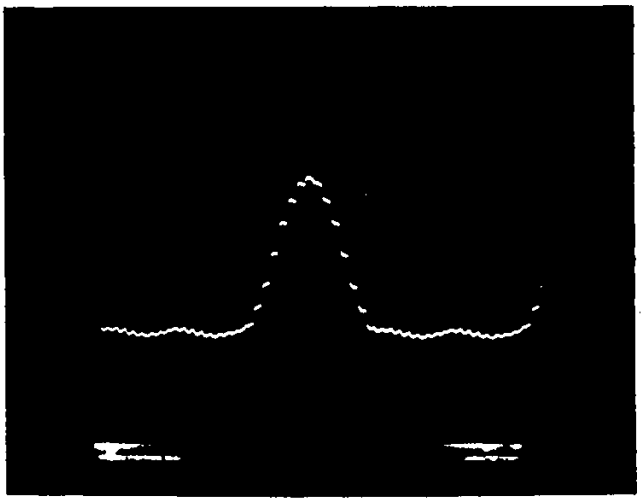

Ver: 20 usec/div
Hor: 0.1V/div

Fig. 5.7a. Pulse Shape $S_1(t)$ before Filtering(*)

* Note that: Input of the TSI encoder is a single pulse with duration T_s = 1/32 (msec)

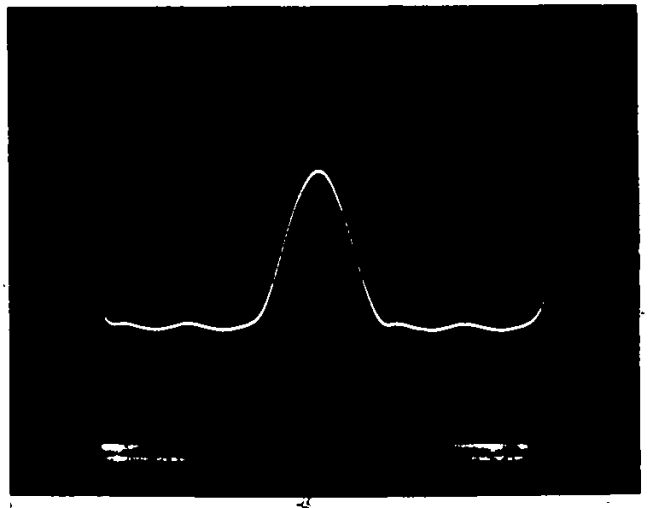

Ver: 20 usec/div
Hor: 0.1V/div

Fig. 5.7b. Pulse Shape $S_1(t)$ after Filtering(*)

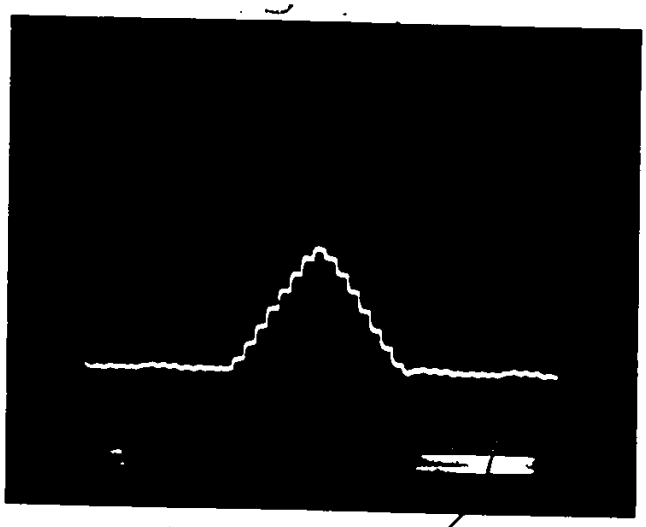

Ver: 20 usec/div
Hor: 0.1 Volt/div

Fig. 5.7c. Pulse shape $S_2(t)$ before filtering(*)

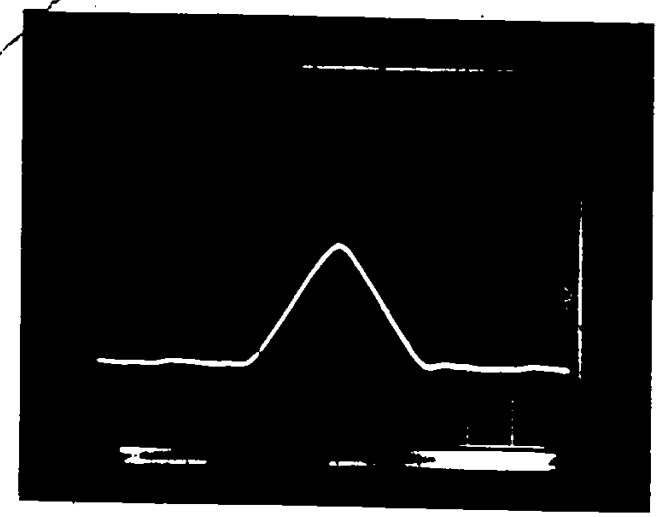

Ver: 20 usec/div
Hor: 0.1 Volt/div

Fig. 5.7d. Pulse shape $S_2(t)$ after filtering(*)

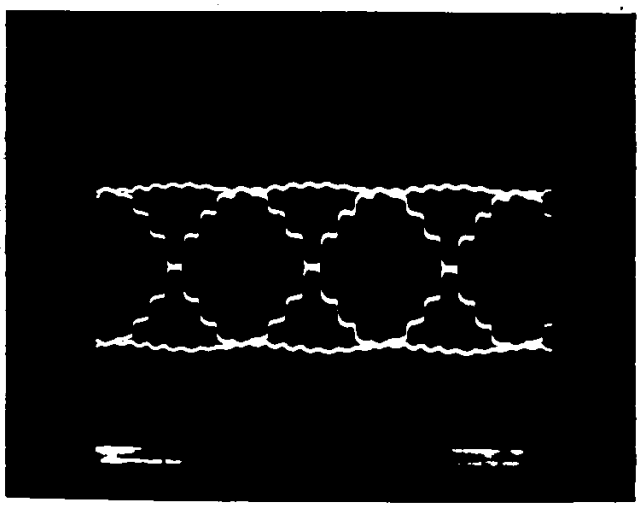

Ver: 10 usec/div
Hor: 0.1 Volt/div

Fig. 5.8a. Eye diagrams y(t) of TSI signals (n = 1) before the "reject" filter

* Note that: Input to the TSI encoder is a pseudo random data with T_s = 1/32 (msec)

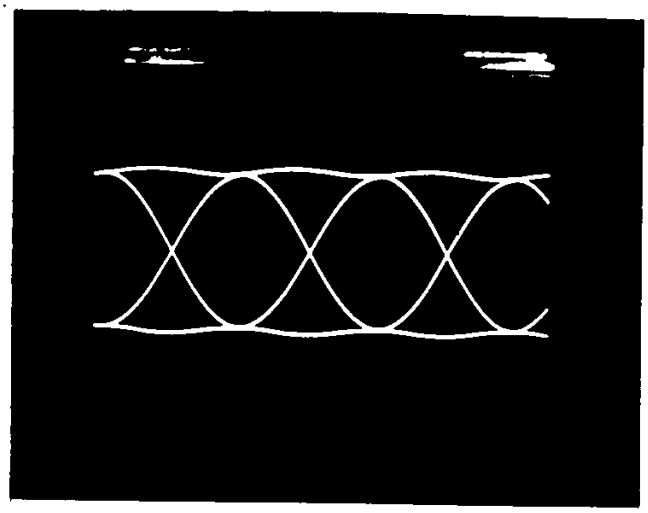

Ver: 10 usec/div
Hor: 0.1 Volt/div

Fig. 5.8b. Eye diagrams y(t) of TSI signal (n = 1) after the "reject" filter (*)

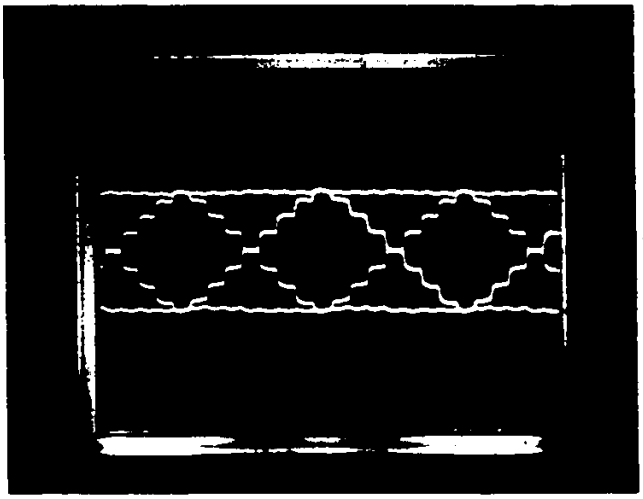

Ver: 10 usec/div
Hor: 0.1 Volt/div

Fig. 5.8c. Eye diagrams y(t) of TSI signal (n = 2) before the "reject" filter (*)

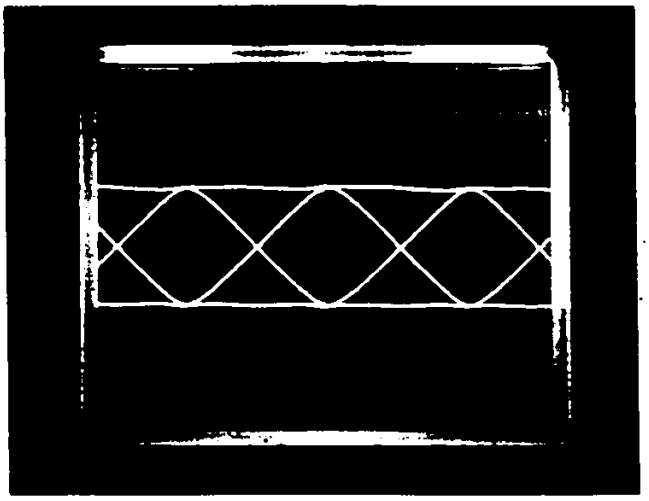

Ver: 10 usec/div
Hor: 0.1 Volt/div

Fig. 5.8d. Eye diagrams y(t) of TSI signal (n = 2) after the "reject" filter

5.1.3 Modulator

The block diagram of the modulator is shown in Fig. 5.9. The input in-phase and quadrature TSI signals are amplified and multiplied by cos $w_c t$ and sin $w_c t$ respectively. The summation of the two mixer outputs is called the TSI-OQPSK signal.

In this design we use 64 kb/s as our data rate and 512 kHz as our carrier frequency. This data rate and carrier frequency have been selected to use in INTELSAT SCPC (Single Channel per Carrier) equipment. The schematic diagram of the modulator is shown in Fig. 5.10. The switches S2 and S3 are set to select IN1 and IN2 respectively. The measured in-phase and quadrature TSI signals (shown in Fig. 5.11) are connected to input IN1 and IN2 respectively. The input level is approximately 300 mvolts peak to peak. We also note that the transitions of one signal occur at the maximum or minimum level of the other. The measured PSD of TSI signals at the input of the modulator is in close agreement with the computer simulated results shown in Fig. 5.12.

The IC U1 is used to adjust the input signal level of the mixers (SRA-6). The signal level at the

mixer's input must be about 300m volts peak to peak. A 512 kHz sine wave is split and modified by U2 to generate cos $w_c t$ and sine $w_c t$ signal respectively ($w_c = 2\pi \times 512$ kHz). The level of the sinusoidal signals must be about 2.5 volts. The two modulated signals of the in-phase and quadrature channel are added to generate TSI-OQPSK signals. Fig. 5.13 shows the PSD and time domain signals of TSI-OQPSK (n = 1) signals. These figures confirm our theoretical derivation in Chapter Two.

In our hardware design we use the LM311 as the hardlimiter which has a threshold at approximately 0 Volt DC.

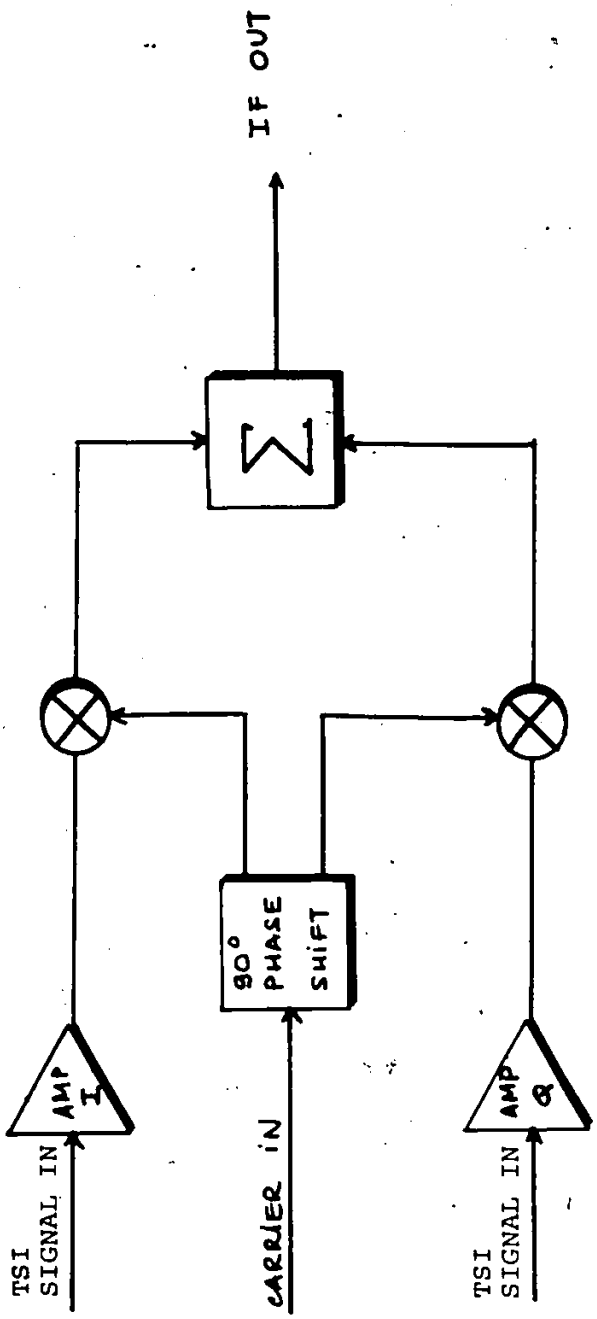

Fig. 5.9 Block Diagram of the Modulator

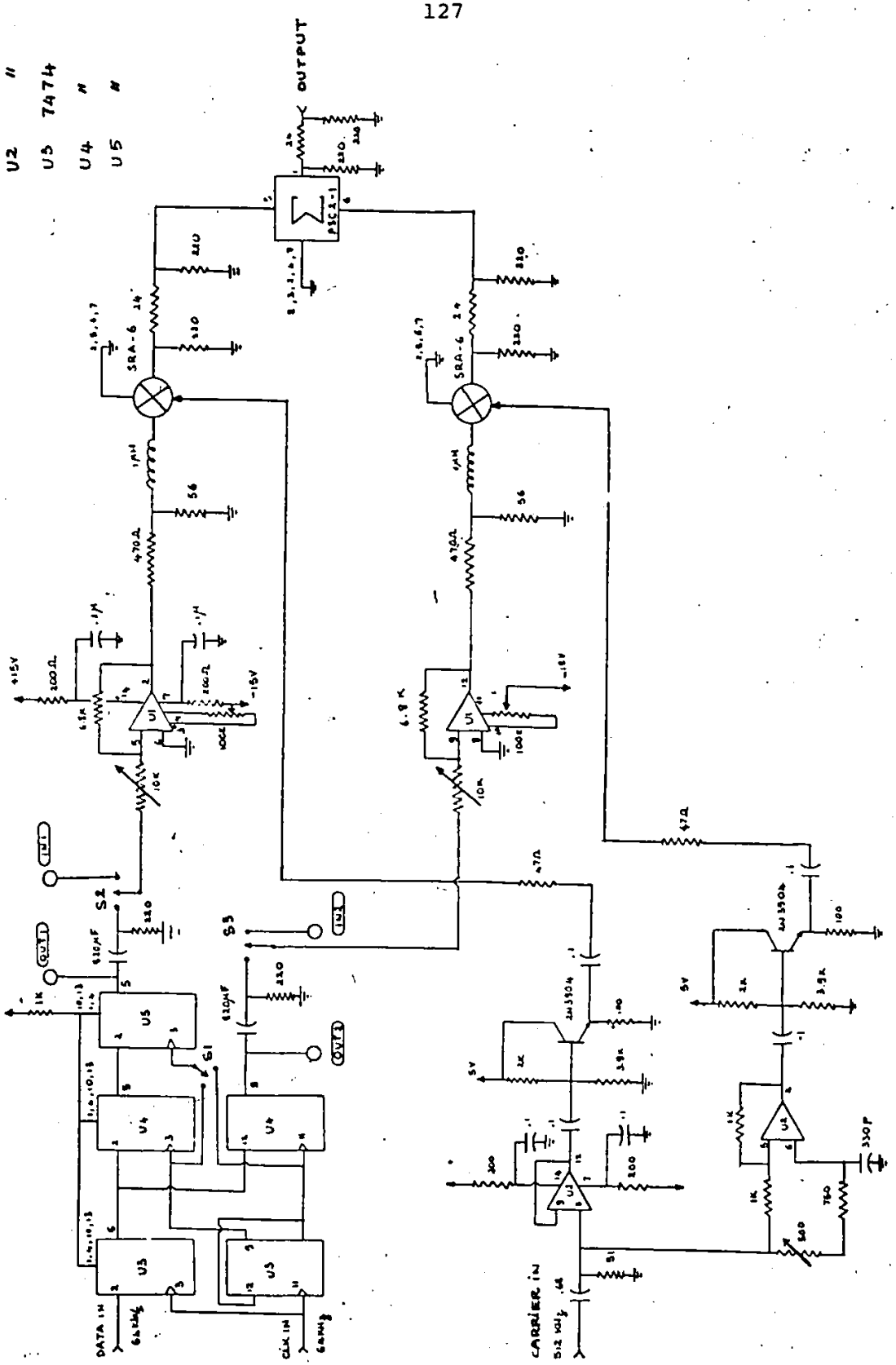

Fig. 5.10. Modulator

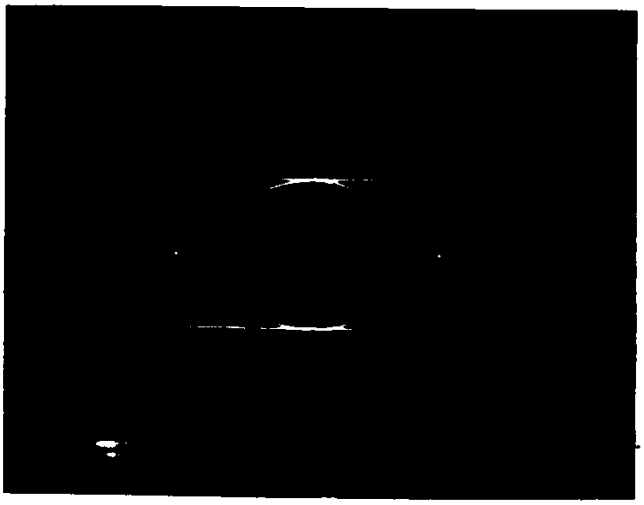

Ver: 5 usec/div
Hor:- 0.1 volt/div

Symbol rate =
32 kb/s

Eye Diagram of I Channel (at IN1)

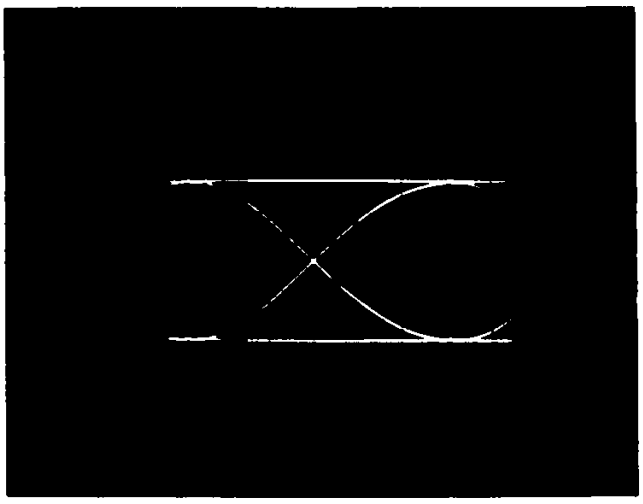

Ver: 5 usec/div
Hor: 0.1 Volt/div

Symbol rate =
32 kb/s

Eye Diagram of Q Channel (at IN2)

Fig. 5.11. Transmit baseband eye diagrams of I and Q channels (prior to modulation) (TSI signal (n = 1))

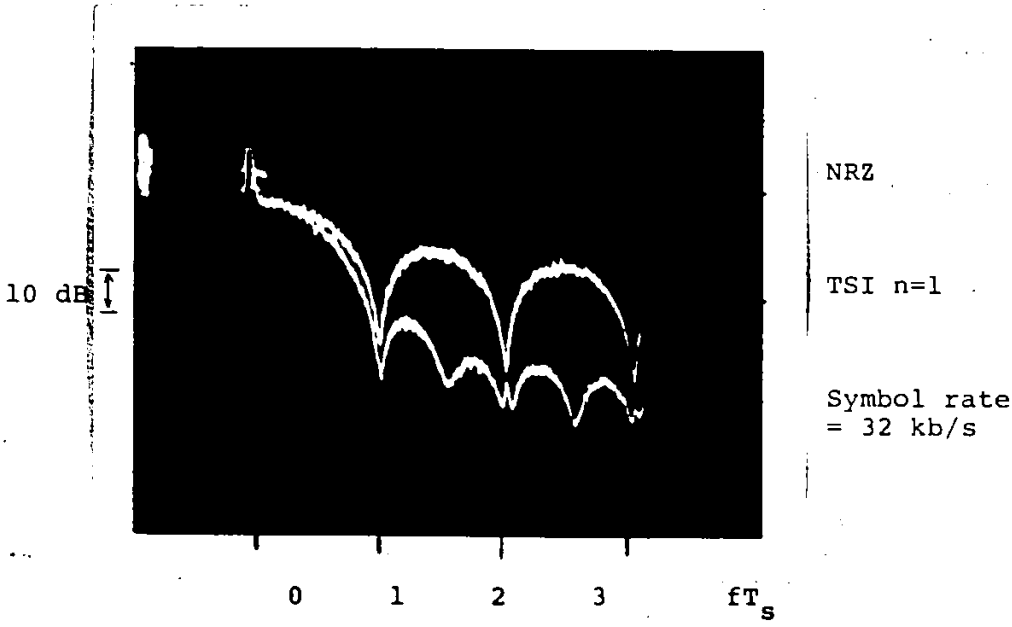

Fig. 5.12. Measured PSDs of NRZ and TSI (n = 1) signals

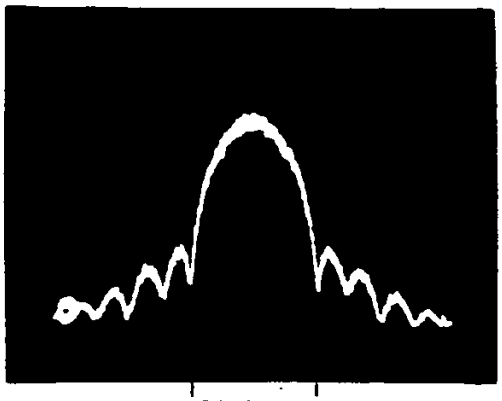

Ver: 10 dB/div
Hor: 20 kHz/div

a/ PSD of TSI-OQPSK Signals

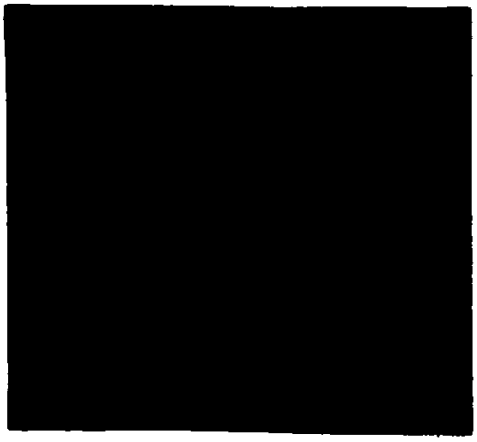

Ver: 0.1 Volt/div
Hor: 10 usec/div

b/ TSI-OQPSK Signals in Time Domain (Triggered by 64 kHZ CLK)

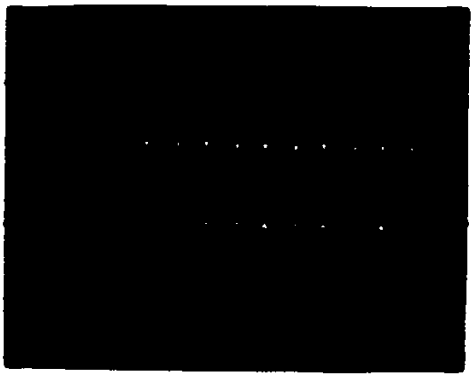

Ver: 0.2 Volt/div
Hor: 0.5 usec/div

c/ TSI-OQPSK Signals in Time Domain (Triggered by 512 kHz Carrier Frequency)

Fig. 5.13 The Modulated Signals from TSI-OQPSK Modulator (64Kb/s) (n=1)

5.2 TSI-OQPSK Demodulator

The block diagram of a TSI-OQPSK demodulator is shown in Fig. 5.14. We note that this demodulator may be the same as a conventional OQPSK demodulator. The carrier and clock signals are hardwired to our demodulator circuit and some delays must be added to these signals to synchronize with the received signal. The schematic diagram of the TSI-OQPSK demodulator board is shown in Fig. 5.15.

The transistor MPSA-12 is used to split the received signal. The carrier signal is amplified and split to generate $\cos w_c t$ and $\sin w_c t$ signal (using U5). The received TSI-OQPSK signal and carrier signal levels must satisfy the requirements specified in section 5.1 (300 mvolts for the TSI-OQPSK signal and 2.5 volts for the carrier signal). U6 to U8 are used to delay and generate the I and Q channel clock. The output signals of the mixers are filtered (by the RC circuits) and amplified (using U1 and U2) before connecting to the input of the threshold comparator (U3 and U4). U8 to U10 serialize the parallel data.

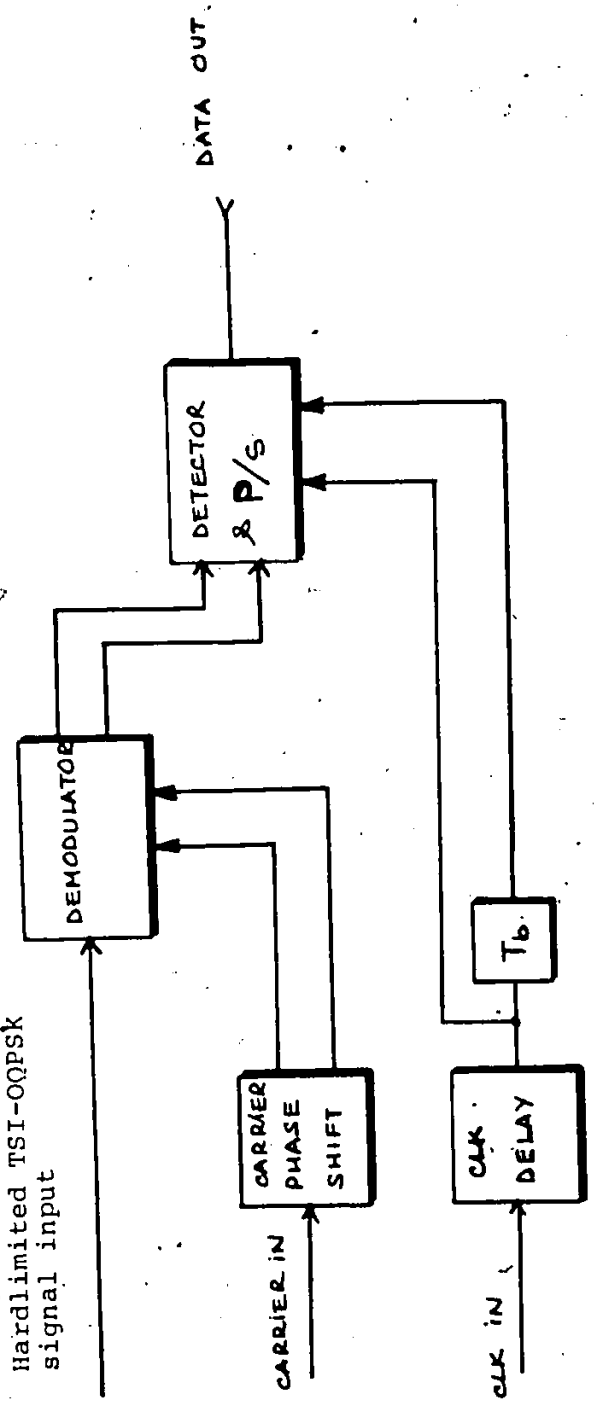

Fig. 5.14 Block Diagram of TSI-OQPSK Demodulator Board

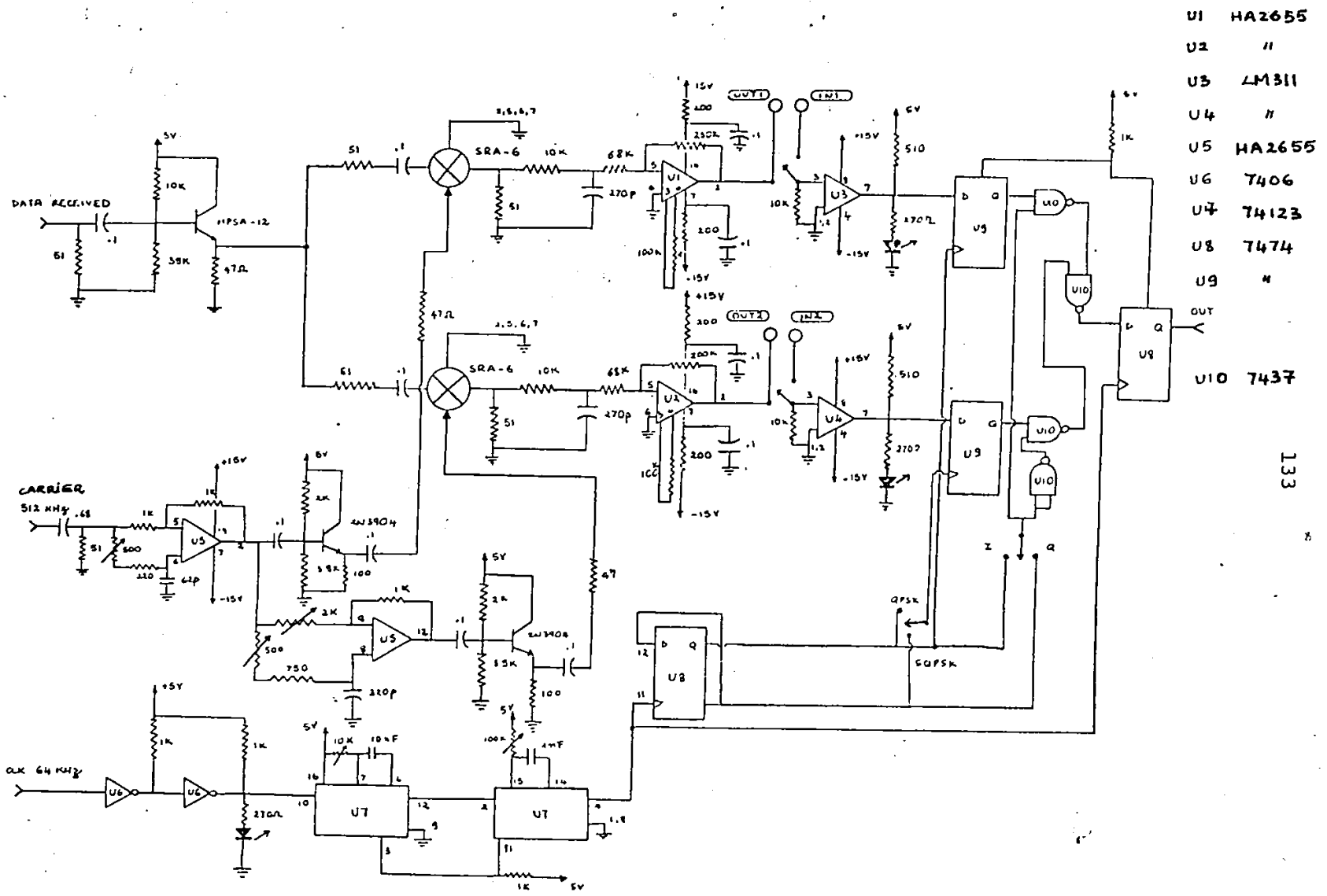

Fig. 5.15. TSI-OQPSK demodulator schematic diagram

The received signal eye diagrams and PSD of hard-limited TSI-OQPSK signals (n = 1) are in close agreement with the computer simulated results and are shown in Fig. 5.16. The PSD of a hardlimited TSI-QPSK signal (n = 1) is also shown in Fig. 5.16. However, the spectral regrowth of TSI-OQPSK signals is much less than that of TSI-QPSK signals.

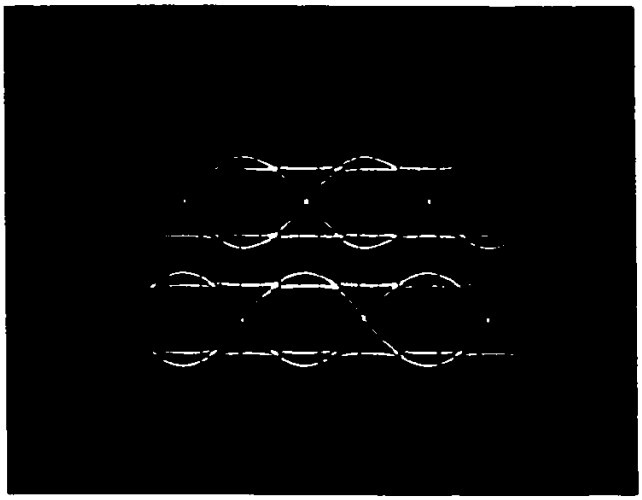

a/ Measured hardlimited TSI-OQPSK signals (n=1) prior to the threshold detector (no receive BPF)

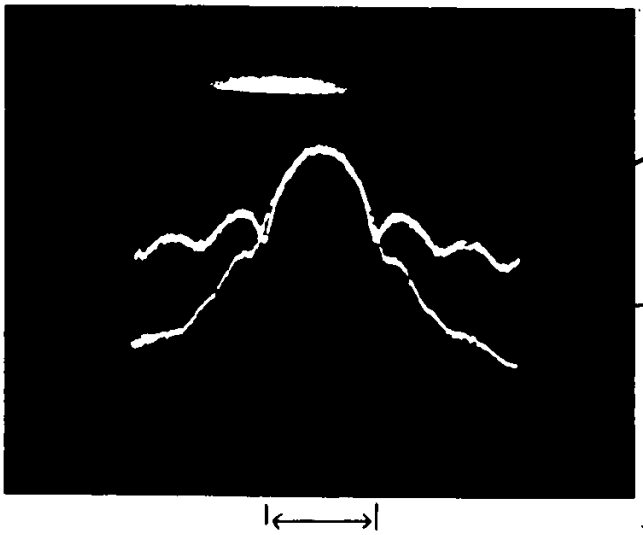

b/ Measured PSDs of hardlimited TSI-OQPSK and TSI-QPSK signals (n=1)

Fig. 5.16 Measured results of hardlimited TSI-OQPSK signals

5.3 P_e Performance of TSI-OQPSK Modems

The following measurements are obtained by using our available equipments and from our TSI-OQPSK modem (n = 1). The block diagram of an adjacent channel experiment is shown in Fig. 5.17. Three TSI-OQPSK modulators (n = 1) (Bit rate = 64 kb/s) with the carrier frequencies 512 kHz and 512 kHz +/- Δf are passed through the hardlimiter and added together. A wideband White Gaussian Noise (WGN) source is added to these summed signals prior to the receive BPF. The receive BPF is a 7^{th} order Butterworth filter with center at 512 kHz and a noise bandwidth of 35 kHz, (this filter has been used in SCPC equipments and is equivalent to zero forcing filter with $\alpha = 0.4$). The received output signal from the demodulator is fed back into the Bit Error Rate measurement device (as shown in Fig. 3.5) to measure the P_e performance.

The measured P_e performances of hardlimited TSI-OQPSK (n = 1) signals when Δf = 45 kHz, 64 kHz are shown in Fig. 5.18 and 5.19 respectively. Computer simulated results are also shown in those figures. The P_e comparison between measured and computer simulated results show an E_b/N_o difference of

approximately 1 dB to 1.5 dB. This is due to the imperfections of the hardware and the filters in use.

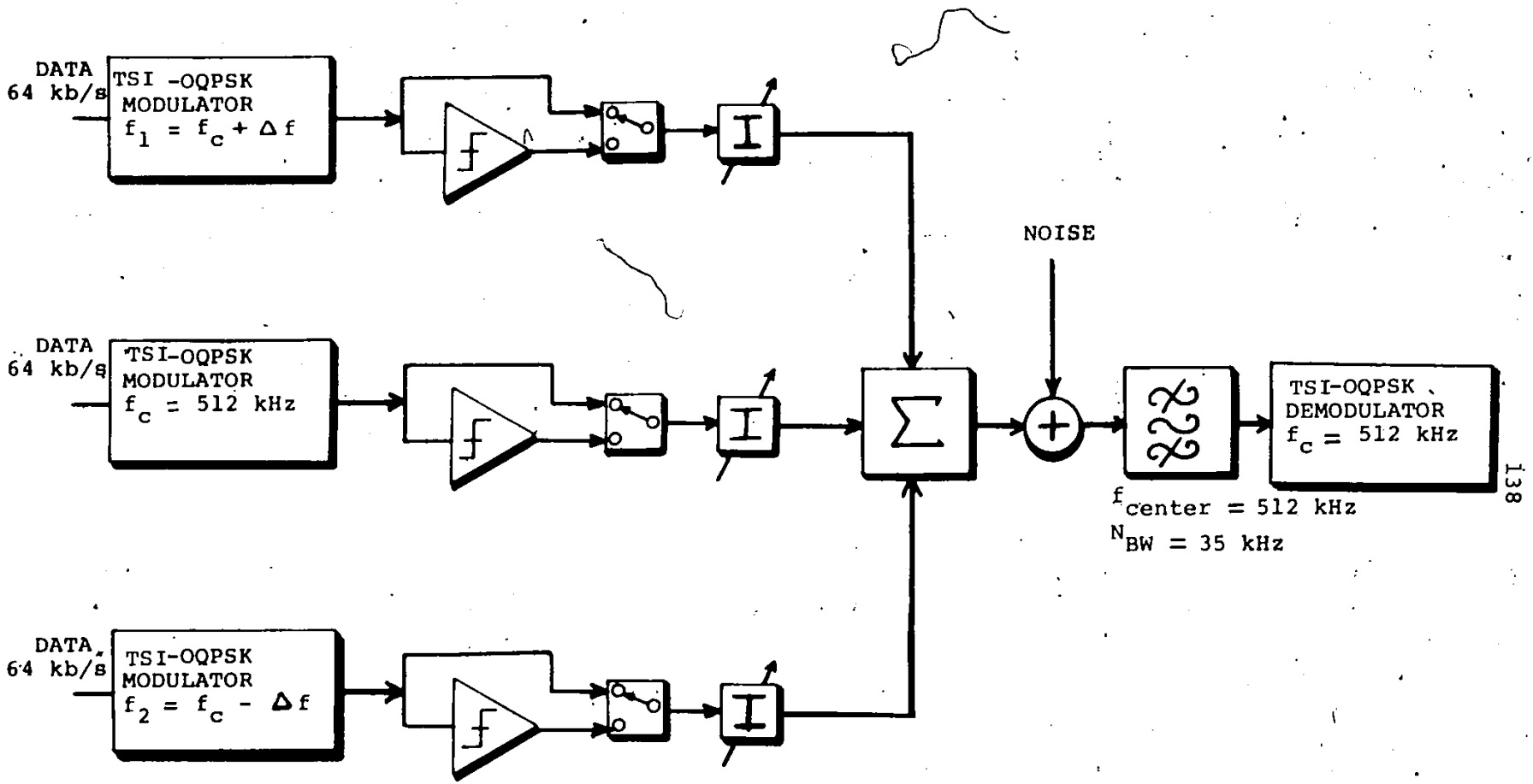

Fig. 5.17. Block diagram of adjacent channel experiement for TSI-OQPSK (n = 1)

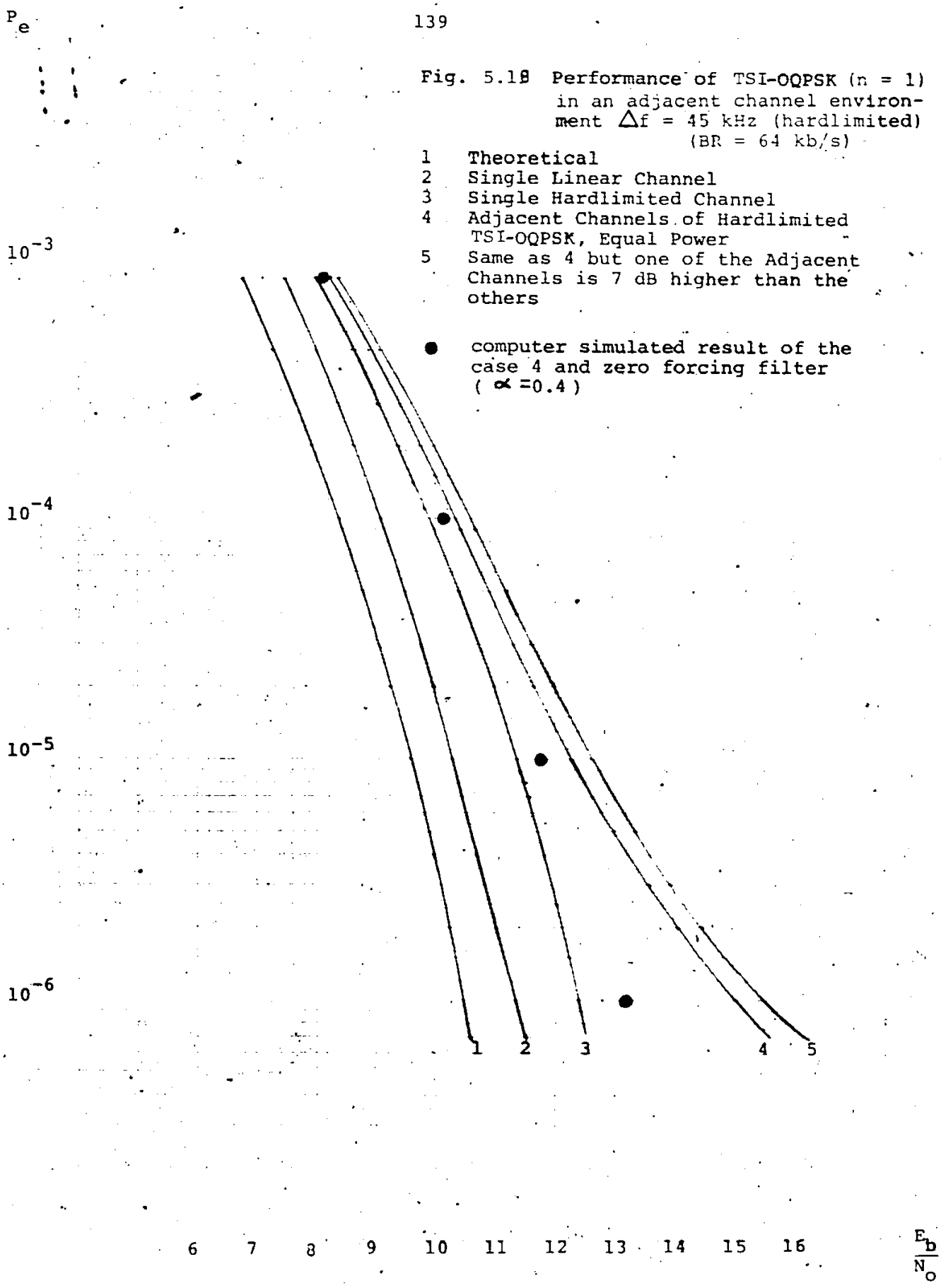

Fig. 5.18 Performance of TSI-OQPSK (n = 1) in an adjacent channel environment Δf = 45 kHz (hardlimited) (BR = 64 kb/s)

1 Theoretical
2 Single Linear Channel
3 Single Hardlimited Channel
4 Adjacent Channels of Hardlimited TSI-OQPSK, Equal Power
5 Same as 4 but one of the Adjacent Channels is 7 dB higher than the others

● computer simulated result of the case 4 and zero forcing filter (α =0.4)

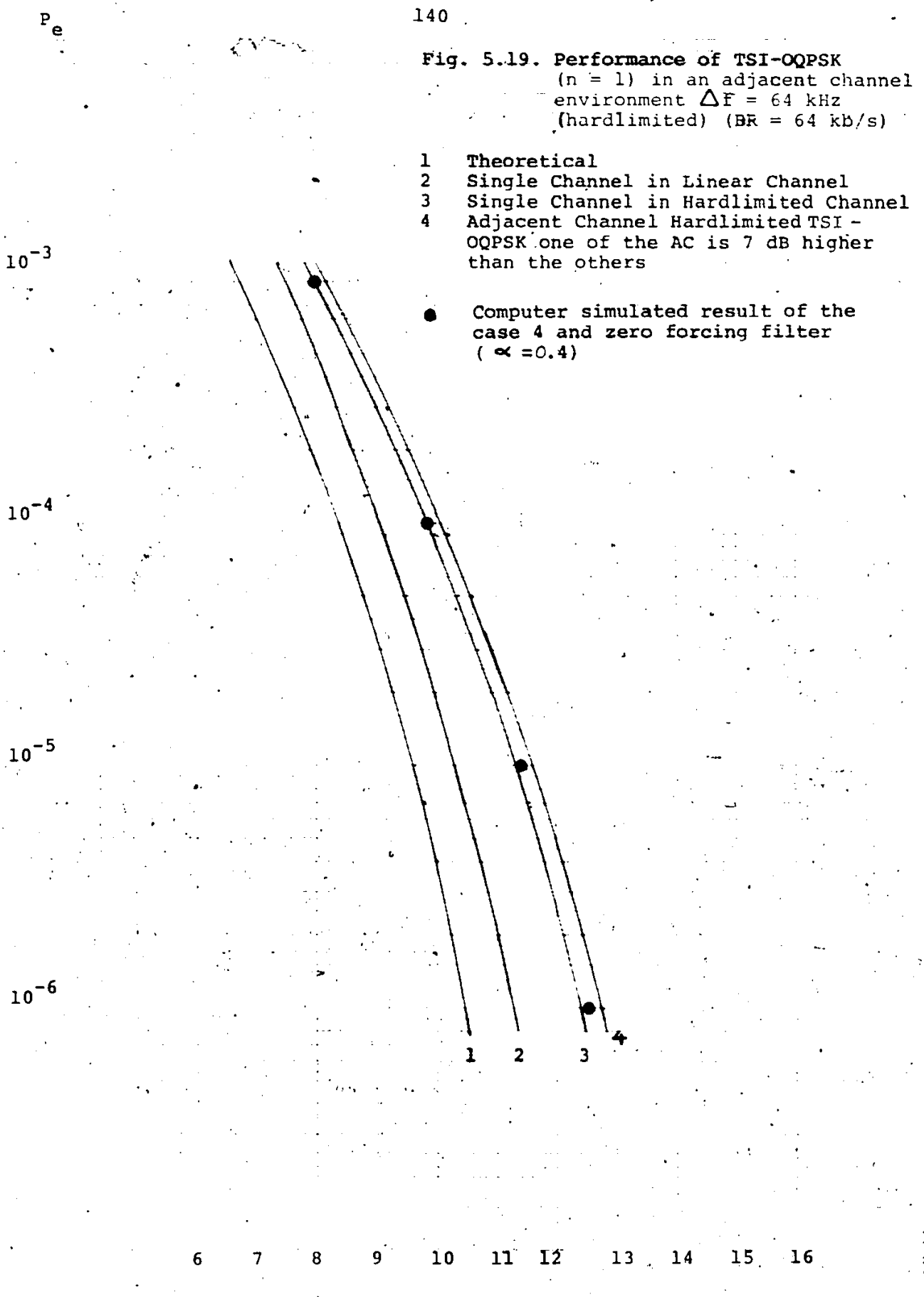

Fig. 5.19. Performance of TSI-OQPSK (n = 1) in an adjacent channel environment Δf = 64 kHz (hardlimited) (BR = 64 kb/s)

1 Theoretical
2 Single Channel in Linear Channel
3 Single Channel in Hardlimited Channel
4 Adjacent Channel Hardlimited TSI - OQPSK one of the AC is 7 dB higher than the others

● Computer simulated result of the case 4 and zero forcing filter (α =0.4)

CHAPTER SIX

CONCLUSION

The basic concepts of TSI-OQPSK system were described in this thesis and the performance of TSI-OQPSK modems was evaluated. The spectral spreading characteristic of TSI-OQPSK signals is their most attractive property. Less spectral spreading means more bandwidth efficiency. Since the HPA of a TSI-OQPSK system may be operated in saturation with minimal degradation, the cost of the HPA is reduced significantly.

A new filtering strategy called Sum of Approximate Eye was introduced in this thesis. This filter improves significantly the performance of TSI-OQPSK modems in a nonlinear channel environment. We also note that the SAE filter can be used as receive filter for all TSI-OQPSK modems (n = 1, 2, ...). In this thesis TSI pulse shapes n = 1 and n = 2 were given special attention because the TSI-OQPSK (n = 1) signal has been published extensively, (TSI-OQPSK (n = 1) is equivalent to SQORC [15-17, 35] and IJF-OQPSK [11, 14, 46]) and TSI-OQPSK (n = 2) has the lowest spectral spreading in a nonlinear and narrow bandwidth channel environment.

Two types of nonlinear amplifier (hardlimiter and saturated INTELSAT V HPA) were used to examine the performance of TSI-OQPSK, OQPSK and QPSK systems. Most of the system comparisons in this thesis are between TSI-OQPSK signals and QPSK, OQPSK signals. We did not include the performance of MSK signals because many recent publications indicated that the performance of OQPSK signals is better than that of MSK signals in a narrow channel spacing environment[2-5].

The Power Spectral Density of TSI-OQPSK signals after passing through a saturated amplifier, were examined. The results indicate that TSI-OQPSK signals have significant spectral advantages over other conventional signals such as QPSK, OQPSK and MSK.

Two different TSI pulse generating circuits (NLSF and Pulse Overlapping) were presented and implemented. Due to the speed limitation of analog switching ICs (Integrated Circuit), the Pulse Overlapping circuit has more advantages than the NLSF circuit in high speed applications. The hardware design of a TSI-OQPSK modem (n = 1) was presented and implemented. Our hardware measurement results are in close agreement with computer simulated results. It is shown that TSI-OQPSK modems have better P_e performance than conventional QPSK, OQPSK and MSK modems in a saturated HPA and narrow channel spacing system configuration ($\Delta f.T_b \leq 1$).

Cost considerations would presumably favor TSI-OQPSK modems since the hardware implementation of TSI encoders and SAE filters are simpler than the conventional raised cosine filters.

Having these attractive spectral properties and P_e performance, TSI-OQPSK modems are expected to find application in power and bandwidth efficient satellite and terrestrial microwave systems.

APPENDIX I

I.1 Derivation of the PSD of the TSI Signal

The Fourier transforms of even and odd pulses $s_e(t)$ and $s_o(t)$ are

$$S_e(f) = S_e^*(f) = 2\int_0^{T_s/2} s_e(t) \cos 2\pi ft \, dt: \text{ real} \qquad (A1.1a)$$

$$S_o(f) = -S_o^*(f) = -2j\int_0^{T_s/2} s_o(t) \sin 2\pi ft \, dt: \text{ imaginary} \qquad (A1.1b)$$

From the definition of $s_i(t)$, $i = 1,2,3,4$, in Eq. (2.2) it follows that

$$S_1(f) = S_1^*(f) = -S_2(f) = -S_2^*(f) = S_e(f) \qquad (A1.1c)$$

$$S_3(f) = -S_3^*(f) = -S_4(f) = S_4^*(f) = S_o(f) \qquad (A1.1d)$$

From transition matrix

$$P = \tfrac{1}{2}\begin{bmatrix} 1 & 0 & 0 & 1 \\ 0 & 1 & 1 & 0 \\ 1 & 0 & 0 & 1 \\ 0 & 1 & 1 & 0 \end{bmatrix}$$

it can be shown that the n-step transition matrix has the form

$$P^n = \underbrace{P \times P \times \ldots \times P}_{n \text{ times}} = \tfrac{1}{4}\begin{bmatrix} 1 & 1 & 1 & 1 \\ 1 & 1 & 1 & 1 \\ 1 & 1 & 1 & 1 \\ 1 & 1 & 1 & 1 \end{bmatrix} \qquad \text{for } n=2,3,\ldots,$$

hence

$$S_{ik} = \sum_{n=1}^{+\infty} P_{ik}^{(n)}\, e^{-j2\pi nfTs}$$

$$= P_{ik}\, e^{-j2\pi fTs} + \tfrac{1}{4} \sum_{n=2}^{\infty} e^{-j2\pi nfTs} \qquad (A1.2)$$

Substituting Eqs. (A1.1c,d) and (A1.2) into Equation (2.10), the PSD funtion of y(t) is obtained as

$$Y(f) = \frac{1}{2T_s} \left\{ \left|S_e(f)\right|^2 + \left|S_o(f)\right|^2 + \mathrm{Re}\left\{ (S_e(f) - S_o(f))^2 e^{-j2\pi fTs} \right\} \right\} \qquad (A1.3a)$$

From Eqs. (A1.1a, b)

$$\left|S_e(f)\right|^2 = S_e(f) \cdot S_e^*(f) = S_e^2(f)$$

$$\left|S_o(f)\right|^2 = S_o(f) \cdot S_o^*(f) = S_o^2(f)$$

Hence Y(f) can be rewritten as

$$Y(f) = \frac{1}{2T_s} \mathrm{Re}\left\{ S_e^2(f) - S_o^2(f) + (S_e(f) - S_o(f))^2 e^{-j2\pi fTs} \right\}$$

$$= \frac{1}{2T_s} \left\{ S_e^2(f) - S_o(f)^2 + S_e^2(f)\cos 2\pi fT_s + S_o^2 \cos 2\pi fT_s + 2jS_e(f)S_o(f)\sin 2\pi fT_s \right\}$$

$$= \frac{1}{T_s} \left\{ S_e^2(f)\cos^2 \pi fT_s - S_o^2(f)\sin^2 \pi fT_s + 2jS_o(f)S_e(f)\sin \pi fT_s \cos \pi fT_s \right\}$$

$$= \frac{1}{T_s} \left\{ S_e(f)\cos \pi fT_s + jS_o(f)\sin \pi fT_s \right\}^2$$

I.2

The Fourier Transforms of $S_{en}(t)$ and $S_{on}(t)$

$$S_{en}(t) = 1$$

$$S_{en}(f) = 2 \int_0^{T_{s/2}} \cos 2\pi ft \, dt$$

$$= \frac{2}{2\pi f} \int_0^{T_{s/2}} 2\pi f . \cos 2\pi ft \, dt$$

$$= \frac{1}{\pi f} \left[\sin 2\pi ft \right]_0^{T_{s/2}}$$

$$S_{en}(f) = \frac{\sin \pi f T_s}{\pi f}$$

$$s_{on}(t) = \sin(\pi t/nT_s)/\sin(\pi/2n) \quad \text{let } A = \frac{1}{\sin(\pi/2n)}$$

then

$$S_{on}(f) = -2j \int_0^{T_s/2} A \sin\frac{\pi t}{nT_s} \cdot \sin 2\pi ft \, dt$$

let $a = \frac{\pi}{nT_s}$ and $b = 2\pi f$ then $S_{on}(f) = \int_0^{T_s/2} \sin(at)\sin(bt)\,dt$. $(-2jA)$

$$= \left[\frac{\sin(a-b)t}{2(a-b)} - \frac{\sin(a+b)t}{2(a+b)}\right]_0^{T_2/2}. \quad (-2jA)$$

$$= S_{on}(f) = -2jA\left\{\frac{\sin(\frac{\pi}{nT_s} - 2\pi f)\,T_s/2}{2(\frac{\pi}{nT_s} - 2\pi f)} - \frac{\sin(\frac{\pi}{nT_s} + 2\pi f)\,T_s/2}{2(\frac{\pi}{nT_s} + 2\pi f)}\right\}$$

$$= -jATn_s\left\{\frac{\sin(\frac{\pi}{2n} - \pi fT_s)}{\pi - 2\pi nfT_s} - \frac{\sin(\frac{\pi}{2n} + \pi fT_s)}{\pi + 2\pi nfT_s}\right\}$$

$$= jAnT_s\left\{\frac{\sin(\frac{\pi}{2n} + \pi fT_s)}{\pi(1 + 2nfT_s)} + \frac{\sin(\pi fT_s - \pi/2n)}{\pi - 2\pi nfT_s}\right\}$$

I.3: DEFINITION OF $v_i(t)$ REQUIRED FOR EQUATION 2.23

$$v_1(t) = -v_{16}(t) = C\, s_e(t) \cdot \left[s_e^2(t) + s_1'^2(t)\right]^{1/2}$$

$$v_2(t) = -v_{15}(t) = C\, s_e(t) \cdot \left[s_e^2(t) + s_2'^2(t)\right]^{1/2}$$

$$v_3(t) = -v_{14}(t) = C\, s_e(t) \cdot \left[s_e^2(t) + s_3'^2(t)\right]^{1/2}$$

$$v_4(t) = v_{13}(t) = C\, s_e(t) \cdot \left[s_e^2(t) + s_4'^2(t)\right]^{1/2}$$

$$v_5(t) = v_{12}(t) = C\, s_o(t) \cdot \left[s_o^2(t) + s_1'^2(t)\right]^{1/2}$$

$$v_6(t) = -v_{11}(t) = C\, s_o(t) \cdot \left[s_o^2(t) + s_2'^2(t)\right]^{1/2}$$

$$v_7(t) = -v_{10}(t) = C\, s_o(t) \cdot \left[s_o^2(t) + s_3'^2(t)\right]^{1/2}$$

$$v_8(t) = -v_9(t) = C\, s_o(t) \cdot \left[s_o^2(t) + s_4'^2(t)\right]^{1/2}$$

where C is a constant and:

$$s_1'(t) = \begin{cases} s_e(t + Ts/2) & \text{for } -Ts/2 \leqslant t < 0 \\ s_e(t - Ts/2) & \text{for } 0 \leqslant t < Ts/2 \end{cases}$$

$$s_2'(t) = \begin{cases} s_o(t + Ts/2), & -Ts/2 \leqslant t \leqslant 0 \\ s_o(t - Ts/2), & 0 \leqslant t < Ts/2 \end{cases}$$

$$s_3'(t) = \begin{cases} s_o(t + Ts/2, & -Ts/2 \leqslant t < 0 \\ s_e(t - Ts/2), & 0 \leqslant t < Ts/2 \end{cases}$$

$$s_4'(t) = \begin{cases} s_e(t + Ts/2, & -Ts/2 \leqslant t < 0 \\ s_o(t - Ts/2), & 0 \leqslant t < Ts/2 \end{cases}$$

APPENDIX II

COMPUTER SIMULATION PROGRAM

This computer program was originally developed by Dr. Arunachalam and P. Vandamme at the University of Ottawa. A number of subroutines have been modified, added and deleted to incorporate the TSI OQPSK signals and SAE filters.

```
C*************************************************************************
C PROGRAM FOR NON-LINEAR CHANNEL WITH ACI WRITTEN BY
C DR.ARUNACHALAM AND P.VANDAMME AT THE U.OF OTTAWA
C*************************************************************************
      COMMON/LLIM
      COMMON/PARA/LSAMPL,NSYMB,NC1,NC2,BAUD,SBANDW
      COMPLEX DATA(2048),TF1(2048),TF2(2048),TF3(2048),TF4(2048)
      COMPLEX DATA1(2048)
      DIMENSION PE1(25),EBNO(25),IPNI(128),IPNQ(128)
      DIMENSION IWK(12),PO(65),IPNI1(128),IPNQ1(128)
      DIMENSION XARRAY(27),YARRAY(27)
      REAL MP,MP1,MP2,MPO,MPF,MPS
C
C     INITIALIZE PROGRAM.
C
      NSYMB=128
      LSAMPL=16
      BAUD=60.
      DATA NSNR/25/
      DATA NRUNS/8/
      DATA FBW1,FBW2,FBW3,FBW4/30.0,30.0,40.0,40.0/
      DATA ALPHA1,ALPHA2/0.4,0.4/
      DATA ALPHA3,ALPHA4/0.1,0.2/
      DATA BAKOFH,BAKOFT/0.0,2.0/
      DATA IOFF,NNN,NTYPE/8,1,1/
      DATA FOF,FOF1,FOF2/0.,100.,-100./
      SBANDW=FLOAT(LSAMPL)*BAUD
      LDIM=LSAMPL*NSYMB
      NC1=LDIM/2+1
      NC2=NC1+1
      DO 501 KH1=1,3
      PSHIF1=1.7
      PSHIF2=3.14
      ITSH1=0
      ITSH2=0
      DO 19 I=1,NSNR
      PE(I)=0.0
   19 CONTINUE
      PE1=0.0
      PRINT 1
    1 FORMAT(5X,'SIMULATION OF QPSK *********************'/)
      OFF=FLOAT(IOFF)/FLOAT(LSAMPL)
      WRITE(6,2) OFF
    2 FORMAT(5X,'OFFSET=',F3.2,' T')
      WRITE(6,999) NNN,NTYPE
  999 FORMAT(5X,'NNN = ',I2,' FILTER TYPE =',I2/)
      WRITE (6,6) BAUD,LSAMPL
    6 FORMAT(5X,'SYMBOL RATE:',F7.2,' BAUD'/,
     &5X,I4,' SAMPLES PER SYMBOL'/)
      DO 500 KM=1,NRUNS
      SSS1=FLOAT(ITSH1)/(16.*.06)
      SSS2=FLOAT(ITSH2)/(16.*.06)
      ITSH11=ITSH1+672
      ITSH12=ITSH2+1344
      OFF=FLOAT(IOFF)/FLOAT(LSAMPL)
C     END OF INITIALIZATION.
C
C     START OF COMPUTATIONS.
      CALL RCOS(FBW1,TF3,ALPHA1,NNN,NTYPE)
      CALL PHGG(TF3,PNOISE)
      CALL LOADS(DATA,IPNI,IPNQ,IOFF,NNN)
      CALL FLIM(DATA,LDIM)
```

```
C     CALL HPA(DATA,BAKCFH,PSHIF0)
      CALL ENERGY (DATA,EB,BAUD)
      CALL FILTER(DATA,TF3)
      CALL POWER(DATA,MF,PF)
      CALL LOADS(DATA1,IPNI1,IPNQ1,ICFF,NNN)
      CALL HLIM(DATA1,LDIM)
C     CALL HPA(DATA1,BAKOFH,PSHIF)
      CALL SACI(DATA1,FCF1)
      CALL FILTER(DATA1,TF3)
      CALL PHASE(DATA1,PSHIF1)
      CALL TIME(DATA1,ITSHI1)
      CALL ATT(DATA1,AT1)
      CALL POWER(DATA1,MP1,PF1)
      DC 10 I=1,LDIM
   10 DATA(I)=DATA(I)+DATA1(I)
      CALL LOADS(DATA1,IPNI1,IPNQ1,ICFF,NNN)
      CALL HLIM(DATA1,LDIM)
C     CALL HPA(DATA1,BAKOFH,PSHIF)
      CALL SACI(DATA1,FCF2)
      CALL FILTER(DATA1,TF3)
      CALL PHASE(DATA1,PSHIF2)
      CALL TIME(DATA1,ITSHI2)
      CALL ATT(DATA1,AT2)
      CALL POWER(DATA1,MP2,PF2)
      DC 20 I=1,LDIM
   20 DATA(I)=DATA(I)+DATA1(I)
      PSHIFT=PSHIF0
      CALL PHASE(DATA,PSHIFT)
      ACI1=10.*ALOG10(MF/MP1)
      N=1
      ACI2=10.*ALOG10(MF/MP2)
      CALL DECOD4(DATA,PNCISE,IPNI,IPNQ,
     #EBNO,PEI,NSNR,EB,IOFF,NERROR)
      DC 5 I=1,NSNR
      PEI(I)=PEI(I)/FLOAT(NSYMB)
    5 EBNO(I)=FLOAT(I)
      DC 23 I=1,NSNR
      PO(I)=PEI(I)+PO(I)
      IF((PEI(I).LT..1E-03.AND.PEI(I).GT..1E-04).AND.(KM.EQ.1)) KL=I
   23 CONTINUE
      PC1=(PEI(KL)**2.)+PC1
C      CALL EYEQ(DATA,LSAMPL,NSYMB)
      ITSHI=ITSHI-1
      PSHIF1=PSHIF1+.11
      PSHIF2=PSHIF2+.23
      ITSH2=ITSH2+1
  500 CONTINUE
      WRITE(6,3) N,FOF1,AT1,ACI1
      N=2
      WRITE(6,3) N,FOF2,AT2,ACI2
    3 FORMAT(///,2X,'CHANNEL ',I1,' CHARACTERISTICS'//,2X,
     &'OFFSET FREQ.: ',F6.1,' MHZ','ATTENUATION:',F4.1,'DB',
     &/' CARRIER TO INT. RATIO: ',F5.1,' DB')
      WRITE (6,9) BAKCFH
    9 FORMAT(5X,'HPA INPUT BACKOFF:',F4.1,' DB')
      DC 64 I=1,25
      PO(I)=PO(I)/FLOAT(NRUNS)
   64 CONTINUE
      WRITE(6,150)
  150 FORMAT(5X,'EB/NO',10X,'PROB. OF. ERROR', /)
      WRITE(6,172) (EBNC(I),PO(I),I=1,NSNR)
  172 FORMAT(5X,F5.1,10X,E13.6)
```

```
FORTRAN IV G LEVEL 21          MAIN          DATE = 81259      19/04/15

0107          WRITE (6,152) NERROR
0108      152 FORMAT(//5X,'ERRORS=',I5,/)
0109          FCF1=FUF1+10.
0110          FCF2=FCF2-10.
0111      501 CONTINUE
0112          STOP
0113          END
```

```
FORTRAN IV G LEVEL  21                HLIM                    DATE = 81250        19/04/15

0001                  SUBROUTINE HLIM(DATA,LOIM)
0002                  COMPLEX DATA(1)
0003                  DO 10 I=1,LOIM
0004               10 DATA(I)=DATA(I)/CABS(DATA(I))
0005                  RETURN
0006                  END
```

```
C*****************************************************************
C RECT-RAISED COSINE FILTER WITH ARBITRARY ALPHA AND X/SINX
C*****************************************************************
      SUBROUTINE RCOS(FBAND*,TF,ALPHA)
      COMMON LDIM
      COMMON/PARA/LSAMPL,NSYMJ,NC1,NC2,JAUD,SBAND*
      COMPLEX TF(1)
      IF (ALPHA.LE.0.0) ALPHA=0.0001.
      FN=LDIM*(FBAND*/SBAND*)
      F1=(1.-ALPHA)*FN
      F2=(1.+ALPHA)*FN
      IFN=IFIX(FN)
      IF1=IFIX(F1)+1
      IF2=IFIX(F2)+1
      A1=3.141516/(2.*FLOAT(IFN))
      DO 8 I=2,IF1
      TF(I)=CMPLX(1.0,0.0)
      J=I-1
      A2=(FLOAT(J)*A1)/(SIN(FLOAT(J)*A1))
      TF(I)=CMPLX(A2,0.0)
    8 CONTINUE
      JK=IF1+1
      DO 9 J=JK,IF2
      I=J-1
      A3=(FLOAT(I)*A1)/(SIN(FLOAT(I)*A1))
      A=(3.141516/(2.0*ALPHA))*((FLOAT(I)/FLOAT(IFN))-1.)
      TF(J)=CMPLX(SQRT(0.5*(1.0-SIN(A))),0.0)
      TF(J)=TF(J)*CMPLX(A3,0.0)
    9 CONTINUE
      JH=IF2+1
      DO 10 I=JH,NC1
      TF(I)=CMPLX(0.0,0.0)
   10 CONTINUE
      DO 5 I=NC2,LDIM
      TF(I)=CONJG(TF(LDIM+2-I))
    5 CONTINUE
      RETURN
      END
```

```
FORTRAN IV G LEVEL 21          MAIN          DATE = 81259          13/04/15

      C*****************************************************************
      C THIS SUBROUTINE ATTENUATES THE SIGNAL
      C*****************************************************************
0001          SUBROUTINE ATT(DATA,AT)
0002          COMMON LDIM
0003          COMMON/PARA/LSAMPL,NSYMD,NO1,NO2,BAUD,SBAND#
0004          COMPLEX DATA(1)
0005          ATT=10.**(-AT/20.)
0006          DO 10 I=1,LDIM
0007    10    DATA(I)=DATA(I)*ATT
0008          RETURN
0009          END
```

```
FORTRAN IV G LEVEL 21          MAIN          DATE = 81259      19/04/15

C*************************************************************
C  THIS SUBROUTINE SHIFTS THE SIGNAL
C*************************************************************
0001          SUBROUTINE TIME(DATA,IT)
0002          COMMON LDIM
0003          COMMON/PARA/LSAMPL,NSYMB,NC1,NC2,BAUD,SDANDW
0004          COMPLEX DATA(1),DAT
0005          DO 10 I=1,IT
0006          DAT=DATA(1)
0007          DO 20 J=2,LDIM
0008       20 DATA(J-1)=DATA(J)
0009       10 DATA(LDIM)=DAT
0010          RETURN
0011          END
```

```
FORTRAN IV G LEVEL 21          MAIN          DATE = 81259      19/04/15

C*************************************************************
C     COMPUTATION OF MEAN POWER
C*************************************************************
      SUBROUTINE POWER(DATA,MP,PF)
      COMMON LOIM
      COMMON/PARA/LSAMPL,NSYMB,N1,NCH,BAUD,BBANDW
      COMPLEX DATA(1)
        REAL MP
      PF=0.
      MP=0.0
      DO 10 I=1,LOIM
      MP=MP+((CABS(DATA(I)))**2.)
      IF(PF.LT.CABS(DATA(I))) PF=CABS(DATA(I))
   10  CONTINUE
      MP=MP/FLOAT(LOIM)/2.
      PF=(PF**2.)/MP
      PF=10.*ALOG10(PF)
      RETURN
        END
```

```
C*************************************************************
C     RAISED COSINE FILTER WITH ARBITRARY ALPHA
C*************************************************************
      SUBROUTINE RCOS1(FBAND,TF,ALPHA)
      COMMON LDIM
      COMMON/PARA/LSAMPL,NSYM,NC1,NC2,BAUD,SBAND
      COMPLEX TF(1)
      IF (ALPHA.EQ.0.0) ALPHA=0.0001
      FN=LDIM*(FBAND/SBAND)
      F1=(1.-ALPHA)*FN
      F2=(1.+ALPHA)*FN
      IFN=IFIX(FN)
      IF1=IFIX(F1)+1
      IF2=IFIX(F2)+1
      A1=3.141516/(2.*FLOAT(IFN))
      DO 8 I=2,IF1
      TF(I)=CMPLX(1.0,0.0)
      J=I-1
      TF(I)=CMPLX(1.,0.0)
    8 CONTINUE
      JK=IF1+1
      DO 9 J=JK,IF2
      I=J-1
      A=(3.141516/(2.0*ALPHA))*((FLOAT(I)/FLOAT(IFN))-1.)
      TF(J)=CMPLX(SQRT(0.5*(1.0-SIN(A))),0.0)
    9 CONTINUE
      JH=IF2+1
      DO 10 I=JH,NC1
      TF(I)=CMPLX(0.0,0.0)
   10 CONTINUE
      DO 5 I=NC2,LDIM
      TF(I)=CONJG(TF(LDIM+2-I))
    5 CONTINUE
      RETURN
      END
```

```
      C*****************************************************************
      C     THE FOLLOWING SUBROUTINE PERFORMS THE FILTERING
      C     PROCESS ON THE DATA SEQUENCE.
      C*****************************************************************
0001        SUBROUTINE FILTER(SIGNAL,TF)
0002        COMMON LDIM
0003        COMPLEX SIGNAL(1),TF(1)
0004        DIMENSION IWK(12)
0005        CALL FFT2C(SIGNAL,11,IWK)
0006        DO 1 I=1,LDIM
0007      1 SIGNAL(I)=CONJG(SIGNAL(I)*TF(I))
0008        CALL FFT2C(SIGNAL,11,IWK)
0009        DO 2 I=1,LDIM
0010      2 SIGNAL(I)=CONJG(SIGNAL(I))/FLOAT(LDIM)
0011        RETURN
0012        END
```

FORTRAN IV G LEVEL 21 MAIN DATE = 81269 19/04/15

```
      C*****************************************************************
      C     THIS SUBROUTINE COMPUTES THE EFFECTIVE NOISE (PNOISE)
      C     AT THE OUTPUT OF THE RECEIVE FILTER
      C*****************************************************************
0001          SUBROUTINE NFSG(TF,PNOISE)
0002          COMMON LOIM
0003          COMMON/PARA/LSAMPL,NSYMS,NSI,NSP,BAUD,SBANDW
0004          COMPLEX TF(1)
0005          SUM=0.0
0006          DO 1 L=1,LOIM
0007          HH=(CABS(TF(L)))**2
0008        1 SUM=SUM+HH
0009          PNOISE=SUM*SBANDW/FLOAT(LOIM)/2.
0010          PP=PNOISE*2./BAUD
0011          RETURN
0012          END
```

160

```
FORTRAN IV G LEVEL 21          MAIN          DATE = 81259      19/04/15

      C*************************************************************
      C BIT ENERGY COMPUTATION
      C*************************************************************
0001          SUBROUTINE ENERGY(DATA,EB),                              &
0002          COMMON LDIM
0003          COMMON/PARA/LSAMPL,NSYMB,NC1,NC2,BAUD,SBANDW
0004          COMPLEX DATA(1)
0005          WATTS=0.
0006          DO 1 I=1,LDIM
0007          WATTS=WATTS+((CABS(DATA(I)))**2.)
0008        1 CONTINUE
0009          WATTS=WATTS/FLOAT(LDIM)
0010          EB=WATTS/(2.*BAUD)
0011          RETURN
0012          END
```

FORTRAN IV G LEVEL 21 MAIN DATE = 81259 19/34/15

```
C*************************************************************
C  THIS SUBROUTINE GENERATES AN EQUIVALENT BASEBAND QPSK SIGNAL.
C*************************************************************
      SUBROUTINE LOAD4(DATA,IPNI,IPNQ)
      COMMON LDIM
      COMMON/PARA/LSAMPL,NSYM1,NC1,NC2,BAUD,SBANDW
      COMPLEX DATA(1)
      DIMENSION NX(7),NY(7),IPNI(1),IPNQ(1)
      DATA NX(1),NX(2),NX(3),NX(4),NX(5),NX(6),NX(7)/-1,-1,1,
     #-1,-1,-1,-1/
      DATA NY(1),NY(2),NY(3),NY(4),NY(5),NY(6),NY(7)/-1,-1,
     #1,1,1,-1/
      DATA JLAST,JTAP/7,1/
      KKK=2**JLAST
      I=0
      DO 1 K=1,KKK
C     GENERATING ONE SYMBOL.
      IF (I.EQ.JLAST) I=0
      I=I+1
      J=I-JTAP
      IF (J.LE.JTAP) J=J+JLAST
      NX(I)=NX(J)*NX(I)
      NY(I)=NY(J)*NY(I)
      IPNI(K)=NX(I)
      IPNQ(K)=NY(I)
C     LOAD INTO THE ARRAY TO BE FOURIER TRANSFORMED.
      J1=(K-1)*LSAMPL+1
      J2=K*LSAMPL
      DO 2 J3=J1,J2
    2 DATA(J3)=CMPLX(FLOAT(NX(I)),FLOAT(NY(I)))
    1 CONTINUE
      RETURN
      END
```

```
C*****************************************************************
C THIS SUBROUTINE DECODES THE PROCESSED DATA
C*****************************************************************
      SUBROUTINE DECOD4(DATA,PNOISE,IPNI,IPNQ,
     #EBNO,PEI,NSNR,EB,ICFF,NERROR)
      COMMON LDIM
      COMMON/PARA/LSAMPL,NSYMB,NC1,NC2,BAUD,SBANDW
      DIMENSION EBNO(1),PEI(1),IPNI(1),IPNQ(1)
      COMPLEX DATA(1),AMP
      NERROR=0
      IF (ICFF.EQ.0) GO TO 111
      DO 6 K=1,ICFF
      XX=AIMAG(DATA(LDIM))
      DO 7 KI=2,LDIM
      KK=LDIM+2-KI
    7 DATA(KK)=CMPLX(REAL(DATA(KK)),AIMAG(DATA(KK-1)))
    6 DATA(1)=CMPLX(REAL(DATA(1)),XX)
C     SYNCHRONIZE THE RECEIVED DATA
  111 NOLD=0
      NCF=0
      K=1
  300 CONTINUE
      NEW=0
      DO 200 J=1,NSYMB
      J1=K+(J-1)*LSAMPL
      IF(J1.GT.LDIM) J1=J1-LDIM
      XB=REAL(DATA(J1))
      YB=AIMAG(DATA(J1))
      IF (SIGN(1.,XB).EQ.IPNI(J)) NEW=NEW+1
      IF (SIGN(1.,YB).EQ.IPNQ(J)) NEW=NEW+1
  200 CONTINUE
      IF(NOLD.GE.NEW) GO TO 399
      NOLD=NEW
      NCF=K
  399 K=K+1
      LFU=2*NSYMB
      IF (NOLD.LT.LFU.AND.K.LE.LDIM) GO TO 300
      IF (NCF.EQ.0) GO TO 230
      LC=LDIM-1
      DO 250 I=1,NCF
      AMP=DATA(1)
      DO 240 J=1,LC
      DATA(J)=DATA(J+1)
  240 CONTINUE
      DATA(LDIM)=AMP
  250 CONTINUE
  230 MI=1
      MQ=1
      EOI=FLOAT(NSYMB)+1.
      EOQ=FLOAT(NSYMB)+1.
      SNR=PNOISE*EB/5.
      SIGMA=SQRT(SNR)
      DO 110 J=1,LSAMPL
      EI=0.
      EQ=0.
      DO 100 K=1,NSYMB
      J1=(K-1)*LSAMPL+J
      AXBAR=(REAL(DATA(J1))+REAL(DATA(J1+1)))/2.
      AYBAR=(AIMAG(DATA(J1))+AIMAG(DATA(J1+1)))/2.
      IF(SIGN(1.,AXBAR).NE.IPNI(K)) EI=EI+1
      IF(SIGN(1.,AYBAR).NE.IPNQ(K)) EQ=EQ+1
      ARGI=ABS(AXBAR)/SIGMA
```

17


```
      ARGQ=ABS(AYBAR)/SIGMA
      EI=EI+ERFC(ARGI)/2.
      EQ=EQ+ERFC(ARGQ)/2.
  100 CONTINUE
      IF(ECI.LE.EI) GO TO 120
      ECI=EI
      MI=J
  120 CONTINUE
      IF (ECQ.LE.EQ) GO TO 110
      ECQ=EQ
      MQ=J
  110 CONTINUE
      MOFF=IABS(MI-MQ)
      MOFF=MOFF+MI
      OFF=(FLOAT(MOFF)+FLOAT(NOF))/FLOAT(LSAMPL)
      DO 2 K=1,NSYMB
      JI=(K-1)*LSAMPL+MI
      JQ=(K-1)*LSAMPL+MQ
      AXBAR=(REAL(DATA(JI))+REAL(DATA(JI+1)))/2.
      AYBAR=(AIMAG(DATA(JQ))+AIMAG(DATA(JQ+1)))/2.
      INDEXX=0
      IF(SIGN(1.,AXBAR).NE.IPNI(K)) INDEXX=1
      INDEXY=0
      IF(SIGN(1.,AYBAR).NE.IPNQ(K)) INDEXY=1
      IF((INDEXX.EQ.1).OR.(INDEXY.EQ.1)) NERROR=NERROR+1
C     COMPUTE THE PROBABILITY OF ERROR FOR THIS SYMBOL
      DO 4 M=1,NSNR
      XM=FLOAT(M)/10.
      SNR=PNOISE*EB/(10.**XM)
      SIGMA=SQRT(SNR)
      ARG=(ABS(AXBAR))/(SIGMA*SQRT(2.))
      IF (ARG.GT.12.) ARG=12.
      EX=ERFC(ARG)/2.
      IF (INDEXX.EQ.1) EX=1.-EX
      ARG=(ABS(AYBAR))/(SIGMA*SQRT(2.))
      IF (ARG.GT.12.) ARG=12.
      EY=ERFC(ARG)/2.
      IF (INDEXY.EQ.1) EY=1.-EY
      IF (EX.LT.1.E-15) EX=0.
      IF (EY.LT.1.E-15) EY=0.
    4 PEI(M)=PEI(M)+((EX+EY)/2.)
    2 CONTINUE
      RETURN
      END
```

```
FORTRAN IV G LEVEL 21          MAIN          DATE = 81259          19/04/15

C*****
C     RAISED COSINE FILTER WITH ARBITRARY ALPHA
C*****
      SUBROUTINE RCOS2(FBANDW,TF,ALPHA)
      COMMON LDIM
      COMMON/PARA/LSAMPL,NSYMB,NC1,NC2,BAUD,SBANDW
      COMPLEX TF(1)
      IF (ALPHA.EQ.0.) ALPHA=0.0001
      FN=LDIM*(FBANDW/SBANDW)
      F1=(1.-ALPHA)*FN
      F2=(1.+ALPHA)*FN
      IFN=IFIX(FN)
      IF1=IFIX(F1)+1
      IF2=IFIX(F2)+1
      A1=3.141516/(2.*FLOAT(IFN))
      DO 8 I=2,IF1
      TF(I)=CMPLX(1.0,0.0)
      J=I-1
      TF(J)=CMPLX(1.,0.0)
    8 CONTINUE
      JK=IF1+1
      DO 9 J=JK,IF2
      I=J-1
      A=(3.141516/(2.0*ALPHA))*((FLOAT(I)/FLOAT(IFN))-1.)
      TF(J)=CMPLX((0.5*(1.0-SIN(A))),0.0)
    9 CONTINUE
      JF=IF2+1
      DO 10 I=JF,NC1
      TF(I)=CMPLX(0.0,0.0)
   10 CONTINUE
      DO 5 I=NC2,LDIM
      TF(I)=CONJG(TF(LDIM+2-I))
    5 CONTINUE
      RETURN
      END
```

```
FORTRAN IV G LEVEL 21          MAIN          DATE = 81259          19/04/15

C*****
C     THIS SUBROUTINE SIMULATES THE EQUIVALENT BASEBAND
C     NONLINEARITY OF THE INTELSAT-V HPA
C*****
      SUBROUTINE HPA(DATA,BAKOFF,PSHIFT)
      COMMON LDIM
      COMPLEX DATA(1)
      REAL MPS
      DATA ZPMAX,ZQMAX,VMAX,VC/1.068,0.928,1.414,1./
      DATA A1,A3,A5,A7,A9,A11,A13,A15,A17/1.916288,-9.358132E-1,
     #1.942392E-1,-2.832262E-2,1.940305E-2,-4.282407E-3,0.0,0.0,0.0/
      DATA B1,B3,B5,B7,B9,B11,B13,B15,B17/-5.9659E-2,1.907669,
     #-1.864724,8.615525E-1,-1.990954E-1,1.815157E-2,0.0,0.0,0.0/
      P(X)=((((((((A17*X**2+A15)*X**2+A13)*X**2+A11)*X**2+A9)*
     #X**2+A7)*X**2+A5)*X**2+A3)*X**2+A1
      ZP(X)=P(X)*X
      Q(X)=((((((((B17*X**2+B15)*X**2+B13)*X**2+B11)*X**2+B9)*
     #X**2+B7)*X**2+B5)*X**2+B3)*X**2+B1
      ZQ(X)=Q(X)*X
      Z(X)=SQRT(ZP(X)**2+ZQ(X)**2)
      TWTIN=VC*10.**(-BAKOFF/20.)
      PSHIFT=ATAN(ZQ(TWTIN*1.414)/ZP(TWTIN*1.414))
      CALL PCALC(DATA,MPS,PR)
      FNORMI=TWTIN/SQRT(MPS)
      DO 11 I=1,LDIM
      DATA(I)=DATA(I)*FNORMI
   11 CONTINUE
      DO 10 I=1,LDIM
      X=REAL(DATA(I))
      Y=AIMAG(DATA(I))
      R=SQRT(X**2+Y**2)
      IF(R.GT.VMAX) GOTO 12
      DATA(I)=CMPLX(P(R)*X-Q(R)*Y,P(R)*Y+Q(R)*X)
      GO TO 10
   12 DATA(I)=CMPLX(ZPMAX*X-ZQMAX*Y,ZQMAX*X+ZPMAX*Y)/R
   10 CONTINUE
      RETURN
      END
```

166

2962931

```
FORTRAN IV G LEVEL 21                    MAIN                    DATE = 81259          19/04/15

                C*************************************************************
                C     THIS SUBROUTINE SIMULATES THE EQUIVALENT BASEBAND
                C     NONLINEARITY OF THE INTELSAT-V TWTA .
                C*************************************************************
     0001               SUBROUTINE TWT(DATA,BAKOFF,PSHIFT)
     0002               COMMON LDIM
     0003               COMPLEX DATA(1)
     0004               REAL MP1
     0005               DATA ZPMAX,ZQMAX,VMAX,VO/.886,1.017,1.414,1./
     0006               DATA A1,A3,A5,A7,A9,A11,A13,A15,A17/2.185509,-1.934083,
                       #9.907856E-1,-2.313386E-1,1.963265E-2,0.0,0.0,0.0,0.0/
     0007               DATA B1,B3,B5,B7,B9,B11,B13,B15,B17/2.641891E-1,1.338875,
                       #-9.973067E-1,2.675212E-1,-2.400961E-2,0.0,0.0,0.0,0.0/
     0008               P(X)=((((((((A17*X**2+A15)*X**2+A13)*X**2+A11)*X**2+A9)*
                       #X**2+A7)*X**2+A5)*X**2+A3)*X**2+A1
     0009               ZP(X)=P(X)*X
     0010               Q(X)=((((((((B17*X**2+B15)*X**2+B13)*X**2+B11)*X**2+B9)*
                       #X**2+B7)*X**2+B5)*X**2+B3)*X**2+B1
     0011               ZQ(X)=Q(X)*X
     0012               Z(X)=SQRT(ZP(X)**2+ZQ(X)**2)
     0013               TWTIN=VO*10.**(-BAKOFF/20.)
     0014               PSHIFT=ATAN(ZQ(TWTIN*1.414)/ZP(TWTIN*1.414))
     0015               CALL POWER(DATA,MP1,PR)
     0016               FNORMI=TWTIN/SQRT(MP1)
     0017               DO 11 I=1,LDIM
     0018               DATA(I)=DATA(I)*FNORMI
     0019            11 CONTINUE
     0020               DO 10 I=1,LDIM
     0021               X=REAL(DATA(I))
     0022               Y=AIMAG(DATA(I))
     0023               R=SQRT(X**2+Y**2)
     0024               IF(R.GT.VMAX) GOTO 12
     0025               DATA(I)=CMPLX(P(R)*X-Q(R)*Y,P(R)*Y+Q(R)*X)
     0026               GO TO 10
     0027            12 DATA(I)=CMPLX(ZPMAX*X-ZQMAX*Y,ZQMAX*X+ZPMAX*Y)/R
     0028            10 CONTINUE
     0029               RETURN
     0030               END
```

```
FORTRAN IV G LEVEL 21.          MAIN            DATE = 81259        19/04/15

      C*************************************************************
      C  THIS SUBROUTINE COMPENSATES FOR THE PHASE SHIFT
      C*************************************************************
0001          SUBROUTINE PHASE(DATA,PSHIFT)
0002          COMMON LDIM
0003          COMPLEX EPS,DATA(1)
0004          EPS=CMPLX(COS(PSHIFT),-SIN(PSHIFT))
0005          DO 10 I=1,LDIM
0006          DATA(I)=DATA(I)*EPS
0007       10 CONTINUE
0008          RETURN
0009          END
```

FORTRAN IV G LEVEL 21 MAIN DATE = 81259 19/04/15

```
C*************************************************************
C     THIS SUBROUTINE DRAWS PROBABILITY OF ERROR CURVES FOR
C     P(E) AS LOW AS 1.0E-10 AND A C/N RATIO AS HIGH AS 30 DB.
C*************************************************************
      SUBROUTINE DRAW(XARRAY,YARRAY,NSNR,JCURV,JLAST)
      DIMENSION XARRAY(27),YARRAY(27),X(15),Y(15)
      M=NSNR
      DO 1 K=1,NSNR
      IF(YARRAY(K).LE.1.0E-10) GOTO 3
      GOTO 1
    3 M=K-1
      GOTO 4
    1 CONTINUE
    4 CONTINUE
      I=M+1
      II=I+1
      XARRAY(I)=0.0
      XARRAY(II)=2.0
      YARRAY(I)=1.E-10
      YARRAY(II)=0.4
      IF(JCURV.GT.1) GOTO 2
C
C     ESTABLISH THE SURFACE AREA.
C
      CALL PLOTS(30.0,27.5)
C
C     ESTABLISH THE ORIGIN.
C
      CALL PLOT(3.0,2.0,-3)
C
C     DRAW THE LOGARITHMIC Y-AXIS.
C
      CALL LGAXS(0.0,0.0,20HPROBABILITY OF ERROR,20,24.,
     +90.,1.0E-10,.4)
C
C     DRAW THE LINEAR X-AXIS.
C
      CALL AXIS(0.0,0.0,11HEB/NO IN DB,-11,
     +16.0,0.0,0.0,2.0)
C
C     WRITE THE TITLE OF THE GRAPH.
C
      CALL SYMBOL(4.0,23.0,0.49,15HDPSK SIMULATION,0.0,15)
C     PLOT THE IDEAL CURVE.
      DO 5 J=1,13
      X(J)=FLOAT(J)
    5 Y(J)=.5*ERFC(SQRT(10.**(.1*J)))
      X(14)=0.0
      X(15)=2.0
      Y(14)=1.E-10
      Y(15)=0.4
      CALL LGLIN(X,Y,13,1,2,JCURV,1)
    2 CONTINUE
C
C     PLOT THE DATA IN LOG-LINEAR MODE.
C
      CALL LGLIN(XARRAY,YARRAY,M,1,2,JCURV,1)
      IF(JCURV.EQ.JLAST) CALL PLOT(0.0,0.0,999)
      RETURN
      END
```

159

2952937

FORTRAN IV G LEVEL 21 MAIN DATE = 81259 19/04/15

```
C*****************************************************************
C       THIS SUBROUTINE DRAWS THE EYE DIAGRAM FOR A
C       SYMBOL DURATION.
C*****************************************************************
      SUBROUTINE EYEQ(DATA)
      COMMON/PARA/LSAMPL,NSYMB,NO1,NO2,BAUD,SBANDW
      DIMENSION DATA2(64),DATA3(64)
      COMPLEX DATA(1)
C     ESTABLISH THE SURFACE AREA.
      CALL PLOTS(35.0,27.5)
C     ESTABLISH THE ORIGIN.
      CALL PLOT(3.0,13.0,-3)
C     WRITE THE TITLE OF THE GRAPH.
      CALL SYMBOL(10.0,12.0,0.49,16HQPSK EYE DIAGRAM,0.0,16)
C     DRAW THE TIME AXIS.
      CALL AXIS(0.0,0.0,1H ,-1.31,0.0,1.0,1.0)
C     DRAW THE AMPLITUDE AXIS.
      CALL AXIS(0.0,-12.0,1H ,1,26.0,90.0,-3.0,0.25)
C     PLOT THE DATA.
      JJ=2*LSAMPL
      DATA2(JJ+1)=0.0
      DATA2(JJ+2)=0.25
      DATA3(JJ+1)=1.0
      DATA3(JJ+2)=1.)
      M2=NSYMB
      DO 4 KK=1,M2
      DO 2 I=1,JJ
      II=(KK-1)*LSAMPL+I+(LSAMPL/2)
      IF (II.GT.LDIM) II=II-LDIM
      DATA2(I)=REAL(DATA(II))
    2 DATA3(I)=FLOAT(I)
      CALL LINE(DATA3,DATA2,JJ,1,0,0)
    4 CONTINUE
      CALL PLOT(0.0,0.0,+999)
      RETURN
      END
```

170

```
FORTRAN IV G LEVEL 21          SACI          DATE = 81259          19/04/15

0001                  SUBROUTINE SACI(TF,FCF)
0002                  COMMON LDIM
0003                  COMMON/PARA/LSAMPL,NSYMB,NC1,NC2,BAUD,SBANDW
0004                  COMPLEX TF(1)
0005                  COMPLEX XX
0006                  DIMENSION IWK(12)
0007                  CALL FFT2C(TF,11,IWK)
0008                  IFCF=IFIX(FCF*FLOAT(LDIM)/SBANDW)
0009                  IF(IFCF.EQ.0) RETURN
0010                  IF(IFCF.LT.0) GO TO 50
0011                  DO 20 K=1,IFCF
0012                  XX=TF(LDIM)
0013                  JJ=LDIM-1
0014                  DO 30 I=1,JJ
0015                  TF(LDIM+1-I)=TF(LDIM-I)
0016            30    CONTINUE
0017                  TF(1)=XX
0018            20    CONTINUE
0019                  GO TO 100
0020            50    IFCF=-IFCF
0021                  JJ=LDIM-1
0022                  DO 70 K=1,IFCF
0023                  XX=TF(1)
0024                  DO 60 I=1,JJ
0025            60    TF(I)=TF(I+1)
0026                  TF(LDIM)=XX
0027            70    CONTINUE
0028           100    DO 1  I=1,LDIM
0029             1    TF(I)=CONJG(TF(I))
0030                  CALL FFT2C(TF,11,IWK)
0031                  DO 2  I=1,LDIM
0032                  TF(I)=CONJG(TF(I))/FLOAT(LDIM)
0033                  RETURN
0034                  END
```

```
FORTRAN IV G LEVEL 21          MAIN          DATE = 81259      19/04/15

      C*****************************************************
      C              PARABOLIC GROUP DELAY
      C*****************************************************
0001          SUBROUTINE PARSE(TF,PI)
0002          COMMON LDIM
0003          COMMON/PARA/LSAMPL,NSYMB,NC1,NC2,BAUD,BRANDW
0004          COMPLEX TF(1)
0005          DO 20 I=1,NC1
0006          AI=FLOAT(I-1)*BRANDW/FLOAT(LDIM)
0007          PHI=4.*PI*.1415926/3.*((PI*(AI**3.))/(10.**3.))
0008          TF(I)=TF(I)*CMPLX(COS(PHI),-SIN(PHI))
0009       20 CONTINUE
0010          DO 21 I=NC2,LDIM
0011          TF(I)=CONJG(TF(LDIM+2-I))
0012       21 CONTINUE
0013          RETURN
0014          END
```

172

```
FORTRAN IV G LEVEL  21                MAIN              DATE = 81259          19/04/15

      C*********************************************************************
      C TO LOAD THE DATA IN QUADRATURE FORM FOR PROCESSING WITH
      C PROVISION TO GENERATE OVERLAPPED PULSES
      C*********************************************************************
            SUBROUTINE LOADS(DATA,IPNI,IPNQ,IOFF,NNN )
            COMMON LDIM
            COMMON/PARA/LSAMPL,NSYMB,NC1,NC2,BAUD,SBANDW
            COMPLEX DATA(1)
            DIMENSION NX(7),NY(7),IPNI(1),IPNQ(1),P(48),Q(16)
            DIMENSION DF(2048)
            DATA NX(1),NX(2),NX(3),NX(4),NX(5),NX(6),NX(7)/
           *-1,-1,-1,-1,-1,-1,-1/
            DATA NY(1),NY(2),NY(3),NY(4),NY(5),NY(6),NY(7)/
           *-1,-1,1,1,1,1,-1/
            DATA JLAST,JTAP/7,1/
            I=0
            DO 1 K=1,NSYMB
            IF (I.EQ.JLAST) I=0
            I=I+1
            J=I-JTAP
            IF (I.LE.JTAP) J=J+JLAST
            NX(I)=NX(J)*NX(I)
            NY(I)=NY(J)*NY(I)
            IPNI(K)=NX(I)
          1 IPNQ(K)=NY(I)
            CALL PULSE(P,LSAMPL,NNN)
            DO 2 I=1,NSYMB
            J1=(I-1)*LSAMPL+1
            J2=I*LSAMPL
            J=0
            DO 3 L=J1,J2
            J=J+1
            L1=I-1
            L2=I+1
            PR=FLOAT(IPNI(I))*P(16+J)
            PQ=FLOAT(IPNQ(I))*P(16+J)
            IF(I.EQ.1) L1=NSYMB
            PR=PR+FLOAT(IPNI(L1))*P(32+J)
            PQ=PQ+FLOAT(IPNQ(L1))*P(32+J)
            IF(I.EQ.NSYMB) L2=1
            PR=PR+FLOAT(IPNI(L2))*P(J)
            PQ=PQ+FLOAT(IPNQ(L2))*P(J)
            DATA(L)=CMPLX(PR,0.)
            DF(L)=PQ
          3 CONTINUE
          2 CONTINUE
            DO 4 I=1,LDIM
            L=I+IOFF
            IF(L.GT.LDIM) L=L-LDIM
          4 DATA(I)=DATA(I)+CMPLX(0.,DF(L))
            RETURN
            END
```

FORTRAN IV G LEVEL 21 DATE = 81259 19/04/15

```
0001          FUNCTION F(X,N)
0002          A=FLOAT(N)
0003          B=(3.14159*ABS(X)+3.14159/2.)/A
0004          C=SIN(3.14159/2./A)
0005          F=.5*(1.-SIN(B)/C)
0006          RETURN
0007          END
```

```
FORTRAN IV G LEVEL 21          PULSE          DATE = 81259      19/04/15

0001                SUBROUTINE PULSE(P,LSAMPL,NNN)
0002                DIMENSION P(1)
0003                D=1./FLOAT(LSAMPL)
0004                K=2*LSAMPL
0005                KK=3*LSAMPL
0006                DO 10 I=1,KK
0007             10 P(I)=0.
0008                DO 20 I=1,K
0009                AI=FLOAT(I-1)*D+(D/2.)-1.
0010             20 P(I+8)=F(AI,NNN)
0011                RETURN
0012                END
```

```
FORTRAN IV G LEVEL  21                FF                DATE = 81259      19/04/15

0001                FUNCTION FF(X,N)
0002                A=SIN(2.*X)/2./X
0003                B=FLOAT(N)*SIN(X)/SIN(3.14159/2./FLOAT(N))
0004                C1=SIN(X+3.14159/2./FLOAT(N))/(3.14159+2.*FLOAT(N)*X)
0005                C2=SIN(X-3.14159/2./FLOAT(N))/(3.14159-2.*FLOAT(N)*X)
0006                G=A-B*(C1+C2)
0007                FF=1./G
0008                RETURN
0009                END.
```

```
FORTRAN IV G LEVEL  21                FFHH                DATE = 81259        19/09/15

0001                  FUNCTION FFHH(X)
0002                  Y=X/3.14159
0003                  DDD=ABS(Y-.5)
0004                  IF(DDD.LT.0.0001) GOTO 111
0005                  G=2.0*X
0006                  H=SIN(G)/G
0007                  A=.5+SQRT(2.)/4.
0008                  B=.5-SQRT(2.)/4.
0009                  C1=H*(1.0/(1.0-4.*Y**2.0)+A-1.0)
0010                  IF(Y.EQ.1.0) Y=Y-.0001
0011                  C2=H*Y**2./(1.-Y**2.)*B
0012                  S2=(ABS(C1-C2))**2.
0013                  S1=H/(1.-4.*Y**2.)
0014                  S1=.5*(ABS(S1)**2.)
0015                  DEM=.5+A**2.
0016                  SS=(S1+S2)/DEM
0017            111   IF(DDD.LT.0.0001) SS=.3
0018                  FFHH=1./(SQRT(SS))
0019                  RETURN
0020                  END
```

177

```
FORTRAN IV G LEVEL  21                FF1                DATE = 81259          19/04/15

0001                FUNCTION FF1(X)
0002                FF1=2.*X*(1.-(4./(3.141592**2))*(X**2))/SIN(2.*X)
0003                RETURN
0004                END
```

```
FORTRAN IV G LEVEL  21                PULS                DATE = 81259        19/04/15

0001                  SUBROUTINE PULS(G,S)
0002                  COMMON LDIM
0003                  COMMON/PARA/LSAMPL,NSYMB,NC1,NC2,BAUD,SBAND
0004                  DIMENSION G(10)
0005                  J=IFIX(10.*S)
0006                  DO 1 I=1,J
0007                  G(I)=(FLOAT(I)-1.)/FLOAT(J)
0008              1   CONTINUE
0009                  J1=J+1
0010                  J2=LSAMPL-J
0011                  DO 2 I=J1,J2
0012                  G(I)=1.0
0013              2   CONTINUE
0014                  J3=J2+1
0015                  DO 3 I=J3,LSAMPL
0016                  G(I)=G(LSAMPL-I+1)
0017              3   CONTINUE
0018                  RETURN
0019                  END
```

```
FORTRAN IV G LEVEL  21          MAIN            DATE = 81259        19/04/15

C*****************************************************************
C     RAISED COSINE FILTER WITH ARBITRARY ALPHA AND SHAPE CORRECTION
C*****************************************************************
0001          SUBROUTINE RCOS( FBAND#,TF,ALPHA,NNN,NTYPE)
0002          COMMON LDIM
0003          COMMON/PARA/LSAMPL,NSYMB,NC1,NC2,BAUD,SBAND#
0004          COMPLEX TF(1)
0005          QQ=3.14159265/2.
0006          IF (ALPHA.EQ.0) ALPHA=0.0001
0007          FN=LDIM*(FBAND#/SBAND#)
0008          F1=(1.-ALPHA)*FN
0009          F2=(1.+ALPHA)*FN
0010          IFN=IFIX(FN)
0011          IF1=IFIX(F1)+1
0012          IF2=IFIX(F2)+1
0013          A1=3.141592/(2.*FLOAT(IFN))
      C       AMOD=FLOAT(IMOD)
0014          TF(1)=CMPLX(1.0,0.0)
0015          DO 8 I=2,IF1
0016          J=I-1
0017          A2=FF(FLOAT(J)*A1,NNN)
0018          AA3=FFHH(FLOAT(J)*A1)
0019          IF(NTYPE.EQ.2) A2=AA3
      C       IF(ABS(AMOD).GT.1) A2=FF1(FLOAT(J)*A1)
0020          TF(I)=CMPLX(A2,0.0)
0021        8 CONTINUE
0022          JK=IF1+1
0023          DO 9 J=JK,IF2
0024          I=J-1
0025          A3=FFHH(FLOAT(I)*A1)
0026           IF(NTYPE.EQ.2)GOTO 119
0027          A3=1./(.5+1./3.1415927)
0028          IF(NNN.EQ.1)A3=2.
0029          BBB=FN
0030          IF(NNN.EQ.2) BBB=BBB/2.
0031          IF(I.NE.BBB)A3=FF(FLOAT(I)*A1,NNN)
0032      119 A=(3.141592/(2.0*ALPHA))*((FLOAT(I)/FLOAT(IFN))-1.)
0033          TF(J)=CMPLX(0.5*(1.0-SIN(A)),0.0)
0034          TF(J)=TF(J)*CMPLX(A3,0.0)
0035        9 CONTINUE
0036          JH=IF2+1
0037          DO 10 I=JH,NC1
0038          TF(I)=CMPLX(0.0,0.0)
0039       10 CONTINUE
0040          DO 5 I=NC2,LDIM
0041          TF(I)=TF(LDIM+2-I)
0042        5 CONTINUE
0043          RETURN
0044          END
```

180

F64-LEVEL LINKAGE EDITOR OPTIONS SPECIFIED LIST,MAP,LET,SIZE=(120K,24K)
VARIABLE OPTIONS USED - SIZE=(122880,24576)

MODULE MAP

CONTROL SECTION NAME	ORIGIN	LENGTH	ENTRY NAME	LOCATION	NAME	LOCATION	NAME	LOCATION
MAIN	00	197E2						
HLIM	197E8	1BC						
TCOS	199A8	60E						
ATT	19FB8	1E4						
TIME	1A1A0	1E4						
POWER	1A388	29A						
RCOS1	1A628	4E4						
FILTER	1AB10	2C8						
HHGG	1ADD8	1FA						
ENERGY	1AFD8	208						
LOAD4	1B1E0	354						
DECOD4	1B538	CF4						
RCOS2	1C230	4C6						
HPA	1C6F8	330						
I*T	1CF28	830						
PHASE	1D758	1E6						
DRA*	1D940	5C4						
EYEQ	1DF08	5B2						
SACI	1E4C0	4D2						
PARGD	1E998	320						
LOAD5	1ECB8	272C						
F	213E8	1EA						
PULSE	215D8	258						
FF	21830	322						
FFHH	21B58	336						
FF1	21EF0	184						
PULS	22078	2BE						
RCOS	22338	71A						
IHCSLOG *	22A58	1BC	ALOG10	22A58	ALOG	22A70		
IHCCSABS*	22C10	B4	CABS	22C10				
IHCCSAS *	22CC8	C4	CMPY#	22CC8	CDVD#	22CE2		
FFT2C *	22D90	9E6						
IHCFIXPI*	23778	14F	FIXPI#	23778				
IHCFRXPR*	238C8	183	FRXPR#	238C8				
IHCECOMH*	23A50	F62	IBCOM#	23A50	FDIOCS#	23B0C	INTSWTCH	24996
IHCCOMH2*	249B8	6C1	SEQDASD	24D94				
IHCSSCN *	25080	1D9						

181

NAME	ORIGIN	LENGTH
IHCSSQRT*	25260	145
IHCSATN2*	253A8	1CB
AXIS *	25578	796
IHCSERF *	25D10	1EC
IHCERRM *	25F00	9DC
LGAXS *	264E0	8DC
LGLIN *	26DC0	5A8
LINE *	27368	57E
PLOTS *	278E0	104E
SYMBOL *	28930	ED2
IHCFCVTH*	29808	1105
IHCERNTH*	2A9C0	542
IHCSEXP *	2AF08	192
IHCERIOS*	2B0A0	F48
IHCFIOS2*	2BFE8	556
IHCUOPT *	2C540	300
IHCFMAXR*	2C840	C9
IHCETRCH*	2C910	28E
IHCUATBL*	2CBA0	298
NUMBER *	2CE26	532
PLTERR *	2D360	DE6
IHCFRXPI*	2E148	141
$BLANKCOM	2E290	4
PARA	2E298	18

NAME	LOCATION	NAME	LOCATION	NAME	LOCATION
COS	25080	SIN	25098		
SQRT	25260				
ATAN2	253A8	ATAN	253BC		
ERFC	25D10	ERF	25D26		
ERFMON	25F00	IHCERRE	25F18		
PLOT	27826	FACTOR	27F0C	NEWPEN	27F4C
ADCCN#	29808	FCVAOUTP	29982	FCVLOUTP	29942
FCVIOUTP	29E52	FCVEOUTP	2A354	FCVCOUTP	2A56E
ARITH#	2A9C0	ADJSWTCH	2AA5C		
EXP	2AF08				
FIOCS#	2B0A0	FIOCSBEP	2B0A6		
MAX1	2C840	MIN1	2C956	AMAX1	2C86C
IHCTRCH	2C910	ERRTRA	2C918		
FRXPI#	2E148				

182

ENTRY ADDRESS 00

TOTAL LENGTH 2E2B0

****GO DOES NOT EXIST BUT HAS BEEN ADDED TO DATA SET

AUTHORIZATION CODE IS 0.

REFERENCES

1. S. Gronemeyer, A. McBride, "MSK and Offset QPSK Modulation", IEEE Trans on Communications, Vol. COM-24, August 1976

2. V.K. Prabhu, "MSK and Offset QPSK Modulation with Band-Limiting Filters" IEEE Trans on Aerospace & Electronic System, January 1981

3. J. Huang and K. Feher, "Performance of QPSK, OK-QPSK and MSK Signals Through a Satellite Link" IEEE Canadian Communications and Power Conference, Montreal, October 1978

4. D.H. Morais and K. Feher, "The Effects of Filtering and Limiting on the Performance of QPSK, Offset QPSK and MSK System" IEEE Trans on Communications, Vol. COM-28, December 1980

5. S. A. Rhodes, "Effects of Hardlimiting on Bandlimited Transmissions with Conventional and Offset QPSK Modulation", Proc. of the IEEE NTC Conference 1972, pp. 20F/1-7

6. G. Satoh, T. Mizuno, "Nonlinear Satellite Channel Design for QPSK/TDMA Transmission" The Fifth International Conference on Digital Satellite Communications, March 23-26, 1981, Genoa, Italy

7. J. Huang, K. Feher and M. Gendron, "Techniques to Generate ISI and Jitter-Free Bandlimited Nyquist Signals and a Method to Analyze Jitter Effects", IEEE Trans on Comm. Vol. COM-27, No. 11, November 1979

8. F. Jager, C.B. Dekker, "Tamed Frequency Modulation", A Novel Method to Achieve Spectrum Economy in Digital Transmission", IEEE Trans on Communications, Vol, COM-26, May 1978

9. T. Le-Ngoc, K. Feher, and H. Pham Van, "Power and Bandwidth Efficient IJF Quadrature Modulation Techniques for Linear and Nonlinear Channels" part of CRC report "Regenerative Transponders for More Efficient Digital Satellite Systems", No. OSU80-00197

10. Intelsat TDMA/DSI System Specification BG-42-65, May 1981

11. T. Le-Ngoc, K. Feher, "Performance of IJF-OQPSK Modulation Schemes in the Presence of Noise, Interchannel and Cochannel Interference", Proc. of the IEEE-NTC, New Orleans, Nov. 1981

12. R. Lucky, J. Salz and E. Weldon, Principles of Data Communication, New York: McGraw Hill 1968

13. K. Feher, Digital Communications: Microwave Applications Englewood Cliffs, N.J. Prentice-Hall 1980

14. T. Le-Ngoc, K. Feher and H. Pham-Van, "New Modulation Techniques for Low Cost Power and Bandwidth Efficient Satellite Earth Stations", IEEE Trans. on Communications, January 1982

15. M.C. Austin and M.U. Chang, "Quadrature Overlapped Raised Cosine Modulation", IEEE Trans. on Communications, Vol COM-29 March 1981

16. W. Foster, M. Chang, "Performance of Several Pulse Shaping Techniques in Nonlinear TDMA Environment" Proc of the IEEE ICC-1981, Denver June 1981

17. D. Divsalar, M.K. Simon, "Performance of Quadrature Overlapped Raised Cosine Modulation Over Nonlinear Satellite Channels" Proc. of the IEEE-ICC 1981, Denver June 1981

18. K. Feher "Filter", U.S. Patent No. 4,339,724, issued July 13, 1982, Canada Disclosure No. 327,365, filed May 10, 1979.

19. K. Feher, "Digital Modulation Techniques in an Interference Environment", Don White Consultants, Inc., Gainesville, Virginia, 22065, 1977

20. K. Feher, "Digital Communications: Satellite/Earth Station Engineering", Prentice-Hall, Inc., Englewood Cliffs, N.J. December 1982

21. Ash, R., Information Theory, John Wiley & Sons, Inc., New York, 1965

22. Lindsey, W. S., M.K. Simon, Telecommunication Systems Engineering, Prentice-Hall, Inc., New Jersey 1973

23. D.H. Morais, K. Feher, "Bandwidth Efficiency and Probability of Error Performance of MSK and Offset QPSK Systems", IEEE Trans on Communications, Vol COM-27 December 1979

24. Shanmugam, K.S., Digital and Analog Communication Systems, John Wiley & Sons, New York, 1979

25. Bennet, W.R., J.R. Davey, Data Transmission, McGraw Hill, New York 1965

26. H.P. Van, K. Feher, "A Class of Two Symbol Interval Modems for Nonlinear Radio Systems" IEEE Trans on Communications, March 1983

27. H.P. Van, K. Feher., "TSI-OQPSK for Multiple Carrier Satellite Systems" Globecom 82, Miami, Florida 1982

28. M.J. Eric, "Intermodulation Analysis of Nonlinear Devices for Multiple Carrier Inputs" CRC report No. 1234, Ottawa, November 1972

29. D. Prendergast, K. Feher, "Low Cost Implementation of Variable Bit Rate ISI-Free Filter/Processor" Satellite Communication Conference, Ottawa, June 1983

30. Mueller, K.H., "A New Approach to Optimum Pulse Shaping in Sampled Systems Using Time-Domain Filtering", BSTJ, Vol. 52, No. 5, May-June, 1973, pp. 723-729

31. Chalk, J.H.H., "The Optimum Pulse Shape for Pulse Communication", Proc. IEEE, Vol. 97, No. 3, March, 1950, pp. 88-92

32. F. Amoroso, "Experimental Results on Constant Envelope Signalling with Reduced Spectral Sidelobes" Proc of the IEEE-ICC, Denver, June 1981

33. T. Aulin, C.E.W. Sundberg, "Continuous Phase Modulation - Part I: Full response signalling", IEEE Trans on Communications, Vol. COM-29, March 1981

34. T. Aulin, N. Rydbeck, C.E.W. Sundberg, "Continuous Phase Modulation - Part II: Partial response signalling", IEEE Trans on Communications, Vol COM-29, March 1981

35. M.C. Austin, M.U. Chang, "Quadrature Overlapped Raised Cosine Modulation" IEEE Trans on Communications, Vol. COM-29, March 1981

36. V.K. Prabhu, "MSK and Offset QPSK Modulation with Band-limiting Filters", IEEE Trans on Aerospace and Electronic System, Vol. AES-17, January 1981

37. R.G. Lyons, "Effects of PSK Spectral Spreading in a Satellite Transponder", ICC 74, pp 36B-116, Minneapolis, Minn., June 17-19-, 1974

38. S.Y. Kwon and R.S. Simpson, "Effect of Hardlimiting on a Quadrature PSK Signal", IEEE Trans on Communications, Vol. COM-22, August 1973

39. S. Murakami, Y. Furuya, Y. Matsuo, M. Sugiyama, "Optimum Modulation and Channel Filters for Nonlinear Satellite Channels", IEEE Trans on Communications, Vol. COM-27, Dec 1979

40. M.K. Simon "A Generalization of Minimum-Shift Keying (MSK) Type signalling based upon Input Data Symbol Pulse Shaping", IEEE Trans on Comm., Vol. COM-24, Aug 1976

41. M. Rabzel, S. Pasupathy, "Spectral Shaping in Minimum Shift Keying (MSK) type Signals", IEEE Trans on Communications, Vol. COM-26, Jan. 1978

42. B. Bazin, "A Class of MSK Baseband Pulse Formats with Sharp Sepctral Roll-Off", IEEE Trans on Communications Vol. COM27, May 1979

43. N. Boutin, S. Morisette, L. Dussault, "Constant Amplitude PSK signal with minimum out of band energy", NTC 1978, pp. 6.3/1.3, Dec. 1978

44. J.G. Anderson, D.P. Taylor, "A Bandwidth Efficient Class of Signal Space Codes", IEEE Trans on Inf. Theory V-1, IT-24, Nov. 1978

45. S. Rhodes, "FSOQ, A New Modulation Technique that Yields a Constant Envelope", NTC 80, Dec. 1980

46. T. Le-Ngoc, K. Feher, "A New Class of IJF-OQPSK Modems for Regenerative Satellite Systems", ICC 81, Denver, Colorado, June 1981

47. H. Pham Van and K. Feher, "New Modulation Techniques for Digital Satellite Systems" IEEC & E 81, Toronto, Canada 1981

48. D. Docherty and C. Pallemaertz, "Spectral Compatibility of 16-state QAM", ICC 80, Seattle, WA June 1980

49. William J.W., Philip H.S. and Joe T.S., "A Bandwidth Compressive Modulation System using Multi-Amplitude Minimum Shift Keying (MAMSK)", IEEE Trans on Communications Vol. COM26, May 1978

50. R. deBuda, "Coherent Demodulation of Frequency Shift Keying with Low Deviation Ratio", IEEE Trans on Comm. Aug. 1972

51. Peter Galko, S. Pasupathy, "The Mean Power Spectral Density of Markov Chain Driven Signals", IEEE Trans on IT, Nov. 1981

52. T. Le-Ngoc and K. Feher, "Performance of IJF-OQPSK Modulation Schemes in a Complex Interference Environment", IEEE Trans on Communications, January 1983